POLYHYDROXYALKANOATES PRODUCTION FROM *Novosphingobium* sp. THA_AIK7 FOR MICROCARRIER FABRICATION USING IN ANIMAL CELL CULTURE

SASINA PROMDEE

A THESIS SUBMITTED IN PARTIAL FULLFILLMENT OF THE REQUIREMENT FOR THE DEGREE OF MASTER OF SCIENCE PROGRAM IN APPLIED BIOLOGY

FACULTY OF SCIENCE AND TECHNOLOGY

RAJAMANGALA UNIVERSITY OF TECHNOLOGY THANYABURI

ACADEMIC YEAR 2023

POLYHYDROXYALKANOATES PRODUCTION FROM *Novosphingobium* sp. THA_AIK7 FOR MICROCARRIER FABRICATION USING IN ANIMAL CELL CULTURE

SASINA PROMDEE

A THESIS SUBMITTED IN PARTIAL FULLFILLMENT OF THE REQUIREMENT FOR THE DEGREE OF MASTER OF SCIENCE PROGRAM IN APPLIED BIOLOGY

FACULTY OF SCIENCE AND TECHNOLOGY

RAJAMANGALA UNIVERSITY OF TECHNOLOGY THANYABURI

ACADEMIC YEAR 2023

Thesis Title	Polyhydroxyalkanoates Production from *Novosphingobium* sp. THA_AIK7 for Microcarrier Fabrication Using in Animal Cell Culture
Name – Surname	Miss Sasina Promdee
Program	Applied Biology
Thesis Advisor	Assistant Professor Jantima Teeka, Ph.D.
Academic Year	2023

THESIS COMMITTEE

Kanokwan Poomputsa .....Chairman

(Assistant Professor Kanokwan Poomputsa, Ph.D.)

N. Buddhakala .....Committee

(Associate Professor Nopparat Buddhakala, Ph.D.)

Atsadawut Areesirisuk .....Committee

(Assistant Professor Atsadawut Areesirisuk, Ph.D.)

Manoch Posung .....Committee

(Mr.Manoch Posung, Ph.D.)

Jantima Teeka .....Committee

(Assistant Professor Jantima Teeka, Ph.D.)

Approved by the Faculty of Science and Technology, Rajamangala University of Technology Thanyaburi in Partial Fulfillment of the Requirements for the Master's Degree

Nipat Jongsawat .....Dean of Faculty of Science and Technology

(Assistant Professor Nipat Jongsawat, Ph.D.)

25 January 2024

Thesis Title	Polyhydroxyalkanoates Production from *Novosphingobium* sp. THA_AIK7 for Microcarrier Fabrication Using in Animal Cell Culture
Name – Surname	Miss Sasina Promdee
Program	Applied Biology
Thesis Advisor	Assistant Professor Jantima Teeka, Ph.D.
Academic Year	2023

ABSTRACT

This research aimed to: 1) investigate an appropriate carbon, nitrogen, and phosphorus source, 2) optimize the condition of PHA recovery using silica gel, 3) study the fabrication process of microcarriers by emulsion technique and 4) study the use of microcarriers in dynamic animal cell culture.

Novosphingobium sp. THA_AIK7 was cultured in a mineral salt medium (MSM) with various carbon, nitrogen, and phosphorus sources. Factor effecting PHAs extraction included temperature, loaded cell, and the amount of silica gel were analyzed using BBD. Fabrication of microcarrier from PHAs was designed using independent variables included PHA (mg), PVA (%), NH_5CO_3 (%), and stirrer (rpm). Fabricated microcarriers were tested for Vero and L929 cells culture.

Crude glycerol, MSG, and $Na_2HPO_4 \cdot 7H_2O$ were the best carbon, nitrogen, and phosphorus sources for growth and PHA production with a maximum PHA content of 27.54%. The highest HV monomer derived from crude glycerol was at 10.85 mol%. The extracted yield of PHAs from silica gel was 41 mg, accounting for 51.25% of CDW. The average diameter and average pore size of fabricated microcarriers MC-PHAs were 125.864 µm and 0.970 µm, respectively. The viability of Vero and L929 cells were 92% and 100%, respectively. PHAs can be fabricated into microcarriers and are not toxic to animal cells. However, the properties of MC-PHAs would be improved to enhance cell adhesion and proliferation in the next step.

Keywords: carbon, microcarrier, nitrogen, polyhydroxyalkanoates, phosphorus

Acknowledgments

This thesis was supported by the National Research Council of Thailand and the Fundamental Fund of RMUTT Research and Innovation Fair for Sustainable Change.

Secondly, I would like to express sincere gratitude to my advisor, Assistant Professor Dr. Jantima Teeka, for the valuable guidance, encouragement, help, and support until this thesis was completed.

Thirdly, I acknowledge my co-advisors, Assistant Professor Dr. Atsadawut Areesirisuk and Dr. Manoch Posung for also making suggestions and supporting my thesis.

Fourth, I would like to thank the thesis committee, Assistant Professor Dr. Kanokwan Poomputsa and Associate Professor Dr. Nopparat Buddhakala for valuable comments and helpful suggestions.

Subsequently, I would especially like to thank my friends, sister, Bioengineering lab members, Animal cell technology lab and the Division of Biology, Faculty of Science and Technology, RMUTT and Innovation and Medical Biotechnology Center (iMBC), Medical Life Sciences Institute, Department of Medical Sciences, Ministry of Public Health, Thailand, for their help and support throughout this research.

Finally, I am especially thankful to my mother, brother and family for their major encouragement, sincere love, and support of everything.

Sasina Promdee

Table of Contents

Table of Contents (Continued)

List of Tables

Page

List of Figure

Page

List of Figure (Continued)

Page

List of Abbreviations

BBD	Box Behnken design
CDW	Cell dry weight
FBS	Fetal bovine serum
MC-PHAs	Microcarrier Polyhydroxyalkanoates
MEM	Minimum essential medium
MSG	Monosodium glutamate
MSM	Mineral salt medium
NB	Nutrient broth
NMR	Nuclear magnetic resonance
PBS	Phosphate buffer saline
PHAs	Polyhydroxyalkanoates
PVA	Polyvinyl alcohol
P_{max}	Maximum product concentration (g/L)
r_{max}	Maximum product production rate (g/L h)
R^2	Coefficient of determination
$W_1/O/W_2$	Water-in-oil-in-water
Q_p	Volumetric production rate of PHA (g/L h)
Q_x	Volumetric production rates of biomass (g/L h)
X	Biomass concentration (g/L)
X_{max}	Maximum biomass concentration (g/L)
μ_{max}	Maximum specific growth rate (h^{-1})
$Y_{p/s}$	PHAs yield from substrate (g/g)
$Y_{x/s}$	Biomass yield from substrate (g/g)

CHAPTER 1
INTRODUCTION

1.1 Background and Statement of Problems

Polyhydroxyalkanoates (PHA) are intracellular polyesters naturally produced by a variety of bacterial species [1]. Under nutrient-limiting conditions with plenty of carbon sources, bacteria store PHA as their carbon and energy reserve materials. More than 150 different monomers can be combined into PHA polymer chain, making them a diverse polyester family. PHA have gained a great interest due to their biodegradability and biocompatibility. Since PHA was first discovered by Lemoigne [2], many attempt has been done to develop the production process of PHA. The first commercial PHA was lunched by ICI under the tradename Biopol® in early 1980 [3]. Unfortunately, PHA unable to compete in the plastic market because of their higher cost compare with a petroleum-based plastic, the average cost of PHA is 6 USD/kg whereas petroleum-based plastic is only 1 USD/kg [4]. Two bottlenecks in the PHA production are carbon source price and the recovery process [4].

Novosphingobium sp. THA_AIK7 is a gram-negative bacteria isolated from biodiesel-contaminated wastewater [5]. *Novosphingobium* sp. THA_AIK7 can produce PHA from a low-price carbon source, crude glycerol waste from biodiesel process, and $(NH_4)_2SO_4$ up to 45% of cell dry weight in small scale culture. PHA biosynthesis by *Novosphingobium* sp. THA_AIK7 was the first report of endotoxin-free PHA produced from gram-negative bacteria, as the lack of lipopolysaccharide (LPS) in their outer membrane [5]. Therefore, the polymer derived from *Novosphingobium* sp. THA_AIK7 could be the alternative choice for biomedical application.

In polymer production or synthesis the use of biological processes, many factors must be taken into account that will affect the type and properties of the polymer produced because it has a complex synthesis mechanism [6]. PHA is synthesized in the form of granules within the cell. Under nutrient imbalance conditions, such as a lack of nitrogen, phosphorus or oxygen, and there should be more than enough carbon sources to produce energy [7]. For optimal conditions for PHA synthesis, the most important factors are temperature, time, pH, and nutrients, of which the important nutrients are carbon sources,

nitrogen sources, and phosphorus sources [6]. In PHA research field, different type and concentration of nitrogen, carbon and phosphorus sources has been investigated to achieve the highest PHA productivity. *Novosphingobium* sp. THA_AIK7 was firstly isolated from biodiesel-contaminated wastewater using crude glycerol, a biodiesel by-product, as carbon source. *Novosphingobium* sp. THA_AIK7 could accumulate PHBV containing up to 9 mol% of HV monomer from crude glycerol plus monosodium glutamate (MSG). Biomass yields from small scale culture were about 3-5 g/L. The PHA yields recovered from bacterial cell using silica gel [8], were vary in the range 40-50% cell dried weight. Increasing the efficiency of biomass and polymer production yield, it is necessary to optimize the nutrient source and recovery process. Moreover, the nutrient source is the main effected to polymer composition and consequently affect the application of polymer.

In our research, we are attempting to apply PHA into medical related research field because of the production cost of PHA are still high and cannot replace conventional plastic. The study of medical research related to animal cell culture when scaling up in the bioreactor culture required microcarriers in the adhesion of cells to increase the area for cell adhesion [9]. Two types of materials are used in the manufacture of microcarriers, synthetic polymers such as polystyrene, polyacrylamide polyhydroxyethylmethacrylate and polyurethane, and biopolymers such as alginate, dextran, collagen, PHA, and PLA [10]. The high-priced of microcarrier, for example, 100 g of Sigma-Solohill microcarrier beads (collagen coated) cost 515 SGD dollar, is obstructed the research work.

In this research, we aim to increase the PHA accumulation in *Novosphingobium* sp. THA_AIK7 by optimizing carbon, nitrogen, and phosphorus source. The extraction condition by silica gel will be investigated to increase the PHA yield. The emulsion technique (water-in-oil-in-water) will be studied to fabricate microcarrier using PHA-based material. The dynamic cell culture will be tried out on porous fabricated-microcarrier.

1.2 Purpose of the Study

1.2.1 To investigate an appropriate carbon, nitrogen, and phosphorus source for PHA production from *Novosphingobium* sp. THA_AIK7.

1.2.2 To optimize the condition of PHA recovery from *Novosphingobium* sp. THA_AIK7 using silica gel.

1.2.3 To study the fabrication process of microcarriers from PHA by emulsion technique.

1.2.4 To study the use of microcarriers in dynamic animal cell culture.

1.3 Scope of Thesis

The scope of this research is to investigate an appropriate carbon, nitrogen, and phosphorus source for PHA production from *Novosphingobium* sp. THA_AIK7. The extraction condition of PHA using silica gel will be also investigated. Microcarrier fabrication by emulsion technique (water-in-oil-in-water) using PHA to produce microcarriers will be studied. The feasibility of using microcarrier for cell adhesion and proliferation of Vero and L929 cell in dynamic culture condition will be investigated. Cytotoxicity of porous microcarrier to Vero and L929 cell line by MTT assay will be done. The structural characteristics of the fabricated porous microcarriers will be examined by scanning electron microscope. The average diameter and pore sizes of the fabricated porous microcarriers will be calculated from the SEM images using Image J software.

1.4 Expectations of Thesis

In this research, the researcher expectations are the able to optimize the production, extraction, and fabrication of PHA to produce porous microcarriers that can be used for adhesion and proliferation of culture cells in dynamic condition.

CHAPTER 2
REVIEWS OF THE LITERATURE

2.1 Polyhydoxyalkanoates (PHA)

Plastic materials have become an integral part of contemporary life and are increasingly used due to their durability, simplicity of molding, and resistance to biodegradation [11].

Plastic produced from conventional fossil fuels are also used in every aspect of life because of their unique properties that can be processed into specialized products that are usable and durable [12]. Bioplastics are materials that can be biodegraded by microorganisms such as fungi and bacteria. Polyhydroxyalkanoates (PHA) are one of the most famous bioplastics. PHA is recognized as a fully biosynthetic substance that produces zero toxic waste and is completely recyclable as organic waste [13].

PHA intracellular polyester naturally produced by a variety of bacterial species [14]. Under nutrient-limited conditions with a large carbon source, bacteria store PHA as carbon and energy reserves. More than 150 different monomers can be combined to form PHA polymer chains, making them a diverse polyester family [3]. PHA is normally non-toxic, biodegradable, biocompatible, soluble in chloroform and other chlorinated solvents but insoluble in water. The melting and transition temperatures range from 40 to 180°C, contingent upon the chemical composition and length of the chain. However, these characteristics vary widely depending on the type, content, and molecular weight of PHA. Modifying the chemical microstructure of these polymers can be considered a powerful tool to tune their mechanical and thermal properties, thus reaching materials suitable for a wide range of applications that may replace conventional plastics [15].

PHAs have biodegradability, biocompatibility, immunological inertness, and degradation in human tissue making them suitable for various medical and pharmaceutical uses [16]. PHAs have been researched for various medical applications, including orthopaedics, urology, heart valves, wound care, and medication delivery [17].

2.1.1 Structure of PHA granules

PHA can be attributed to its structural and biophysical properties related to the specific method of storing PHA chains within cells. Bioaccumulating PHA chains are stored in the form of granules [18].

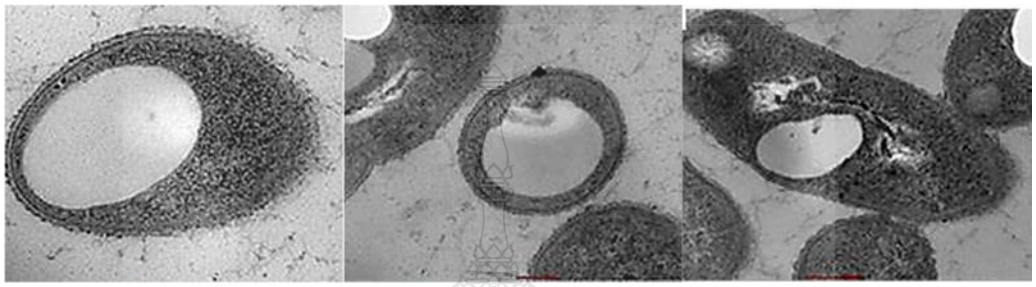

Figure 2.1 PHA granules in PHA-producing cells of the *Novosphingobium* sp. THA_AIK7

Source: Teeka *et al*. (2012) [5].

2.1.2 Chemical structure of PHAs polymer

The amount of carbons in the monomeric subunits of these polymers typically divides them into three categories [19]. PHA polymers with a short chain length (scl-PHA) consist of monomers with three to five carbon atoms, whereas those with a medium chain length (mcl-PHA) consist of monomers with six to fourteen carbon atoms [20].

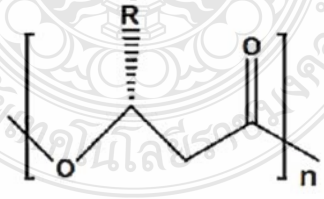

R = Functional alkyl group

n = Repetitions of the monomer

Figure 2.2 PHA molecule general structure

Source: Tan *et al*. (2014) [19].

Table 2.1 PHA polymer types and chemical structures

	Alkyl "R" group	N^0 Carbon Atoms	PHA polymer
Short-chain-length	CH_3	C_4	Poly(3-hydroxybutyrate)
PHAs (Scl-PHA)	CH_2-CH_3	C_5	Poly(3-hydroxyvalerate)
Medium-chain-length	$(CH_2)_2$-CH_3	C_6	Poly(3-hydroxyhexanoate)
PHAs (Scl-PHA)	$(CH_2)_3$-CH_3	C_7	Poly(3-hydroxyheptanoate)
	$(CH_2)_4$-CH_3	C_8	Poly(3-hydroxyoctanoate)
	$(CH_2)_5$-CH_3	C_9	Poly(3-hydroxynonanoate)
	$(CH_2)_6$-CH_3	C_{10}	Poly(3-hydroxydecanoate)
	$(CH_2)_7$-CH_3	C_{11}	Poly(3-hydroxyundecanoate)
	$(CH_2)_8$-CH_3	C_{12}	Poly(3-hydroxydodecanoate)
	$(CH_2)_9$-CH_3	C_{13}	Poly(3-hydroxytridecanoate)
	$(CH_2)_{10}$-CH_3	C_{14}	Poly(3-hydroxytetradecanoate)

Source: Tan *et al*. (2014) and Peregrina *et al*. (2021) [19, 21].

PHAs are separated into two groups: heteropolyesters, which can be further divided into copolyesters and terpolyesters, and homopolyesters, which have only one kind of monomer [22, 23]. The most popular homopolymer PHA is known as polyhydroxybutyrate (PHB) [24, 25]. PHB mechanical qualities are similar to those of traditional fossil-based plastics like polypropylene or polyethylene [20, 26], and it is gaining popularity for use in medical applications where product purity and chemical composition are essential [27]. Among the applications include wound care, medication delivery, orthopedic, urological, and cardiovascular devices, as well as tissue engineering. [28, 29]. Numerous bacterial species such as *Pseudomonads*, *Bacillus* sp., *Escherichia* coli, and *Novosphingobium* sp., have been examined for the production of mcl and lcl-PHA able to be generated from different substrates [30, 31].

2.1.3 Application of PHA

Since PHA is biocompatible and degradable, manufacturing is meant to replace synthetic, non-biodegradable polymers in various applications, packaging, agriculture, leisure, and medical and biomedical fields [32]. Potential applications of PHAs in medical industries are shown in Table 2.2

Table 2.2 PHAs and their derivatives in medical industries

Bioproducts	Microorganism	Applications	References
PHA	*Pseudomonas fluorescens*	Drug delivery, protein microarray, protein purification, antibody immobilization in clinical diagnostics	[33]
PHBV	*Ralstonia eutropha* B5785	Suture	[34]
Poly-3-hydroxybutyrate, Poly4-hydroxybutyrate	*Cupriavidus eutrophus* B-10646	Elastic nonwoven membranes-helps in reducing inflammation, enhancing angiogenic properties of skin, facilitate wound healing capacity	[35]
3HB	*Escherichia coli*	Immobilized cell factories for biocatalysis and bio-transformation, Chaperone protein levels	[36]
PHB-Hydroxyapatite composite	*Ralstonia eutropha* B5786	Bone regeneration	[35]
PHB	Biomer and Roth	Scaffolds for tissue engineering	[37]

2.2 *Novosphingobium* sp. THA_AIK7

Novosphingobium sp. THA_AIK7 is a gram-negative bacterium that was found in wastewater contaminated with biodiesel [5]. can produce PHAs from a low-price carbon source as crude glycerol waste from the biodiesel process. PHA biosynthesis by *Novosphingobium* sp. THA_AIK7 was the first report of endotoxin-free PHAs produced from gram-negative bacteria that lack lipopolysaccharide (LPS) in their outer membrane [5]. Therefore, polymers derived from *Novosphingobium* sp. THA_AIK7 showed promise as an alternative choice for biomedical applications [5]. Figure 2.3 shown Sudan black B staining of the THA_AIK7 isolate exhibiting a black fraction of lipid storage granules under a light microscope.

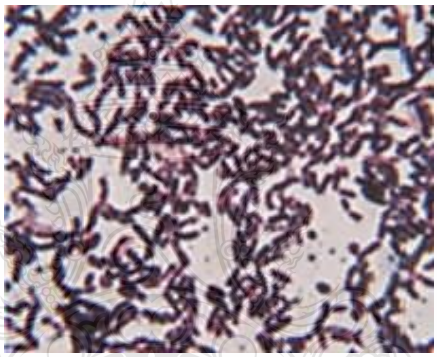

Figure 2.3 Sudan black B staining of the *Novosphingobium* sp. THA_AIK7
Source: Teeka *et al*. (2012) [5].

2.3 Effect of nutrient on PHA production

Complete nutrient depletion procedures are typically two-stage fed-batch processes, with PHA buildup mostly happening in the depleted stage [38, 39, 40]. The growth-limiting factor is usually a critical nutrient usually N, but all other nutrients are continually supplied. This is accomplished by either reducing the amount of nitrogen fed or modifying the feed's C to N ratio [41]. Because PHA synthesis continues unabated, rest biomass, or biomass other than PHA, grows more slowly than PHA does. This leads to an increasing PHA content, which is frequently the outcome of nutritional deficiency or constraint [42].

In polymer production or synthesis the use of biological processes, many factors must be taken into account that will affect the type and properties of the polymer produced because it has a complex synthesis mechanism [43]. For optimal conditions for PHA synthesis, the most important factors are temperature, time, pH, and nutrients, of which the important nutrients are carbon sources, nitrogen sources, and phosphorus sources [6].

2.3.1 Carbon sources

Carbon sources are the main constituents in the microbial culture medium. Microorganisms will use carbon sources to generate energy and PHA produce such as wheat flour, tapioca starch, glucose, sucrose, and molasses [43].

2.3.2 Nitrogen sources

Different microorganisms are capable of using different nitrogen source compounds some species can grow in inorganic compounds Some species grow in organic compounds [43].

2.3.3 Phosphorus sources

It is a catalyst for energy generation and transfer for microorganisms [43].

Design and implementation of effective bioprocess techniques to enhance the overall process kinetics can significantly reduce PHA production cost, leading to higher polymer concentrations and productivity [44, 45]. Providing optimal levels of carbon supply and limited nitrogen availability in the culture medium during fermentation is one of the most crucial fermentation conditions for improving PHB production [46]. However, high substrate concentrations may also impede microbial growth and impact total biomass and PHA generation rates [47]. Therefore, a thorough grasp of PHA generation kinetics is crucial when developing fermentation strategies that maintain appropriate substrate concentrations to maximize PHA accumulation [45, 48].

Table 2.3 Polyhydroxyalkanoates (PHAs) production by bacteria

Microorganism	Substrate	Types of PHA	Biomass (g/L)	PHA (g/L)	PHA Content (%)	References
B. sacchari IPT101	Ensiled grass press	mcl-PHA	44.5	13.8	35	[49]
Cupriavidus necator DZM 545	Glucose	PHB	164	125	76.2	[50]
C. necator H16	Glucose	PHB	148	113	76	[51]
C. necator H16	Palm olein	PHB	161	109	68	[52]
C. necator DSM 4058	Crude glycerol	PHB	28.86	24.75	85.76	[53]
Escherichia coli(genetically modified)	Sucrose	PHB	9.84	3.76	38.21	[54]
P. putida LS46	Octanoic acid	mcl-PHA	28.9	17.7	60.6	[55]
Paracoccus sp. LL1	Glucose	PHBV	113	43.9	38.8	[56]
Paracoccus sp. LL1	Corn stover hydrolysate	PHB	14.8	9.71	72.4	[57]
Paracoccus sp. LL1	Brown algae hydrolysate	PHBV	13.46	4.98	37	[58]

Source: Moungprayoon *et al*. (2022) [59].

2.4 Recovery of PHA

PHA recovery usually begins after cell separation from the growth medium at the end of the high cell density culture process. The successful recovery of intracellular biopolymers depends on efficient cell shell rupture and subsequent purification processes. Additionally, successful processes must be broadly applicable and in the case of biological processes, must also be tightly controlled at high cell densities. To make cell disruption easier, pretreatment steps may be applied first to the bacterial biomass [60]. In Table 2.4 all methods are summarized and the advantages and disadvantages of PHA recovery

Table 2.4 Advantages and disadvantages of PHA recovery methods

Method	Advantages	Disadvantages
Solvent extraction	high product purity, no degradation of the polymer, low endotoxin content of PHA extracted from Gram negative bacteria	with most solvents only applicable to small scale, often dried cells required, economically not feasible, hazardous to human beings and the environment, most suitable for lab scale
Disruption by sodium hypochlorite	high product purity, no drying of cells necessary, applicable to large scale, applicable to environmental samples	digestion of the cell matter strongly exothermic, hypochlorite may also digest the polymer, thereby reducing the molecular weight
Disruption by surfactants	PHA can be recovered directly from the culture broth, limited degradation of the polymer	high costs, SDS is difficult to recover and to remove from the isolated polymer
Disruption by chelate hydrogen peroxide treatment	high product purity	depending on the conditions, degradation of the polymer may occur with concomitant reduction of molecular weight
Disruption by dissolution of non-PHA cell mass by acids	inexpensive and ecologically friendly, high yield and purity of PHA	acids may degrade PHA, leading to a reduced molecular weight
Enzymatic cell disruption	high recovery rate and purity of the polymer, mild operating conditions	high costs for enzymes

Table 2.4 Advantages and disadvantages of PHA recovery methods (Continued)

Method	Advantages	Disadvantages
Disruption by high pressure homogenization	good performance at high biomass concentrations, applicable for large scale treatment	poor disruption at low biomass concentrations
Disruption by ultrasonication	combination with other extraction methods leads to high purity of the product	difficult to apply to large scale
Supercritical fluids	low-cost chemical treatment with moderate operating conditions, nonflammable, low toxicity and reactivity	requires strict process parameters, further chemicals needed for a high degree of disruption
Dissolved-air flotation	no chemicals necessary	consecutive batch flotation steps required
Spontaneous release of PHA granules	no chemicals necessary	genetically engineered producing strains required, not all cells may secrete PHA granules

Source: Madkour *et al*. (2013) and Pérez Rivero *et al*. (2019) [60, 61].

2.5 Microcarrier

Biomaterial scaffolds that have been transformed into microcarriers have been thoroughly investigated in the field of tissue engineering and provide numerous advantages over traditional static scaffolds [62]. Microspherical scaffolds known as microcarriers have biofunctional properties that enable them to be used in cell culture, proliferation, and transportation [63]. Microcarriers are a novel type of scaffold used in tissue engineering that have several advantages over other scaffolding materials such as hydrogels, films, and bulk scaffolds. These advantages include the ability to load a sufficient number of cells, maintain the phenotype of the cells during differentiation, and

make it easier to regulate and monitor the environments in which the cells are cultured [64].

Two types of materials are utilized as microcarriers: natural and synthetic polymers. Most synthetic polymers used to make early microcarriers included polystyrene, polyacrylamide, polyurethane foam, polyhydroxyethylmethacrylate, and glucose. Synthetic polymer microcarriers had good mechanical and repeatability qualities but lacked cell recognition sites, which hindered cell attachment and growth [65]. Because natural polymers, such as gelatin, collagen, cellulose, and dextran, are readily available, biocompatible, and reasonably priced, they are now the preferred material for subsequent innovations of microcarriers [66, 67].

2.6 Types of microcarrier

Microcarriers enable the amplification of cells by offering a vast surface area for cell development during proliferation in dynamic cultures [68]. The dynamic system provides improved gas exchange and nutrition intake. [69]. Therefore, choosing the right microcarriers is essential since it will directly affect cell growth.

Microcarriers have 3 types: non-porous, microporous, and macroporous. Depending on the porosity of the microcarrier, cells adhere in different ways.

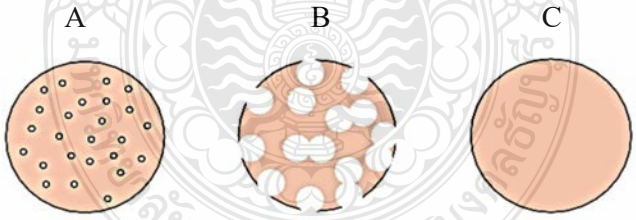

A = Microporous microcarrier

B = Microporous microcarrier

C = Non-porous microcarrier

Figure 2.4 Microcarrier types according to porosity

Source: Koh *et al*. (2020) [70].

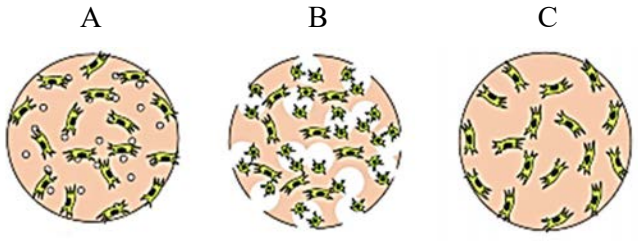

A = Microporous microcarrier

B = Macroporous microcarrier

C = Non-porous microcarrier

Figure 2.5 MSC attachment on microcarriers

Source: Koh *et al*. (2020) [70].

Generally, cells adhere to the non-porous and microporous microcarrier surfaces, while microporous microcarrier has bigger gaps that enable cells to adhere to the interior of the microcarrier [70].

Table 2.5 Examples of microcarriers that are sold commercially

Name	Type	Diameter (μm)	Density (g/mL)	Matrix and surface modifications	Properties and applications	Refs.
Cytodex 1	Solid	190 ± 58	1.03	Dextran matrix with positively-charged diethylaminoethyl groups	Substrates for the propagation of articular bovine chondrocytes	[71]
Cytodex 2	Solid	135–200	1.04	Dextran matrix with N,N,N-trimethyl-2-hydroxyaminopropyl groups	High biocompatibility and injectable for cartilage regeneration	[72]
Cytodex 3	Solid	175 ± 36	1.04	Dextran beads coated with denatured porcine-skin collagen	Natural microcarrier that permits prolonged and rapid cell growth	[73]

Table 2.5 Examples of microcarriers that are sold commercially (Continued)

Name	Type	Diameter (μm)	Density (g/mL)	Matrix and surface modifications	Properties and applications	Refs.
Hillex II-170	Solid	170 ± 10	1.12	Polystyrene with treated surface	Use in cell culture systems for bioreactor scale up	[74, 75]
ProNectin ® F	Solid	169 ± 44	1.02	Polystyrene with Recombinant proteins	Shaped 3D cell carrier for 3D culture analysis	[76]
FACT III	Solid	169 ± 44	1.02	Charged polystyrene and collagen coated	Cell expansion	[77]
CGEN 102-L	Solid	169 ± 44	1.02	Polystyrene coated with Type I porcine collagen	Good biocompatibility, for tissue-healing processes	[74]
Cytopore 1, 2	Macro porous	240 ± 40	1.03	Cross-linked cellulose with positively-charged diethylaminoethyl groups	Suitable for stirred-tank cultures	[71]
Cultispher G, S and GL	Macro porous	255 ± 125	1.04	Cross-linked Type I porcine collagen	Suitable for all types of cultures	[78]

2.7 Properties of porous microcarriers

In tissue engineering, porous cell microcarriers' bulk and surface characteristics are especially important. Generally speaking, the interaction between a biomaterial and a cell primarily, attachment, development, and differentiation determines the effectiveness of tissue engineering [79]. In addition, the microcarriers should have characteristics like large specific surface area, high porosity, injectable particle size distribution, suitable density, and interconnected open pore structures to improve the quality of regenerated tissues in vivo, and number of cells loaded [80].

Important characteristics of microcarriers to take into account include cytocompatibility and biocompatibility. Microcarriers roles include delivering seeded cells for tissue regeneration or tissue defect repair in the body, as well as serving as a place for cell adhesion, proliferation, and functional differentiation [75]. Microcarriers should therefore have high levels of biocompatibility and cytocompatibility. Materials that are biocompatible and cytocompatibility help to increase the survival rate of loaded cells and reduce the host reaction brought on by the implantation of microcarriers [81]. Degradation and toxicity, charge, hydrophobic–hydrophilic balance, and surface finish (smooth, rough, and surface porosity) are some of the factors that affect cytocompatibility and biocompatibility [82]. Therefore, a biomaterial's biocompatibility increases with its ability to replicate the tissue microenvironment [83].

2.8 Fabrication technique of microcarriers

The application-related characteristics, such as the average size of microcarriers, the physical and chemical properties of biomaterials, and the use of cultivated cells, influence the choice of microcarrier preparation processes. To date polymer-based microcarriers can now be prepared using a variety of methods, most commonly involving emulsion-solidification, extrusion, spray-drying, and their combinations [83].

2.8.1 Emulsion-solidification technique

The most popular method for creating polymer-based microcarriers is the emulsion-solidification process, which works best with porogens such as water, gelatin, sodium bicarbonate, ammonium bicarbonate, and sodium chloride [84]. The polymer is coupled with porogens to create emulsions of W/O (water-in-oil), O/W (oil-in-water), $W_1/O/W_2$ (water-in-oil-in-water), or O/W/O (oil-in-water-in-oil), with the porogen in the internal dispersed phase. Various solvent removal methods are employed, contingent on the characteristics of the solvent, such as evaporation, diffusion, or extraction. The microcarriers' porous structure is achieved by eliminating the porogen using gas-foaming, filtration, or alternative methods based on the porogen characteristics [85, 86].

2.8.2 Extrusion-solidification technique

The process of extrusion-solidification is frequently used to prepare microparticles. Like emulsion-solidification, it often requires solidification after

extrusion [87]. To facilitate solidification, a hydrophilic polymeric solution is first put in a syringe tube and then injected with a needle into a container containing a solidifying agent (polyvalent ions, for example). The needle diameter, flow rate, viscosity of the solution, injection height, and concentration of the polymer primarily determine the extrusion-solidification technique's microsphere size [88].

2.8.3 Spray-solidification technique

Spray drying is a popular method for implementing the spray-solidification process. This method creates microcarriers by spraying a natural or synthetic polymer solution in an inert gas, such as nitrogen, to facilitate splitting, additional drying, and solidification [89]. Polymer concentration, nozzle diameter, gas temperature, and spray flow rate are just a few variables that can alter the size of polymer-based microcarriers made with this method. This allows for the fabrication of microcarriers with diameters ranging from 10 μm to 3 mm, depending on the adjusted manufacturing parameters. The benefits of spray-drying microcarriers are distinct and include a small particle size distribution, low adhesion, easy continuous processing, and high reproducibility [90].

2.9 Vero cell

Product category: Animal cells

Organism**:** *Cercopithecus aethiops*

Morphology**:** epithelial

Tissue: kidney

Applications: 3D cell culture, high-throughput screening, industrial biotechnology, media testing, and toxicology

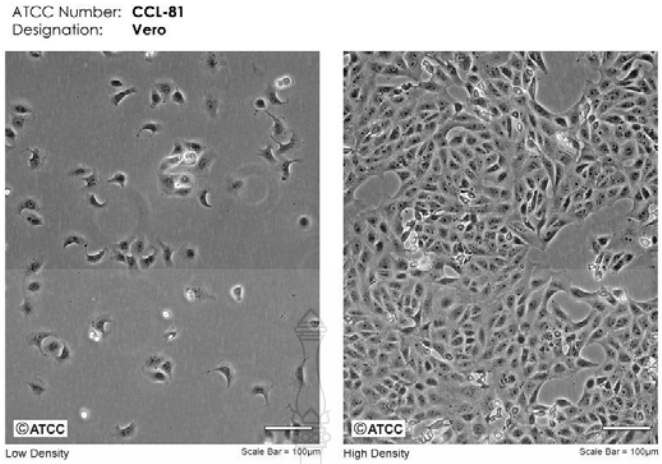

Figure 2.6 Vero cell

Source: Vero | ATCC [91].

2.10 L929 cell

Product category: Animal cells

Organism**:** *Mus musculus*, mouse

Morphology**:** fibroblast

Tissue: Subcutaneous connective tissue; Adipose; Areolar

Applications: 3D cell culture

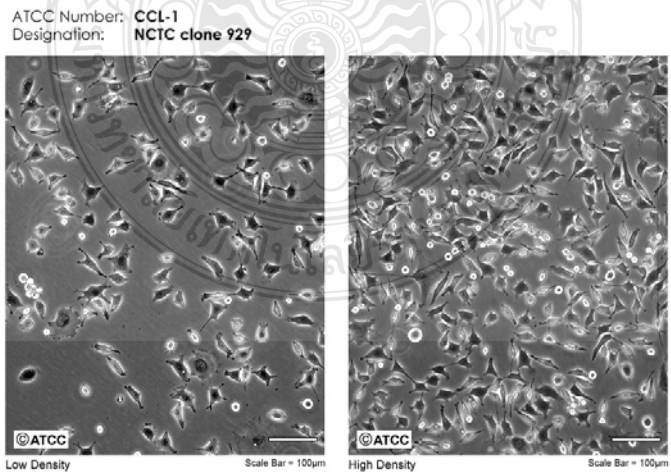

Figure 2.7 L929 cell

Source: NCTC clone 929 [L cell, L-929, derivative of Strain L] - CCL-1 ATTC [92]

2.11 Reviews of the literature

Teeka *et al.* [93] studied the impact of different nitrogen and carbon sources on *Novosphingobium* sp. THA_AIK7 growth and PHA synthesis. The was cultured on Mineral Salt Medium (MSM) supplemented with four distinct nitrogen and carbon sources (urea, ammonium sulfate, ammonium chloride, and monosodium glutamate (MSG)): molasses, starch hydrolysate, glucose, and crude glycerol. It was discovered that the optimal source for PHA production was crude glycerol combined with MSG, which resulted in a flexible and white PHA-casted film. After 96 h, under these conditions, the PHA concentration, PHA content, and $Y_{p/s}$ were found to be 0.407 g/L, 14.59% of dry cell weight, and 0.298 g PHA/g crude glycerol, respectively.

Chung *et al.* [94] studied the Usage of PLGA, by using the method of gas foaming was used to create biodegradable injectable porous microcarriers in a $W_1/O/W_2$ double emulsion. Highly porous injectable microcarriers with an average pore diameter of about 29 μm and a mean size of around 175 μm. While retaining their distinct phenotypes, chondrocytes cultivated on porous microcarriers proliferated more than those in nonporous microcarriers or monolayer cultures. Different primary cells for tissue regeneration can be grown and delivered using biodegradable porous microcarriers.

Wei *et al.* [95] studied the suspension culturing system's mammalian cell behaviours are compared with biopolyester PHBVHHx microspheres. based on solid microspheres (SMSs), hollow microspheres (HMSs), and porous microspheres (PMS) containing 3-hydroxybutyrate (HB), 3-hydroxyvalerate (HV), and 3-hydroxyhexanoate (HHx) in a microbial terpolyester PHBVHHx. PMSs have pore widths of 10 to 60 μm and diameters that range from 330 to 400 μm. In comparison to PHBVHHx made by the conventional solvent evaporation process, the pores inside the PMSs were found to be well linked, yielding the highest water uptake ratio. PMS demonstrated significantly greater cell adhesion and proliferation after a 6-day inoculation with human osteoblast-like cells. Compared to highly porous PMSs, less porous SMSs or HMSs were shown to have a higher frequency of dead or apoptotic cells. Thus, it can be said that porous PHBVHHx microspheres with bigger open pores on the surface and interconnected inside pores can act as a scaffold or carrier that promotes greater and better cell growth for injectable applications or just general cell growth.

Kim *et al*. [96] studied Injectable scaffold microcarriers for cell distribution were created using highly porous, biodegradable polymeric microspheres. The microspheres were created using a modified double emulsion solvent evaporation process using water, oil, and water ($W_1/O/W_2$). Ammonium bicarbonate, an effervescent salt, was added to the primary W1 droplets. This caused carbon dioxide and ammonia gas bubbles to form spontaneously during the solvent evaporation process, stabilizing the primary emulsion and forming well-connected pores in the resulting microspheres. Characterization was done on the porous microspheres that were created with different gas foaming conditions. As the ammonium bicarbonate concentration increased, the surface pores grew to a diameter of 20 mm, which was sufficient for cell infiltration and seeding. These porous scaffold microspheres have the potential to be used for both injectable tissue defect delivery of the seeded cells and suspension-based cell culture.

Huang *et al*. [97] studied thermally-induced phase separation (TIPS) based on emulsion, highly porous chitosan microspheres (CSM) were created without the use of hazardous crosslinkers or chemical porogenic agents other than ice. The CSM's interconnecting pores ranged in size from 20 to 50 μm, with an average diameter of about 150 μm. Because of their exceptional biocompatibility and distinctive porous structure, the CSM was used as microcarriers to enable high-performance hepatocyte culture in three-dimensional (3D) space. Multidirectional cell-cell interactions were also observed, and cell growth occurred within the CSM's internal pores and exterior surface. Compared to 2D cell culture, the CSM microcarriers produced increased cellular activity and functionality. These CSM microcarriers are thought to offer a suitable substrate for in vitro 3D cell growth.

CHAPTER 3
MATERIALS AND METHODS

3.1 Chemicals, Apparatus and Equipment

3.1.1 Ammonium Chloride (NH_4Cl)

3.1.2 Ammonium sulfate ($(NH_4)_2SO_4$)

3.1.3 Autoclave (N-BIOTEC / NB-1080)

3.1.4 Beaker

3.1.5 Biosafety cabinet (BSC)

3.1.6 Calcium chloride dihydrate ($CaCl_2 \cdot 2H_2O$)

3.1.7 Centrifuge (SIGMA / 2-16PK)

3.1.8 Centrifuge tube

3.1.9 Chloroform ($CHCI_3$)

3.1.10 Crude glycerol

3.1.11 Culture vessels

3.1.12 di-Sodium hydroren phosphate ($Na_2HPO_4 \cdot 2H_2O$)

3.1.13 Duran bottle

3.1.14 Ferrous ammonium citrate ($C_6H_8O_7 \cdot xFe^{3+} \cdot yNH_3$)

3.1.15 Fetal bovine serum

3.1.16 Flask

3.1.17 Fructose ($C_6H_{12}O_6$)

3.1.18 Glass pipette

3.1.19 Glucose ($C_6H_{12}O_6$)

3.1.20 Glycerol ($C_3H_8O_3$)

3.1.21 Heamecytometer

3.1.22 Hot air oven (Binder)

3.1.23 Incubator and shaker

3.1.24 Lactose ($C_{12}H_{22}O_{11}$)

3.1.25 Magnesium sulfate ($MgSO_4$)

3.1.26 Maltose ($C_{12}H_{22}O_{11}$)

3.1.27 Micropipette

3.1.28 Minimum Essential Medium (MEM)

3.1.29 Mini-multi shaker

3.1.30 Monosodium glutamate (MSG) ($C_5H_8NNaO_4$)

3.1.31 MTT Cell Proliferation Assay Kit (Abcam)

3.1.32 Palm oil

3.1.33 Pipette plastic

3.1.34 Potassium Dihydrogen phosphate (KH_2PO_4)

3.1.35 Potassium nitrate (KNO_3)

3.1.36 Scanning Electron Microscope (SEM)

3.1.37 Silica

3.1.38 Sodium Nitrate ($NaNO_3$)

3.1.39 Trace element solution

3.1.39.1 Boric acid (H_3BO_3)

3.1.39.2 Cobalt (II) Chloride Hexahydrate ($CoCl_2 \cdot 6H_2O$)

3.1.39.3 Zinc sulfate heptahydrate ($ZnSO_4 \cdot 7H_2O$)

3.1.39.4 Manganese (II) Chloride Tetrahydrate ($MnCl_2 \cdot 4H_2O$)

3.1.39.5 Sodium molybdate Heptahydrate ($NaMoO_4 \cdot 7H_2O$)

3.1.39.6 Nickel (II) Chloride Hexahydrate ($NiCl_2 \cdot 6H_2O$)

3.1.39.7 Copper sulphate pentahydrate ($CuSO_4 \cdot 5H_2O$)

3.1.40 1X Trypsin (Gibco)

3.1.41 Urea (CH_4N_2O)

3.1.42 Xylose ($C_5H_{10}O_5$)

3.1.43 6-well plate (Thermo scientific)

3.1.44 96-well plate (Thermo scientific)

3.2 Animal cell and Microorganism

3.2.1 L929 cell

3.2.2 Vero cell

3.2.3 *Novosphingobium* sp. THA_AIK7

3.3 Method

3.3.1 Effect of carbon, nitrogen, and phosphorus on PHAs production

Inoculum of *Novosphingobium* sp. THA_AIK7 was cultured in nutrient broth (NB) and incubated at 30°C, 150 rpm for 24 h [5]. One liter of mineral salt medium (MSM) was used for PHA production, excluding carbon, nitrogen, and phosphorus, consisting of KH_2PO_4 1.50 g, $MgSO_4 \cdot 7H_2O$ 0.2 g, ferrous ammonium citrate 0.06 g, $CaCl_2 \cdot 2H_2O$ 0.01 g, and trace element solution 1 mL. One liter of trace element solution contained H_3BO_3 0.3 g, $CoCl_2 \cdot 6H_2O$ 0.2 g, $ZnSO_4 \cdot 7H_2O$ 0.1 g, $MnCl_2 \cdot 4H_2O$ 0.03 g, $NaMoO_4 \cdot 2H_2O$ 0.03 g, $NiCl_2 \cdot 6H_2O$ 0.02 g, and $CuSO_4 \cdot 5H_2O$ 0.01 g [98]. The initial pH of the medium was set at 7.

3.3.1.1 Optimal carbon source for PHA production

Ten percent inoculum of *Novosphingobium* sp. THA_AIK7 was added to 150 mL of MSM broth supplemented with 10 g/L of various carbon sources (glucose, glycerol, fructose, sucrose, lactose, maltose, xylose, and crude glycerol), 1 g/L of monosodium glutamate (MSG), and 6.7 g/L of $Na_2HPO_4 \cdot 7H_2O$. The culture was incubated at 30°C with an agitation rate of 150 rpm for 96 h. Samples were taken during biomass cultivation and PHA yield determination, while polymer composition and functional groups of casted film from the selected condition were analyzed by nuclear magnetic resonance (NMR) [99].

3.3.1.2 Optimal nitrogen source for PHA production

Ten percent inoculum of *Novosphingobium* sp. THA_AIK7 was added to 150 mL of MSM broth supplemented with 10 g/L of optimized carbon source, 1 g/L of various nitrogen sources ($(NH_4)_2SO_4$, NH_4Cl, urea, KNO_3, $NaNO_3$, and MSG), and 6.7 g/L of $Na_2HPO_4 \cdot 7H_2O$. The culture condition and analysis were similar to 3.3.1.1.

3.3.1.3 Optimal phosphorus source for PHA production

Ten percent inoculum of *Novosphingobium* sp. THA_AIK7 was added to 150 mL of MSM broth supplemented with 10 g/L of optimized carbon, 1 g/L of optimized nitrogen source, and 6.7 g/L of various phosphorus sources ($Na_2HPO_4 \cdot 7H_2O$, K_2HPO_4, and $(NH_4)_2HPO_4$). The culture condition and analysis were similar to 3.3.1.1.

3.3.1.4 Biomass production kinetics

The logistic model was used to describe the growth of microorganisms during culture, and the relationship between growth and stable growth. The model presented the relationship between biomass (X) and initial cell concentration (X_0), maximum cell concentration (X_{max}), and maximum specific growth rate (μ_{max}) at a specific time (t), as shown in equation (1) [100].

$$x = \frac{X_0 \exp(\mu_{max} t)}{1-\left[\left(\frac{X_0}{X_{max}}\right)(1-exp(\mu_{max} t))\right]} \quad (1)$$

3.3.1.5. PHAs production kinetics

The Gompertz model was used to describe the change in product concentration during culture for maximum product concentration (P_{max}), maximum product production rate (r_{max}), and lag time (t_L), as shown in equation (2) [100].

$$P = P_{max} \cdot exp\left[-exp\left(\frac{r_{max} \cdot \exp(1)}{P_{max}}\right)(t_L - t) + 1\right] \quad (2)$$

The logistic and Gompertz models were used to fit the experimental data using Microsoft Excel and SigmaPlot 14.0 for non-linear regression analysis. Values of the fermentation parameters, as well as the statistical indicator for coefficient of determination (R^2), were obtained directly from the software [101].

3.3.1.6 Up-scale production in 10 L bioreactor

The optimized carbon, nitrogen, and phosphorus sources from 3.3.1.1- 3.3.1.3 it is defined as a food recipe for cultivation in bioreactor 10 L, with agitation rate of 150 rpm, aeration rate 1 vvm and initial pH of 7.0. The sample will be taken to analyze biomass yield, PHA yield, glycerol, and pH of culture medium every 12 h until 168 h.

3.3.2 The statistical experimental design to optimization of extraction process using silica gel

The optimization of extraction process using silica gel performed by Box-Behnken design (BBD) experiment using the design expert version 13.0 software. The independent variable will be: Temperature (X_1), Loaded cell (X_2) and amount of Silica gel (X_3) (Table 3.1 and 3.2). The control unit does not contain silica gel. Different amount of loaded cell, in each run, will be first mixed with different amount of hot silica gel. Chloroform 25 mL and water 5 mL will be added to the mixer in glass bottle. The mixed portion will be incubated at temperature assigned in each run. After 24 h of incubation, the chloroform phase will be transfer to glass plate, evaporate, and dry at 60 ^{o}C for 24 h before weigh. The general quadratic equation to predict the optimal point is as follows (3):

$$Y = \sum_{i=1}^{N} \beta_{ii} X_i^2 + \sum_{i=1}^{N} \sum_{j>1}^{N} \beta_{ij} X_i X_j + \sum_{i=1}^{N} \beta_i X_i + \beta_0 \quad (3)$$

Where

Y is the predictive response value (Dependent variable)

X_i and X_j are the predictive response values (Independent variable)

β_0 is the Y-intercept

β_i is the single regression coefficient

β_{ii} is the regression coefficient of the quadratic equation

β_{ij} is the relative regression coefficient of the variable

Table 3.1 The experiment level of the variable for BBD

Independent Variable	Code variable	Experiment levels (code)		
		Low (-1)	Medium (0)	High (+1)
Temperature (°C)	X_1	45	50	55
Loaded cell (mg)	X_2	40	60	80
Amount of silica gel (g)	X_3	18	24	30

Table 3.2 Box-Behnken experimental design (BBD)

Run	Temperature (°C) (X_1)	Loaded cell (mg) (X_2)	Amount of silica gel (g) (X_3)
1	-1	-1	0
2	1	-1	0
3	-1	1	0
4	1	1	0
5	-1	0	-1
6	1	0	-1
7	-1	0	1
8	1	0	1
9	0	-1	-1
10	0	1	-1
11	0	-1	1
12	0	1	1
13	0	0	0
14	0	0	0
15	0	0	0
16	0	0	0
17	0	0	0

Remark: 1 (High level), 0 (Medium level), and -1 (Low level)

The optimum condition derived from quadratic equation will be performed to validate the predicted results.

3.3.3 The statistical experimental design for fabrication of microcarrier PHA by emulsion technique

The fabrication of microcarrier PHA by emulsion technique performed by Box-Behnken design (BBD) experiment using the design expert version 13.0 software. The independent variable will be: PHA (X_1), PVA (X_2), NH_5CO_3 (X_3) and Stirrer (X_4) (Table 3.3) and design a total of 29 RUN experiments as shown in Table 3.4.

Table 3.3 The experiment level of the variable for BBD

Independent Variable	Code variable	Experiment levels (code)		
		Low (-1)	Medium (0)	High (+1)
PHA (g)	X_1	0.08	0.16	0.24
PVA (%)	X_2	0.1	0.5	1
NH_5CO_3 (%)	X_3	1	4	8
Stirrer (rpm)	X_4	200	500	1000

Table 3.4 Box-Behnken experimental design (BBD)

Run	PHA (X_1)	PVA (X_2)	NH_5CO_3 (X_3)	Stirrer (X_4)
1	-1	-1	0	0
2	1	-1	0	0
3	-1	1	0	0
4	1	1	0	0
5	0	0	-1	-1
6	0	0	1	-1
7	0	0	-1	1
8	0	0	1	1
9	-1	0	0	-1
10	1	0	0	-1
11	-1	0	0	1
12	1	0	0	1
13	0	-1	-1	0
14	0	1	-1	0
15	0	-1	1	0
16	0	1	1	0
17	-1	0	-1	0
18	1	0	-1	0

Table 3.4 Box-Behnken experimental design (BBD) (Continued)

Run	PHA (X_1)	PVA (X_2)	NH_5CO_3 (X_3)	Stirrer (X_4)
19	-1	0	1	0
20	1	0	1	0
21	0	-1	0	-1
22	0	1	0	-1
23	0	-1	0	1
24	0	1	0	1
25	0	0	0	0
26	0	0	0	0
27	0	0	0	0
28	0	0	0	0
29	0	0	0	0

Remark: 1 (High level), 0 (Medium level), and -1 (Low level)

The optimum condition derived from quadratic equation will be performed to validate the predicted results.

3.3.3.1 Fabrication of microcarrier PHA by emulsion technique

Microcarriers PHA (MC-PHAs) will be prepared using a gas foaming method in a ($W_1/O/W_2$) double emulsion. 2 mL of NH_5CO_3 (X_3) aqueous solution mixed with PHA (X_1) dissolved in chloroform 8 mL, stirred at 1,000 rpm for 10 min. The resulting solution will then be poured into PVA (X_2) solution and stirred (X_4) at room temperature for 4 h to obtain microcarriers washed 3 times with distilled water and dried at 60°C. A total of 29 experimental runs were performed as per Table 3.4. The morphology and size of the fabricated microcarrier were examined under SEM [94, 102].

3.3.3.2 Cell adhesion and growth in dynamic condition

One gram per liter of Cytodex1 and MC-PHAs will be added in spinner flasks, washed with phosphate buffer saline (PBS), MC-PHAs coated with 0.1%

gelatin solution, and autoclaved at 121° C for 15 min, removal of gelatin solution and add Minimum Essential Medium (MEM) serum-free media for 30 min, then remove Minimum Essential Medium (MEM) serum-free media. Vero and L929 cells in Eagle's Minimum Essential Medium (MEM) with 10% FBS will be added into a spinner flask at cell concentration 1 x 10^7 cell/mL, incubated at 37 ° C and 5% CO_2 at 30 rpm stirring rate. Cell adhesion and growth on fabricated microcarrier will be monitored at 0, 24, 48, 72, 96, and 120 h. Samples will be stained with 1 µg/mL Hoechst 33342 dye for 10 min, washed with distilled water and then observed under a fluorescence microscope. Vero and L929 cell attachment on microcarrier will be visualized by SEM and crystal violet staining.

3.3.3.3 Cytotoxicity

Cytodex1 and MC-PHAs were added in the test tube, washed with phosphate buffer saline (PBS), MC-PHAs coated with 0.1% gelatin solution, and autoclaved at 121° C for 15 min, remove of gelatin solution and add Minimum Essential Medium (MEM) serum-free media for 30 min, add in 96 well and remove MEM serum-free media. Vero and L929 cells in MEM with 10% FBS will be added into a 96 well at cell concentration 3 x 10^3 cell/well, incubated at 37 ° C and 5% CO_2 for 3 days. After discard of old media, 50 µl of serum-free media and 50 µl of MTT reagent will be filled into each well. After 3 h of incubation at 37°C, 150 µl MTT solvent will be added and shook for 15 min. The absorbance will be read at OD 590 nm against cell culture medium. [103]. Percent of cytotoxicity will be calculated as equation below (4).

$$\% \text{ Cytotoxicity} = \left(\frac{(100\times(\text{Control-Sample}))}{\text{Control}}\right)\times 100 \quad (4)$$

Control is the absorbance of cells in media.

Sample is the absorbance of sample.

The result of cytotoxicity of fabricated microcarrier to Vero cell will be expressed as % viability as the equation below.

$$\% \text{ Viability} = 100 - \text{cytotoxicity} \quad (5)$$

3.3.4 Analysis

3.3.4.1 Biomass yield

Two milliliters of cell suspension were centrifuged at 4°C and 6797 × g for 10 min. The supernatant was discarded and the cell was washed twice with distilled water, mixed well, and centrifuged again to reseparate the cell pellet before drying at 80°C for 24 h until the weight was constant. The dried cell pellet was weighed and expressed as grams per liter of biomass.

3.3.4.2 PHA yield

PHA-accumulating cells in a 10 mL sample were harvested following the above method. Five milliliters of 5% sodium hypochlorite were added to the centrifuge tube and incubated at 37°C for 1 h. The cell debris was cleaned twice with distilled water and then transferred to a glass bottle. Each glass bottle was added with 10 mL chloroform and 5 mL distilled water and incubated at 40°C for 6 h. The chloroform phase was transferred onto a glass plate, evaporated, and dried at 60°C for 24 h. The casted film was weighed and expressed as grams per liter of PHAs [104].

3.3.4.3 Sudan Black B Staining

Sudan Black B staining was used to visualize PHA accumulation inside the bacterial cells under a compound microscope. Heat fixation of the bacterial cells was performed before Sudan Black B solution (0.3% (w/v) Sudan Black B in 70% ethanol) was dropped on the slide. After 10 min, the slide was washed with xylene and safranin was dropped for another 45 sec. Dark blue spots scattered on the slide indicated PHA stored inside the bacterial cells.

3.3.4.4 PHAs characterization by NMR

The spectrum of the polymer synthesized by *Novosphingobium* sp. THA_AIK7 was analyzed by ^{1}H nuclear magnetic resonance (NMR) [105]. A 10 mg aliquot of the sample was dissolved in 1 mL deuterochloroform ($CDCl_3$) in a glass tube by heating at 45°C, with spectra recorded at 500 MHz. determined that characteristic peaks in the NMR spectrum at 0.9 ppm (HV unit) and 1.25 ppm (HB unit) could be utilized to calculate the HV composition in the PHBV sample, as shown in equation (6).

$$\text{HV composition (\%)} = \frac{\text{Area}CH_3\text{(HV)}}{\text{Area}CH_3\text{ (HV)}+\text{Area}CH_3\text{(HB)}} \times 100\% \quad (6)$$

3.3.4.5 Glycerol residual

Dilute the sample as appropriate. Then pipette 0.5 mL of the sample into the test tube, add 0.5 mL of ethanol 95.5% (w/v), 0.6 mL of solution D, and 0.6 mL of solution C, respectively. The mixer will be immersed in a water bath at 70°C. for 1 minute, stirring manually. The sample tube will be immediately cooled in cold water to stop the reaction. The samples will be finally read in a spectrophotometer set in double beam mode at 410 nm, against a blank, and compared with the standard curve of the standard glycerol solution [106].

(1) Solution A: 1.6 M acetic acid solution

(2) Solution B: 4.0 M ammonium acetate solution

The solution A and B will be mixed in equal volumes, these solutions result in a buffer solution at pH 5.5.

(3) Solution C: 0.2 M acetyl acetone solution

Pipette 200 mL (195 mg) of acetylacetone in 5 mL of acetic acid stock solution and 5 mL of ammonium acetate stock solution. This reagent must be prepared daily.

(4) Solution D: 10 mM sodium periodate solution

Weigh 21 mg of sodium meta periodate, add 5 mL of acetic acid stock solution, swirl to dissolve the periodate first, add 5 mL ammonium acetate stock solution. This reagent must be prepared daily.

3.3.4.6 SEM

The structural characteristics of the fabricated microcarriers were examined by scanning electron microscope. The average sizes of the microcarriers and pores were calculated from the SEM images using Image J software and expressed as means ± standard deviations.

3.3.4.7 Cell adhesion on microcarriers by SEM

Samples were collected at 96 h, fixed with 2.5% glutaraldehyde in 0.1M phosphate buffer pH 7.2 for 1 h, dropped onto glass coated with Poly- L-lysine was left for 10 minutes, washed with phosphate buffer 2 times and distilled water 1 time, 3-5 minutes each time. Dehydrate with ethanol at various concentrations including 30%, 50%, 70%, 95% and 100% steps, each step was 5 minutes (at 100%, do it 3 times) and then

dried at the critical point using a critical point dryer. The microcarrier samples were placed on a stub, coated with gold, and analyzed using SEM.

3.3.4.8 Number of adherent cells on the microcarrier

The samples were stained in a solution mixed with 0.5 M citric acid + 0.1 % crystal violet + 1.5 % Triton X-100 for 24 h and the number of cells was counted with a hemacytometer.

3.3.4.9 Metabolic profile of cultured cells

Samples were collected at 0, 24, 48, 72, 96, 120, and 144 h. The cells were centrifuged and the supernatant was analyzed for glucose content using a glucose/lactate analyzer [107].

3.3.4.10 Statistical analysis

Significant differences were determined by one-way analysis of variance (ANOVA) at p-value < .05. The effect of each sample was defined by Duncan's multiple comparison test at p-value < .05 using SPSS version 15.

CHAPTER 4

RESULTS AND DISCUSSIONS

4.1 Effect of medium composition on biomass and PHA production

To increase PHAs yield, various carbon sources (10 g/L) namely glucose, glycerol, fructose, sucrose, lactose, maltose, xylose, and crude glycerol were added to the MSM with a 10% (v/v) inoculum and cultivated for 96 h at 30°C with shaking at 150 rpm. Our study revealed that carbon source tested in this study clearly affected PHAs production by *Novosphingobium* sp. THA AIK7. Maximum and minimum biomass were obtained from crude glycerol and xylose at 4.41 and 1.20 g/L, while PHAs concentration were 1.01 and 0.01 g/L, respectively (Figure 4.1(A)). Carbon assimilation is different in each species. AIK7 isolate employed waste glycerol for polymer biosynthesis better than pure glycerol [108]. Glycerol obtained in soy-based biodiesel production (CSBP) would be utilized as a substrate for bacterial growth, while free fatty acid (FFA) and fatty acid methyl esters (FAME) would be a good source for PHA synthesis [109]. Poomipuk *et al*. (2014) stated that lactose and sucrose, a disaccharide, were found to be less preferable than monosaccharides such as glucose and fructose for PHAs production. However, *Cupriavidus* sp. KKU38 could effectively utilize maltose, a disaccharide, and xylose, a monosaccharide for PHAs production [110].

Novosphingobium sp. THA_AIK7 effectively exploited $(NH_4)_2SO_4$ and MSG for growth at 3.48 and 3.46 g/L, respectively whereas urea was less suitable. This occurred because the $(NH_4)_2SO_4$ nitrogen source served as a precursor for vitamins, amino acids, and growth factors [111]. The most favorable nitrogen source for PHA production was MSG at 0.73 g/L, while urea was not appropriate for both biomass and PHA production at 1.23 and 0.04 g/L, respectively (Figure 4.1(B)). These findings showed that PHA yield was not related to growth. PHA synthesis is enhanced by environmental stresses such as nitrogen, phosphate, or oxygen limitation [112]. Optimal biomass and polymer production in *Bacillus megaterium* was recorded using NH_4Cl in 2% sugarcane molasses at 1.27 g/L and 40.10% CDM, respectively [112]. Beaulieu *et al*. (1995) investigated PHB production by *Alcaligenes eutrophus* in a synthetic 3% glucose medium supplemented with various ammonium substrates. They discovered that $(NH_4)_2SO_4$ provided optimal

growth at 25.25 g/L and PHB yield of 43 % CDW after 72 h of fermentation [113]. Quillaguamán *et al*. (2008) concluded that using MSG instead of glutamine in the medium resulted in a significant change in the final cell density of *Halomonas boliviensis*, with a DCW of 44 g/L and PHB content of 81 wt% in fed-batch culture. Similar to carbon sources, each species prefers a different nitrogen source [114].

Three sources of phosphorus salts impacted biomass and PHA production that was maximized in media containing $Na_2HPO_4 \cdot 7H_2O$ at 5.23 and 1.44 g/L, respectively (Figure 4.3(C)). However, $(NH_4)_2HPO_4$ was not suitable for biomass and polymer biosynthesis at 0.65 and 0.08 g/L, respectively. In the "No addition" treatment, the MSM contained the phosphorus source from KH_2PO_4 at 1.50 g/L. Therefore, phosphorus deficiency in the "No addition" treatment gave higher PHA accumulation than addition of $(NH_4)_2HPO_4$. Phosphorus deficiency yielded intracellular concentration of NADPH and stimulated PHA synthesis, while citrate synthase was inhibited in the TCA cycle resulting in higher PHA accumulation in cells [115]. Bustamante *et al*. (2019) found that higher concentration of $(NH_4)_2HPO_4$ together with KH_2PO_4 reduced growth and PHB yield from *Caulobacter segnis* DSM 29236, possibly due to the cytotoxic effect of ammonium on the cells [116]. PHA accumulation in mixed microbial cultures was evaluated by *Gao et al*. (2021) under various phosphorus sources [117]. They determined Na_2HPO_4 as the best phosphorus source that increased 3HB and 3HO contents by 41% and 49%, respectively. Phosphorus supplements as $Na_2HPO_4.7H_2O$ and K_2HPO_4 improved both biomass and PHA content of the AIK7 strain as appropriate forms of nutrients for the cells.

The volumetric production rates of biomass (Q_x) and volumetric production rate of PHA (Q_p) for the above treatments were calculated (Table 4.1). Crude glycerol gave the highest PHA content at 24.45% with xylose at only 0.90%. Highest Q_p was obtained from crude glycerol at 0.011 ± 0.001 g/L h, while highest Q_x was recorded from glycerol at 0.053 ± 0.006 g/L h, proving that the bacteria used glycerol for their growth. Maximum PHA content of nitrogen source was achieved from MSG at 21.32%, with the minimum from urea at 3.49%. MSG and $(NH_4)_2SO_4$ recorded the same level of Q_x at 0.036 ± 0.003 g/L h showing that the AIK7 strain used these two nitrogen sources for growth equally. Highest productivity of polymer Q_p was gained from MSG at 0.008 ± 0.001 g/L h, while $Na_2HPO_4 \cdot 7H_2O$ and $(NH_4)_2HPO_4$ gave maximum and minimum PHA contents at 27.54%

and 12.31%, respectively. Biomass and polymer productivity peaked in media containing $Na_2HPO_4 \cdot 7H_2O$ at Qx 0.073 ± 0.003 and Qp 0.015 ± 0.000 g/L h. PHA production is a complex process, with the final quality and quantity of the product yield depending on the strain, metabolic pathway involved, fermentation parameters, PHA production phase, carbon source, nitrogen source, phosphorus source, and nutrient depletion condition required for PHA synthesis [118]. Results suggested that the appropriate medium for growth and PHA production of *Novosphingobium* sp. THA_AIK7 contained crude glycerol, MSG, and $Na_2HPO_4 \cdot 7H_2O$ as carbon, nitrogen, and phosphorus sources, respectively. Variation in PHA content derived from each condition was low (0.90-27.54%) compared to the observed dark blue spots of stained PHA in Figure 4.5, possibly because the extraction process was unable to recover all the stored polymer inside the bacterial cells.

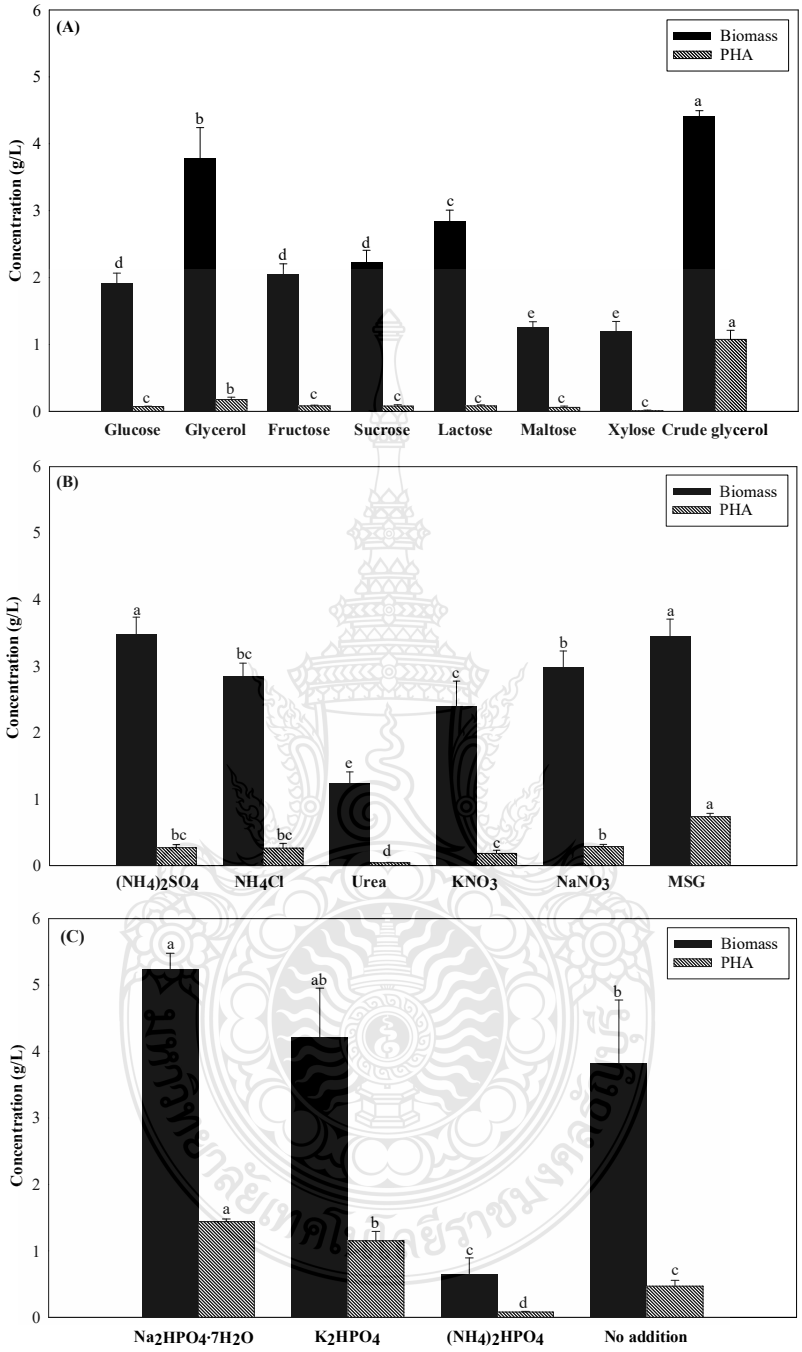

Figure 4.1 Influence of (A) carbon, (B) nitrogen, and (C) phosphorus sources on biomass production and PHA accumulation of *Novosphingobium* sp. THA_AIK7 at 96 h of cultivation. Data are represented as mean ± SD bar. The different superscripts indicate significant differences at p-value ≤ .05.

Table 4.1 Biomass and PHA production of *Novosphingobium* sp. THA_AIK7 under different conditions at 96 h of cultivation.

Condition	PHA content (%)	Q_x (g/L h)	Q_p (g/L h)
Carbon sources			
Glucose	3.87^{b}	0.020±0.002^{de}	0.001±0.000^{bc}
Glycerol	4.66^{b}	0.053±0.006^{a}	0.002±0.000^{b}
Fructose	4.04^{b}	0.021±0.002^{de}	0.001±0.000^{bc}
Sucrose	3.55^{b}	0.023±0.002^{d}	0.001±0.000^{bc}
Lactose	2.92^{bc}	0.030±0.002^{c}	0.001±0.000^{bc}
Maltose	4.77^{b}	0.017±0.001^{e}	0.001±0.000^{bc}
Xylose	0.90^{c}	0.017±0.002^{e}	0.000±0.000^{c}
Crude glycerol	24.45^{a}	0.046±0.001^{b}	0.011±0.001^{a}
Nitrogen sources			
$(NH_4)_2SO_4$	7.76^{b}	0.036±0.003^{a}	0.003±0.000^{b}
NH_4Cl	9.25^{b}	0.030±0.002^{bc}	0.003±0.001^{b}
Urea	3.49^{c}	0.017±0.002^{d}	0.000±0.000^{d}
KNO_3	7.66^{b}	0.025±0.004^{c}	0.002±0.000^{c}
$NaNO_3$	9.64^{b}	0.031±0.003^{ab}	0.003±0.000^{b}
MSG	21.32^{a}	0.036±0.003^{a}	0.008±0.001^{a}
Phosphorus sources			
$Na_2HPO_4{\cdot}7H_2O$	27.54^{a}	0.073±0.003^{a}	0.015±0.000^{a}
K_2HPO_4	27.41^{a}	0.058±0.010^{ab}	0.012±0.001^{b}
$(NH_4)_2HPO_4$	12.31^{b}	0.007±0.003^{c}	0.001±0.000^{d}
No addition	12.31^{b}	0.053±0.013^{b}	0.005±0.001^{c}

Different lowercase superscripts in the same column indicate significant differences at p-value ≤ .05.

4.2 Kinetic modeling of microbial growth and PHA production

The logistic and Gompertz models were used to simulate microbial growth and PHA production under various conditions to calculate the growth kinetics and polymer production rate [100, 101]. Non-linear regression analysis was performed using Microsoft Excel to determine the values of the cultivated parameters and the statistical indicator for

the coefficient of determination (R^2). The microbial growth kinetics and PHA production from *Novosphingobium* sp. THA_AIK7 cultivated under different carbon, nitrogen, and phosphorus sources at 0-96 h are shown in Figures 4.2-4.4, with estimated kinetics of biomass and PHA production obtained from both models summarized in Table 4.2.

The simulation curves of microbial growth by the logistic model showed that crude glycerol, glycerol, and lactose had progressively increasing prediction curves at maximum predicted biomass (X_{max}) of 4.841, 3.939, and 2.969 g/L, respectively (Table 4.2). The predicted specific growth rate (μ_{max}) was highest at 0.104 h^{-1} from fructose, showing that the AIK7 strain used fructose for growth faster than the other carbon sources. The AIK7 strain also utilized glucose, the most common carbon source for bacterial growth, faster than crude glycerol, glycerol, and lactose with predicted μ_{max} of 0.094 h^{-1}, while μ_{max} values from these three carbon sources were 0.044, 0.070, and 0.062 h^{-1}, respectively. The predicted μ_{max} was maximized from fructose and glucose but the maximum predicted X_{max} reached only 1.597 and 1.781 g/L (Table 4.2) with Q_x only 0.021 and 0.020 g/L h, respectively (Table 4.1), indicating that these two monosaccharides were easily assimilated into the cell but might not be used directly for cell growth. Statistical analysis revealed that X_{max} and μ_{max} obtained from glucose and fructose were not significantly different. The simulated curves of crude glycerol, glycerol, and lactose were close to the experimental data with R^2 0.984, 0.990, and 0.984, respectively (Figure 4.2) indicating that this model could be used to explain the growth kinetics of *Novosphingobium* sp. THA_AIK7 under these conditions.

The predicted logistic model curves of MSG, NH_4Cl, and $(NH_4)_2SO_4$ sharply increased and reached X_{max} peak at 13.500, 13.333, and 13.267 g/L, respectively (Table 4.2). Trends of the predicted lines and experimental lines of these nitrogen sources were in the same direction, with R^2 0.991, 0.986, and 0.979, respectively (Figure 4.3) showing that the logistic model could be used to predict the growth of this bacteria. The $(NH_4)_2SO_4$ gave the maximum predicted μ_{max} at 0.026 h^{-1}, while MSG reached the second highest μ_{max} at 0.022 h^{-1}, exhibiting that the AIK7 strain quickly utilized these two sources of nitrogen for biomass generation. The predicted X_{max} and μ_{max} values of urea were lowest among all sources of nitrogen at 6.667 g/L and 0.011 h^{-1} (Table 4.2), corresponding with

the lowest Q_x of 0.017 g/L h (Table 4.1) and suggesting that urea was not suitable for their growth.

The predicted biomass from $Na_2HPO_4{\cdot}7H_2O$, K_2HPO_4, and No addition increased with time. The retrieved biomass values from the model were 5.146, 4.833, and 3.900 g/L, respectively (Table 4.2). The R^2 values of 0.991, 0.940, and 0.977 from $Na_2HPO_4.7H_2O$, K_2HPO_4, and No addition revealed that the model results were similar to the experimental data (Figure 4.4). The μ_{max} of $Na_2HPO_4.7H_2O$ peaked at 0.116 h^{-1}, while the predicted X_{max} and μ_{max} of $(NH_4)_2HPO_4$ were lowest at 0.770 g/L and 0.004 h^{-1}, concurring with the lowest Q_x of 0.007 g/L h (Table 4.1) and confirming that this phosphorus source was not preferred by this bacterium. The estimated kinetic results showed that the logistic model accurately predicted microbial growth under these conditions.

The Gompertz model was chosen to simulate PHA production. Crude glycerol had a progressively increasing prediction curve, with maximum predicted PHA (P_{max}) of 1.200 g/L, while the simulation curve of xylose showed the least amount of PHA with P_{max} at 0.014 g/L. Maximum production rate (r_{max}) was obtained from crude glycerol at 0.030 g/L h, with minimum r_{max} given by xylose, glucose, fructose, and maltose at 0.002 g/L h (Table 4.2). The start time for PHA production from crude glycerol was 44.5 h, with R^2 of 0.995 (Figure 4.2). Xylose was not appropriate for supporting growth or PHA production, with P_{max}, r_{max}, and Q_p of 0.014 g/L, 0.002 g/L h, and 0.000 g/L h, respectively.

The predicted PHA from MSG steadily increased with P_{max} of 2.083 g/L, whereas urea produced the least amount with P_{max} of 0.052 g/L. Maximum and minimum production rates (r_{max}) were also obtained from MSG and urea at 0.016 and 0.001 g/L h, respectively (Table 2). The start time for PHA production of MSG was 50 h with R^2 of 0.995 (Fig. 4.3). The NH_4Cl and $(NH_4)_2SO_4$ showed support for growth, with high predicted X_{max} while the P_{max} values were 0.283 g/L and 0.343 g/L, with r_{max} 0.004 and 0.004 g/L h (Table 4.2), respectively. This result indicated that these two nitrogen sources were used for biomass generation in preference to product formation.

The predicted PHA values for $Na_2HPO_4{\cdot}7H_2O$ and K_2HPO_4 sharply increased and reached P_{max} of 3.367 g/L and 2.767 g/L, respectively. No addition and $(NH_4)_2HPO_4$

produced the lowest amount of PHA with P_{max} 0.883 and 0.387 g/L, respectively. Maximum and minimum production rates (r_{max}) were obtained from $Na_2HPO_4 \cdot 7H_2O$ and $(NH_4)_2HPO_4$ at 0.035 and 0.001 g/L h, respectively (Table 4.2). The start time for PHA production from $Na_2HPO_4 \cdot 7H_2O$ was 50 h with R^2 of 0.965 (Figure 4.4). Results indicated that $(NH_4)_2HPO_4$ was not suitable for both growth and product formation by this bacterium.

These simulation results of PHA production by the Gompertz model suggested that both the experimental and predicted data tend to go in the same direction confirming that this model explained the product formation profile of *Novosphingobium* sp. THA_AIK7. He *et al*. (2022) isolated *Novosphingobium percolationis* sp. nov. and *Novosphingobium huizhouense* sp. nov., from the leachate of a domestic waste treatment plant. They concluded that these two strains had broad carbon metabolic abilities and harbored the complete Embden-Meyerhof-Parnas pathway, citrate cycle, Entner-Doudoroff pathway, pentose phosphate pathway, and glyoxylate cycle for central carbon metabolism [119]. Koller and Obruča (2022) summarized PHA production from glycerol by various bacterial strains. They drew a metabolic pathway generating a pyruvate intermediate from glycerol uptaken into the cell via glycolysis and Entner-Doudoroff pathway [120]. This pyruvate intermediate then converted to central metabolite acetyl-CoA, a common precursor of PHA biosynthesis pathway. Free fatty acids (FFAs) and fatty acid methyl esters (FAMEs) contained in crude glycerol were other sources of PHA production via β-oxidation and fatty acid *de novo* biosynthesis [99, 109], explaining why *Novosphingobium* sp. THA_AIK7 produced more PHA from crude glycerol than from other carbon sources.

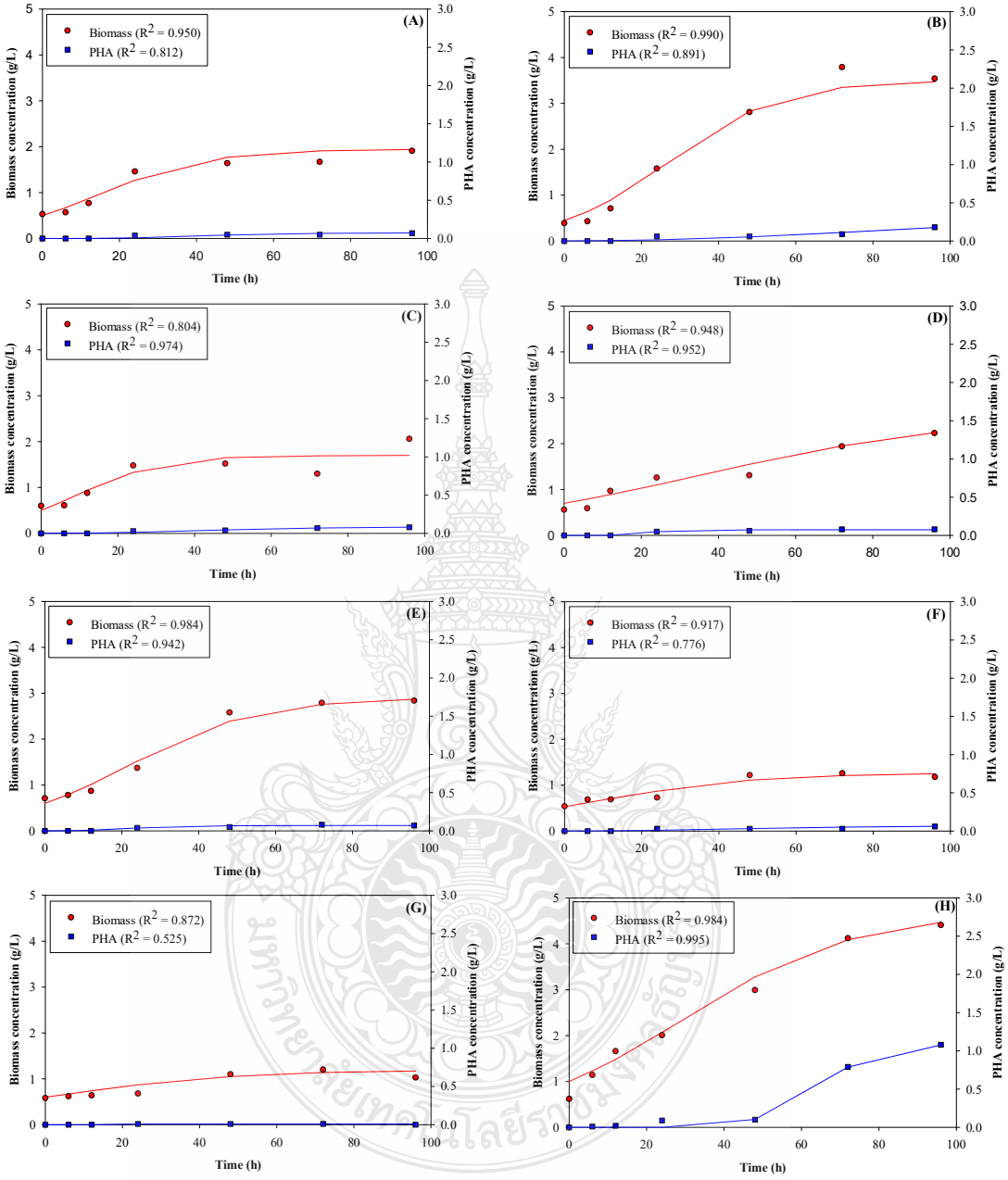

Figure 4.2 Comparison of experimental observations (symbols) and model predictions (lines) of biomass and PHA concentration of *Novosphingobium* sp. THA_AIK7 during fermentation with medium containing (A) glucose, (B) glycerol, (C) fructose, (D) sucrose, (E) lactose, (F) maltose, (G) xylose, and (H) crude glycerol.

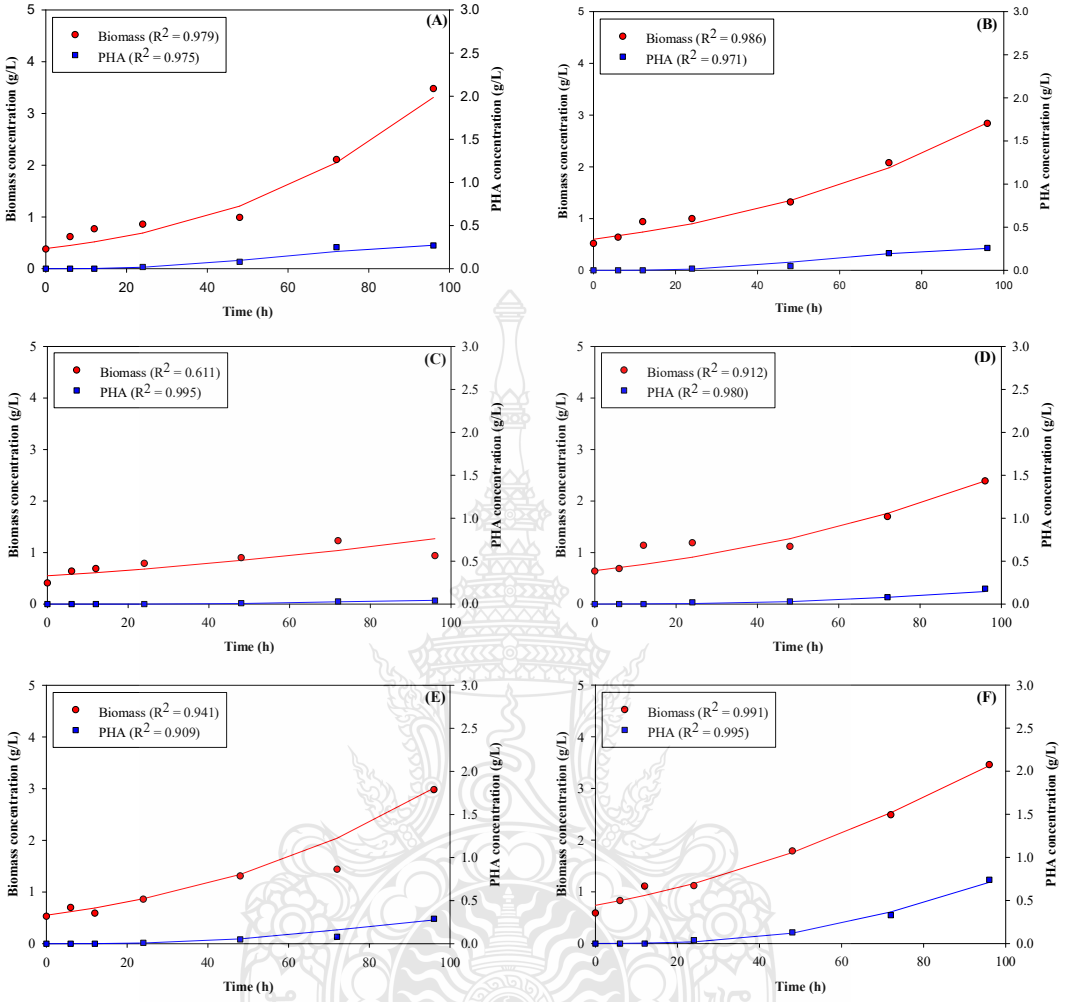

Figure 4.3 Comparison of experimental observations (symbols) and model predictions (lines) of biomass and PHA concentration of *Novosphingobium* sp. THA_AIK7 during fermentation with medium containing (A) $(NH_4)_2SO_4$, (B) NH_4Cl, (C) urea, (D) KNO_3, (E) $NaNO_3$, and (F) MSG

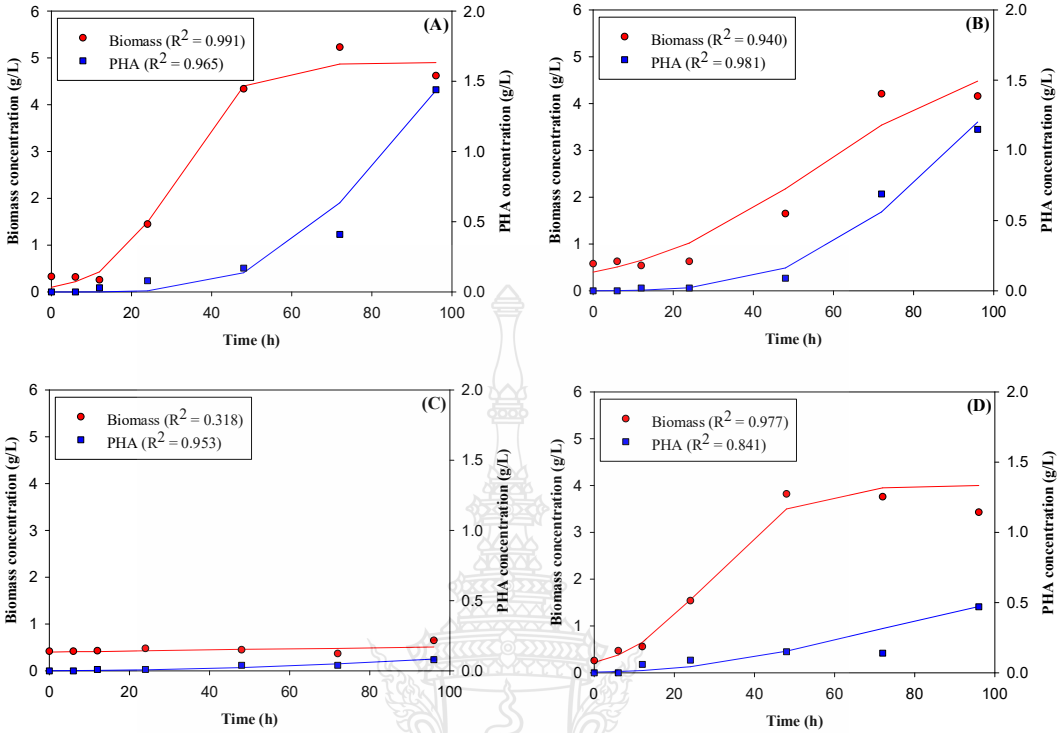

Figure 4.4 Comparison of experimental observations (symbols) and model predictions (lines) of biomass and PHA concentration of *Novosphingobium* sp. THA_AIK7 during fermentation with medium containing (A) $Na_2HPO_4 \cdot 7H_2O$, (B) K_2HPO_4, (C) $(NH_4)_2HPO_4$, and (D) No Phosphorus source addition

Table 4.2 Estimated kinetics of biomass and PHA production of *Novosphingobium* sp. THA_AIK7 under different conditions.

Condition	X_{max} (g/L)	P_{max} (g/L)	μ_{max}(h^{-1})	r_{max} (g/L h)
Carbon sources				
Glucose	1.781±0.030^{d}	0.079±0.008^{c}	0.094±0.009^{a}	0.002±0.001^{b}
Glycerol	3.939±0.467^{b}	0.400±0.100^{b}	0.070±0.013^{b}	0.003±0.001^{b}
Fructose	1.597±0.074^{de}	0.103±0.015^{c}	0.104±0.010^{a}	0.002±0.000^{b}
Sucrose	2.773±0.492^{c}	0.078±0.013^{c}	0.029±0.009^{d}	0.005±0.001^{b}
Lactose	2.969±0.119^{c}	0.083±0.015^{c}	0.062±0.009^{bc}	0.003±0.000^{b}
Maltose	1.416±0.210^{de}	0.090±0.056^{c}	0.040±0.013^{d}	0.002±0.001^{b}
Xylose	1.067±0.115^{e}	0.014±0.006^{c}	0.043±0.015^{cd}	0.002±0.002^{b}
Crude glycerol	4.841±0.439^{a}	1.200±0.200^{a}	0.044±0.006^{cd}	0.030±0.005^{a}
Nitrogen sources				
$(NH_4)_2SO_4$	13.267±1.079^{a}	0.343±0.093^{bc}	0.026±0.002^{a}	0.004±0.001^{b}
NH_4Cl	13.333±3.055^{a}	0.283±0.029^{bc}	0.019±0.002^{bc}	0.004±0.000^{bc}
Urea	6.667±0.289^{b}	0.052±0.003^{c}	0.011±0.001^{d}	0.001±0.000^{c}
KNO_3	13.200±0.346^{a}	0.450±0.278^{b}	0.017±0.001^{c}	0.004±0.001^{bc}
$NaNO_3$	11.333±1.041^{a}	0.400±0.087^{bc}	0.020±0.001^{b}	0.003±0.001^{bc}
MSG	13.500±1.732^{a}	2.083±0.333^{a}	0.022±0.002^{b}	0.016±0.004^{a}
Phosphorus sources				
$Na_2HPO_4{\cdot}7H_2O$	5.146±0.067^{a}	3.367±0.321^{a}	0.116±0.021^{a}	0.035±0.004^{a}
K_2HPO_4	4.833±0.577^{a}	2.767±1.168^{a}	0.045±0.000^{b}	0.034±0.003^{a}
$(NH_4)_2HPO_4$	0.770±0.139^{c}	0.387±0.032^{b}	0.004±0.002^{c}	0.001±0.000^{b}
No addition	3.900±0.656^{b}	0.883±0.362^{b}	0.103±0.023^{a}	0.007±0.002^{b}

Different lowercase superscripts in the same column indicate significant differences at *p*-value ≤ .05.

Preliminary identification of PHA lipid inclusions was carried out using Sudan Black B dye, which is a lipophilic dye that attaches to the ester bond in the polymeric chain of the PHB granule [121]. Dispersed dark blue spots of stained PHA observed under the microscope for oil immersion at 1000x magnification indicated that PHA occupied almost all the cell area, as shown in Figure 4.5. Results revealed that *Novosphingobium* sp. THA_AIK7 accumulated PHA inside their cells under this condition. Yadav *et al*. (2021) found that under the appropriate condition, PHA accumulation as granules inside the cells varied from 1 to 90% of cell dry weight (CDW) [122].

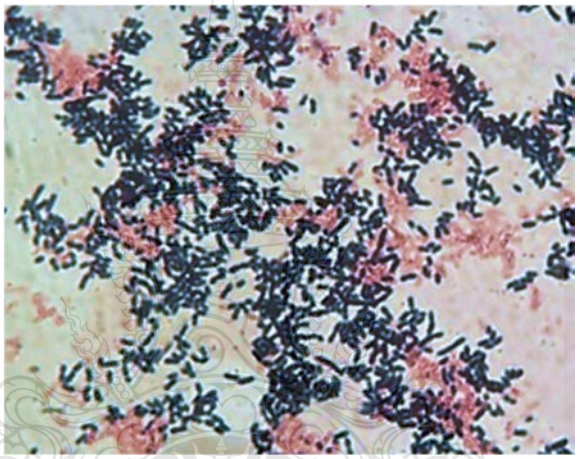

Figure 4.5 Sudan Black B staining of *Novosphingobium* sp. THA_AIK7 cultured in MSM for 96 h (magnification, 1000x).

4.3 NMR spectra of PHA derived from various conditions

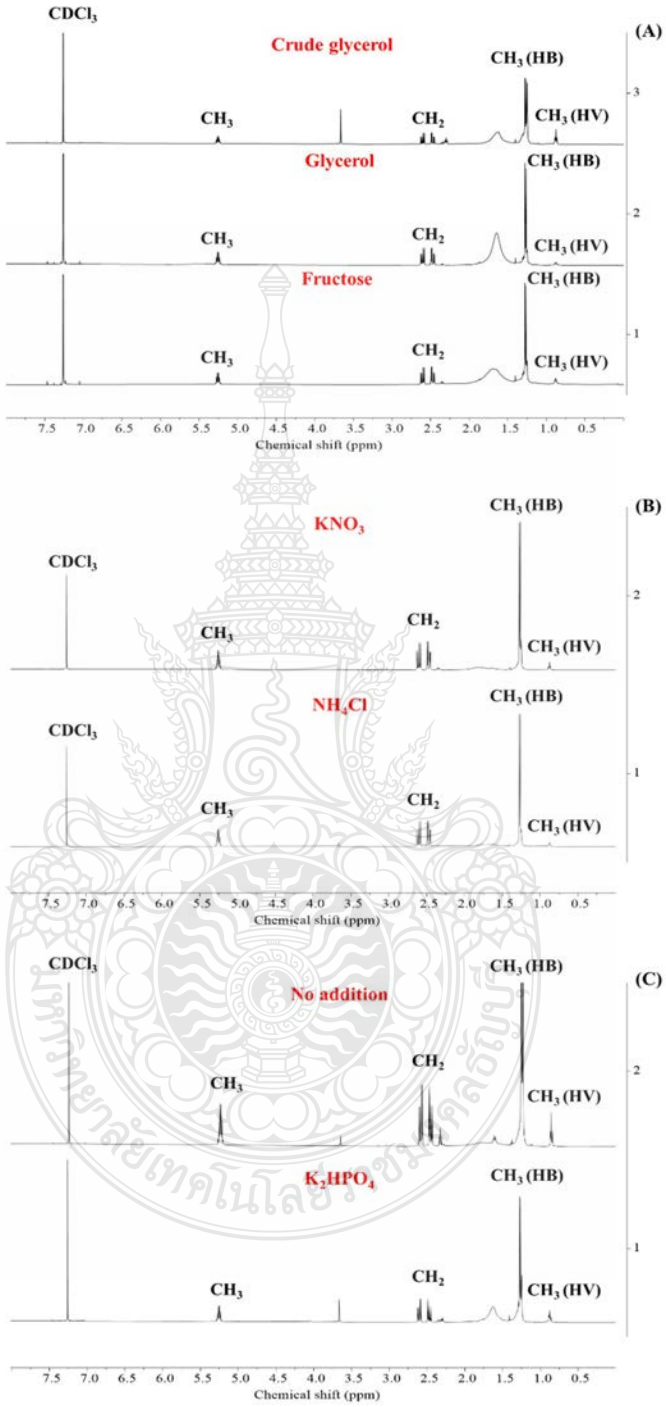

Figure 4.6 ^{1}H nuclear magnetic resonance spectra of (A) carbon, (B) nitrogen, and (C) phosphorus sources.

The extracted polymers from *Novosphingobium* sp. THA_AIK7 cultivated with different sources of carbon, nitrogen, and phosphorus were subjected to ^{1}H NMR spectrometry analysis. ^{1}H NMR peaks of each condition were detected at 0.9, 1.26, 2.6, and 5.2 ppm, as shown in Figure 4.6, corresponding to the absorption resonance of methyl (CH_3), methyl (CH_3), methylene (CH_2), and methane (CH) groups, respectively [123, 124]. The identical peaks of PHBV were designated as methyl group protons in HB and HV at 0.9 and 1.27 ppm, respectively. The detected signals resembled those from an earlier study of pure P(HB-co-HV) polymers [125, 126], proving that the extracted polymer from every condition was PHBV. The NMR spectra at 3.6 ppm revealed the presence of crude glycerol resonance [127, 128, 129], as shown in Figure 4.6(A) in crude glycerol, Figure 4.6(B) in KNO_3 and NH_4Cl, and Figure 4.6(C) in No addition and K_2HPO_4 used as medium composition. Glycerol and fructose were used as carbon sources. This peak confirmed the integration of crude glycerol into the polymer chain.

Table 4.3 Peak area and mol% of PHBV extracted polymer under various conditions

Carbon source	Nitrogen source	Phosphorus source	Peak area at 0.9 ppm	Peak area at 1.25-1.27 ppm	HV monomer (mol%)
Fructose	MSG	$Na_2HPO_4{\cdot}7H_2O$	1.59	14.06	10.16
Glycerol	MSG	$Na_2HPO_4{\cdot}7H_2O$	0.39	5.53	6.59
Crude glycerol	MSG	$Na_2HPO_4{\cdot}7H_2O$	1.61	13.23	10.85
Crude glycerol	NH_4Cl	$Na_2HPO_4{\cdot}7H_2O$	0.19	4.18	4.35
Crude glycerol	KNO_3	$Na_2HPO_4{\cdot}7H_2O$	0.27	4.81	5.32
Crude glycerol	MSG	K_2HPO_4	0.46	7.49	5.79
Crude glycerol	MSG	No addition	0.38	5.65	6.30

The peak areas of HB and HV were calculated to obtain HV mol% in each polymer extract, as shown in Table 4.3. Commercial PHBV polymer from Sigma-Aldrich contained HV units at 8% and 10% [130, 131], while PHBV produced from *Novosphingobium* sp. THA_AIK7 varied from 4.35-10.85 mol%. The highest PHBV percentage of 10.85 mol% was obtained from crude glycerol with MSG and $Na_2HPO_4.7H_2O$ in the medium formula, while the lowest percentage of 4.35 mol% was achieved from crude glycerol with NH_4Cl and $Na_2HPO_4.7H_2O$ in the medium formula. The data in Table 4.3 indicated that PHA produced from *Novosphingobium* sp. THA_AIK7 using only crude glycerol, glycerol, and fructose and the sole carbon source could be polymerized into a PHBV copolymer without addition of propionic acid or valeric acid as a 3HV precursor, suggesting that *Novosphingobium* sp. THA_AIK7 could produce a PHBV copolymer with high 3HV content from a low-priced, carbon source [128].

4.4 Up-scale production in 10 L bioreactor

The bacterial culture *Novosphingobium* sp. THA_AIK7 in a batch-bioreactor 10 L in the MSM formula using crude glycerol as the carbon source, MSG as the nitrogen source, and $Na_2HPO_4 \cdot 7H_2O$ as the phosphorus source, agitation rate of 150 rpm, aeration rate 1 vvm and initial pH of 7.0. Analyzed the cell dry weight (CDW) and found that the cell weight increased continuously, reaching a maximum of 5.48 g/L at 108 h. Meanwhile, the amount of glycerol decreased continuously along with cell growth, the biomass yield ($Y_{x/s}$) was 1.42 g/g. The pH of the culture was in the range of 6.76-6.99 (Figure 4.7). Bacteria began to produce PHA at 24 h with a PHA content of 0.03 g/L and the highest increase at 132 h with a PHA of 1.25 g/L (Figure 4.8), with PHA yield ($Y_{p/s}$) was 0.41 g/g and PHA content of 24.17%. Hermann-Krauss *et al*. (2013) used *Aloferax mediterranei* DSM 1411 to produce PHBHV. It uses crude glycerol phase (CGP) from biodiesel production as a carbon source. It was cultivated in a 10 L bioreactor, it was found that the $Y_{p/s}$ value was 0.19 g/g, which was lower than pure glycerol (0.37 g/g) [132]. Poblete-Castro *et al*. (2014) demonstrate that the chemical mixture used to produce raw glycerol from biodiesel synthesis does not represent a threat to the Pseudomonas genus of bacteria. It also shows inexpensive substances can effectively synthesize mcl-PHA. Using raw

glycerol as its carbon source, *P. putida* KT2440 was the most effective strain tested for mcl-PHA synthesis, yielding CDW 4.23 g/L and PHA 1.46 g/L [133].

The bacterial culture *Novosphingobium* sp. THA_AIK7 in the bioreactor obtained less PHA than in the flask level. Differences between culture at the flask level and in a bioreactor. In flask culture, during sample collection, shaking was stopped for 30 minutes, but in the bioreactor, there was no stopping stirring, and it had an aeration rate of 1 vvm. Kulkarni *et al*. (2010) [134] have demonstrated the impact of many environmental factors, including inoculum density. Influence of incubation temperature, duration, and starting medium pH on *Halomonas campisalis* synthesis of PHA in a flask. Previous studies of Teeka *et al*. (2010) [108] found that Novosphingobium sp. THA_AIK7 at the flask level found that cells could grow in aerobic conditions by shaking at 150 rpm. From this research, it can be concluded that Novosphingobium sp. THA_AIK7 is an aerobic bacterium but requires a small amount of aerobic. The bacteria will produce less PHA if providing too much or too little air.

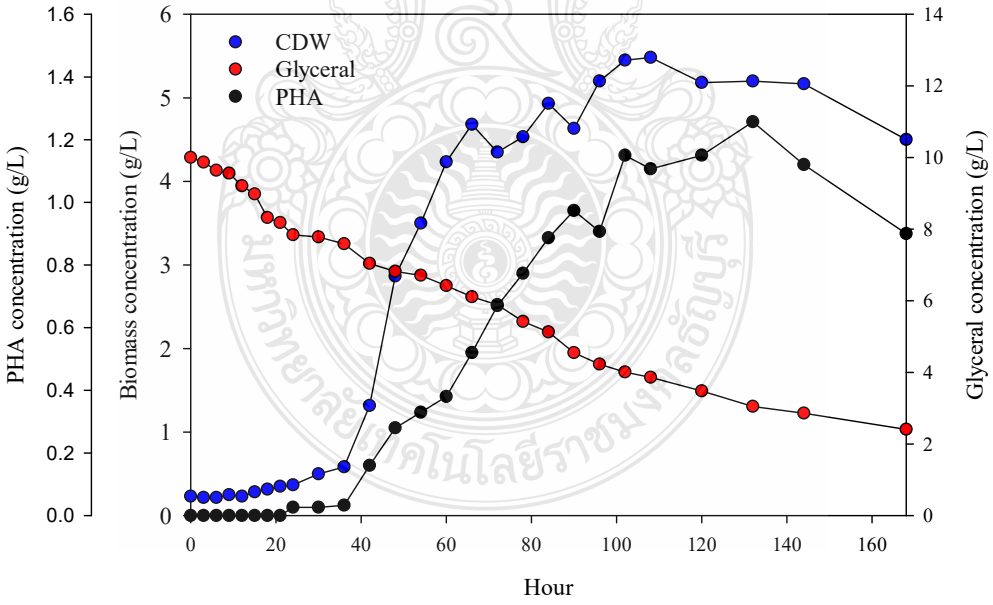

Figure 4.7 Biomass, PHA, and glycerol concentration of *Novosphingobium* sp. THA_AIK7 in a batch bioreactor

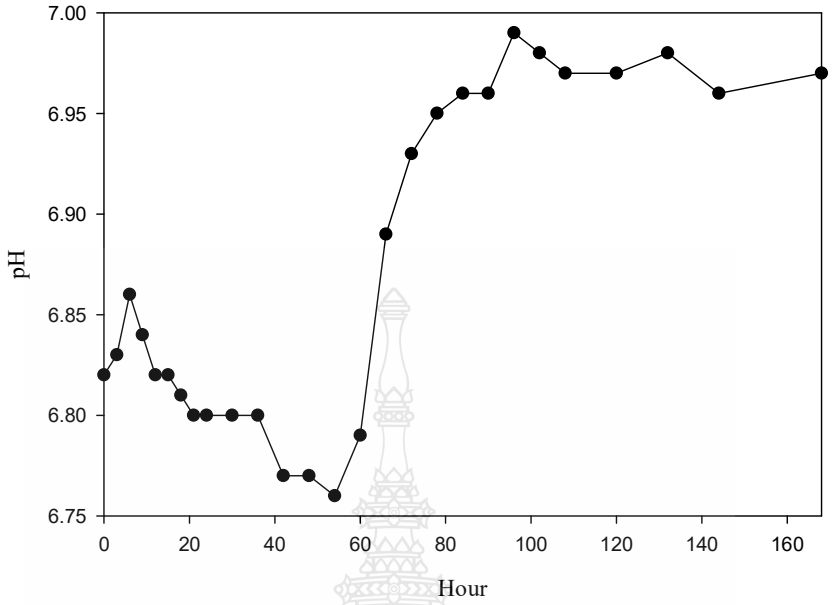

Figure 4.8 The pH profile of medium of *Novosphingobium* sp. THA_AIK7 in a batch-bioreactor

4.5 The statistical experimental design to optimization of extraction process using silica gel

The optimum condition of extraction process using silica gel was arranged as 17 runs of Box-Behnken design (Table 4.4). The influence of three independent variables Temperature (A), Loaded cell (B) and amount of Silica gel (C) were investigated. The experimental results of the extraction process using silica gel found that the amount of PHA extracted were ranged at 14 to 41 mg. The high PHA was obtained from the experimental results which used 80 mg of cell, silica gel 30 g, and temperature at 50°C in run 12. From the experiment, it was found that when the concentration of cells and the amount of silica gel increased, the amount of PHA also increased.

Table 4.4 PHA content of silica gel extraction

Run	PHA (mg)
1	14
2	16
3	37
4	39
5	29
6	30
7	34
8	28
9	20
10	38
11	22
12	41
13	29
14	29
15	29
16	29
17	29

Remark: Experiments 13-17 are the same example.

Silica is an extremely effective adsorbent and non-toxic, along with its remarkable textural properties like high surface area, large pore size/volume, and plenty of open pores, along with its good mechanical, chemical, and thermal stability (non-swelling) up to 1500 ℃, make it an incredibly effective adsorbent [135]. According to Yang *et al*. (2018) and Halamoda-Kenzaoui *et al*. (2015) [136, 137], the silica structure affects how stable silica nanostructures are. Large porous silica nanoparticles, for instance, changed their colloidal stability and had their silica surface scratched by biological and cellular media in a synergistic way. Apart from aqueous colloidal stability, additional significant practical metrics to characterize the reaction activity and selectivity of silica nanostructures are heat stability and reusability [138]. Ferraz *et al*. (2004) [139]

researched the extraction of lipids from human serum using a silica-based extraction, as reported by Neoh *et al*. (1986), which requires a half-hour absorption phase but failed to extract lipids from human serum effectively [140]. This was achieved only after increasing the silica concentration 10 times throughout two successive absorption phases that lasted 2 and 16 h. Probably, the levels of lipids in the samples used were lower than what is typically present in human serum [140]. For this reason, it can be concluded that Silica gel and cells affect PHA extraction. Silica gel is a conventional physical pre-treatment method used to interrupt cell membranes and extract intracellular products. Silica gel, a water adsorbent, was chosen for PHA recovery, attempting to rely on lipid removal from human serum research [139, 141]. The lipid component of the cell extract may be adsorbed in the porous silica gel and sink to the bottom during the chloroform phase, increasing the solvent's lipid dissolution and augmenting the PHA recovery than the sodium hypochlorite basis technique.

The analysis of variance (ANOVA) and code regression coefficients of the quadratic model for find the influencing factors to PHA production were shown in Table 4.4. The statistical analysis results of PHA showed that *p*-value of PHA production models was < .0001. In this silica gel (C^2) is a significant *p*-value of .0142. It was indicated that the PHA model was significant at the confidence level of 95% (*p*-value ≤ .05). The value of the coefficient of determination (R^2) of PHA was 0.9791, indicating that the experimental findings and predicted data were well correlated (Table 4.4)

The model construction was arranged in a series by using all coefficients with symbols of all variables in terms of linear, squares, and interactions. The mathematical equation of full quadratic model was shown in Eqs. (7).

$$\text{PHA} = -151.33625 + 5.89425A + 0.814125B - 0.670625C + 0.001100AB - 0.054917AC + 0.000625BC - 0.046650A^2 - 0.003059B^2 + 0.073160C^2 \quad (7)$$

Table 4.5 ANOVA results of BBD for extraction

Source	Sum of Squares	df	Mean Square	F-value	p-value
Model	910.62	9	101.18	36.41	< 0.0001*
A-Temperature	8.57	1	8.57	3.08	0.1225
B-Cell	7.04	1	7.04	2.53	0.1556
C-Silica gel	0.3803	1	0.3803	0.1368	0.7224
AB	0.0484	1	0.0484	0.0174	0.8987
AC	10.86	1	10.86	3.91	0.0886
BC	0.0225	1	0.0225	0.0081	0.9308
A^2	5.73	1	5.73	2.06	0.1943
B^2	6.31	1	6.31	2.27	0.1757
C^2	29.21	1	29.21	10.51	0.0142*
Residual	19.45	7	2.78		
Lack of Fit	19.45	3	6.48		
Pure Error	0.0000	4	0.0000		
Cor Total	930.07	16			
	$R^2 = 0.9791$				

*p-value ≤ .05 and are significant.

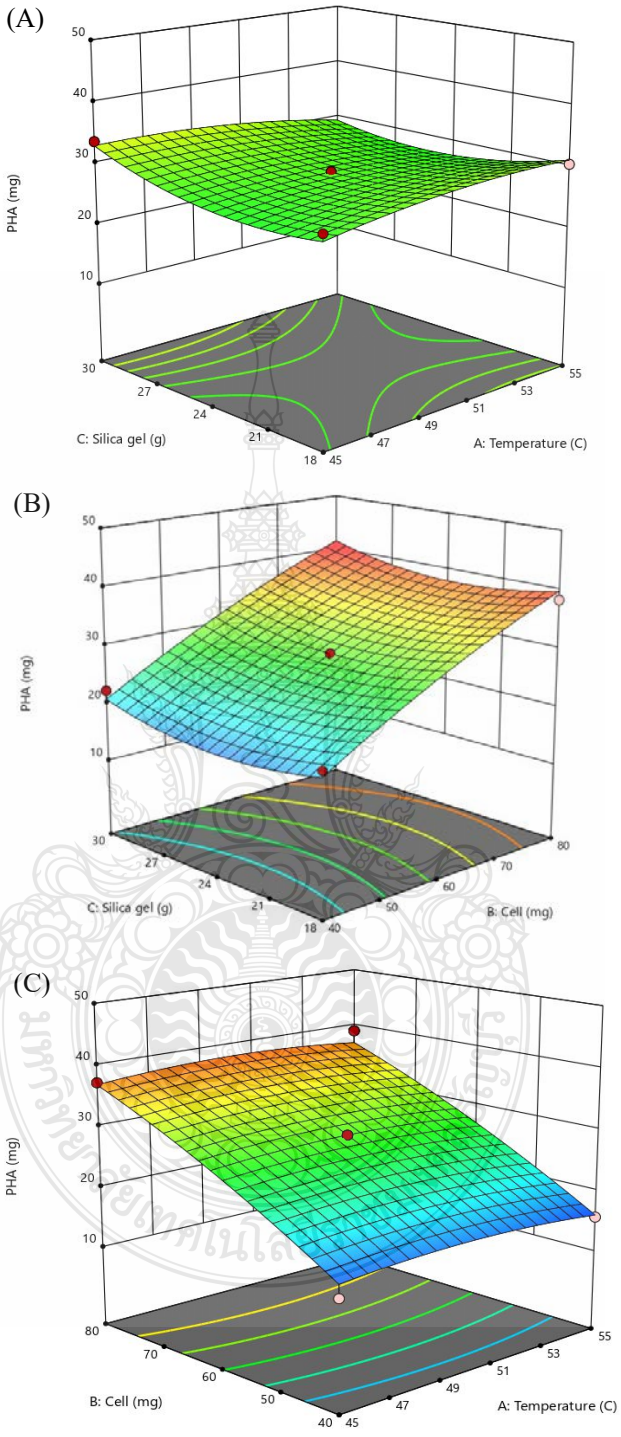

Figure 4.9 3D surface and 2D contour graph of PHA extraction (A), silica gel and temperature; (B), silica gel and cell; and (C), cell and temperature.

The Eqs. (7) were employed to create the three-dimensional (3D) response surface graph and the related two-dimensional (2D) contour to determine the optimum combination of the assessed variables (Figure 4.9 *A* to *C*). The interaction between silica gel + temperature in this range shows that they slightly affected (Figure 4.9 A). While the interaction between silica gel + cell in this range shows that the amount of PHA increases when the cell concentration is higher from 40 to 80 mg and the amount of silica gel is between 18 to 30 g (Figure 4.9 B). The interaction between cell + temperature in this range shows that the amount of PHA increases when the cell concentration is higher from 40 to 80 mg (Figure 4.9 C). However, to increase Extraction PHA efficiency, it is essential to consider all three studied variables and other control factors concurrently.

4.6 The statistical experimental design for fabrication of microcarrier PHA by emulsion technique

The optimum condition of fabrication of microcarrier PHA by emulsion technique was arranged as 29 runs of BBD (Table 4.5). The influence of four independent variables PHA (*A*), PVA (*B*), NH_5CO_3 (*C*) and Stirrer (*D*) were investigated. The experimental results of pore size and diameter ranged at 0.479 – 1.970 μm and 17-125 μm, respectively. The pore size and diameter are the best, accorded by the second-order quadratic model. The best microcarrier has pore size and diameter 0.970 and 125 μm, respectively, were obtained from the experimental results which used PHA 0.24 g, PVA 0.5 %, NH_5CO_3 1 %, and Stirrer 500 rpm in run 18.

The analysis of variance (ANOVA) and code regression coefficients of the quadratic model to find the influencing factors to pore size and diameter were shown in Table 4.5-4.6. The statistical analysis results of pore size and diameter showed that the *p*-values of models were 0.0001 and 0.0017, respectively. It was indicated that the pore size and diameter model was significant at the confidence level of 95% (p-value ≤ .05). The value of the coefficient of determination (R^2) of pore size and diameter models were 0.8957 and 0.8421, respectively, indicating that the experimental findings and predicted data were well correlated (Table 4.5-4.6).

For the pore size model in this stirrer (D), PHA and NH_5CO_3 (AC), NH_5CO_3 (C^2), and stirrer (D^2) are significant model terms with the p-values at .00001, .0013, .0024, and .0001, respectively (Table 4.5). The diameter model in this stirrer (D), PHA (A^2), and stirrer (D^2) are significant model terms with the p-values at .00002, .0339, and .0009, respectively, (Table 4.6).

The model construction was arranged in a series by using all coefficients with symbols of all variables in terms of linear, squares, and interactions. The mathematical equation of the full quadratic model is shown in Eqs. (8).

$$\text{Pore size} = -1.52619 + 2.32689A + 0.637824B + 0.111976C + 0.005072D + 0.405582AB - 1.46623AC + 0.001609AD - 0.046791BC - 0.000704BD - 0.000098CD + 5.27120A^2 - 0.0242991B^2 + 0.025159C^2 - 2.87172\text{E-}06D^2 \quad (8)$$

Table 4.6 ANOVA results of BBD for pore size of MC-PHAs

Source	Sum of Squares	df	Mean Square	F-value	p-value
Model	5.12	14	0.3658	8.59	0.0001
A-PHA	0.0094	1	0.0094	0.2214	0.6452
B-PVA	0.0289	1	0.0289	0.6782	0.4240
C-NH_5CO_3	0.0519	1	0.0519	1.22	0.2881
D-Stirrer	1.19	1	1.19	27.90	0.0001
AB	0.0009	1	0.0009	0.0202	0.8891
AC	0.6833	1	0.6833	16.04	0.0013
AD	0.0110	1	0.0110	0.2591	0.6187
BC	0.0222	1	0.0222	0.5209	0.4823
BD	0.0675	1	0.0675	1.58	0.2287
CD	0.0793	1	0.0793	1.86	0.1940
A^2	0.0074	1	0.0074	0.1732	0.6836
B^2	0.0152	1	0.0152	0.3572	0.5596
C^2	0.5848	1	0.5848	13.72	0.0024
D^2	1.16	1	1.16	27.32	0.0001
Residual	0.5965	14	0.0426		

Table 4.6 ANOVA results of BBD for pore size of MC-PHAs (Continued)

Source	Sum of Squares	df	Mean Square	*F*-value	*p*-value
Lack of Fit	0.5965	10	0.0596		
Pure Error	0.0000	4	0.0000		
Cor Total	5.72	28			
	$R^2 = 0.8957$				

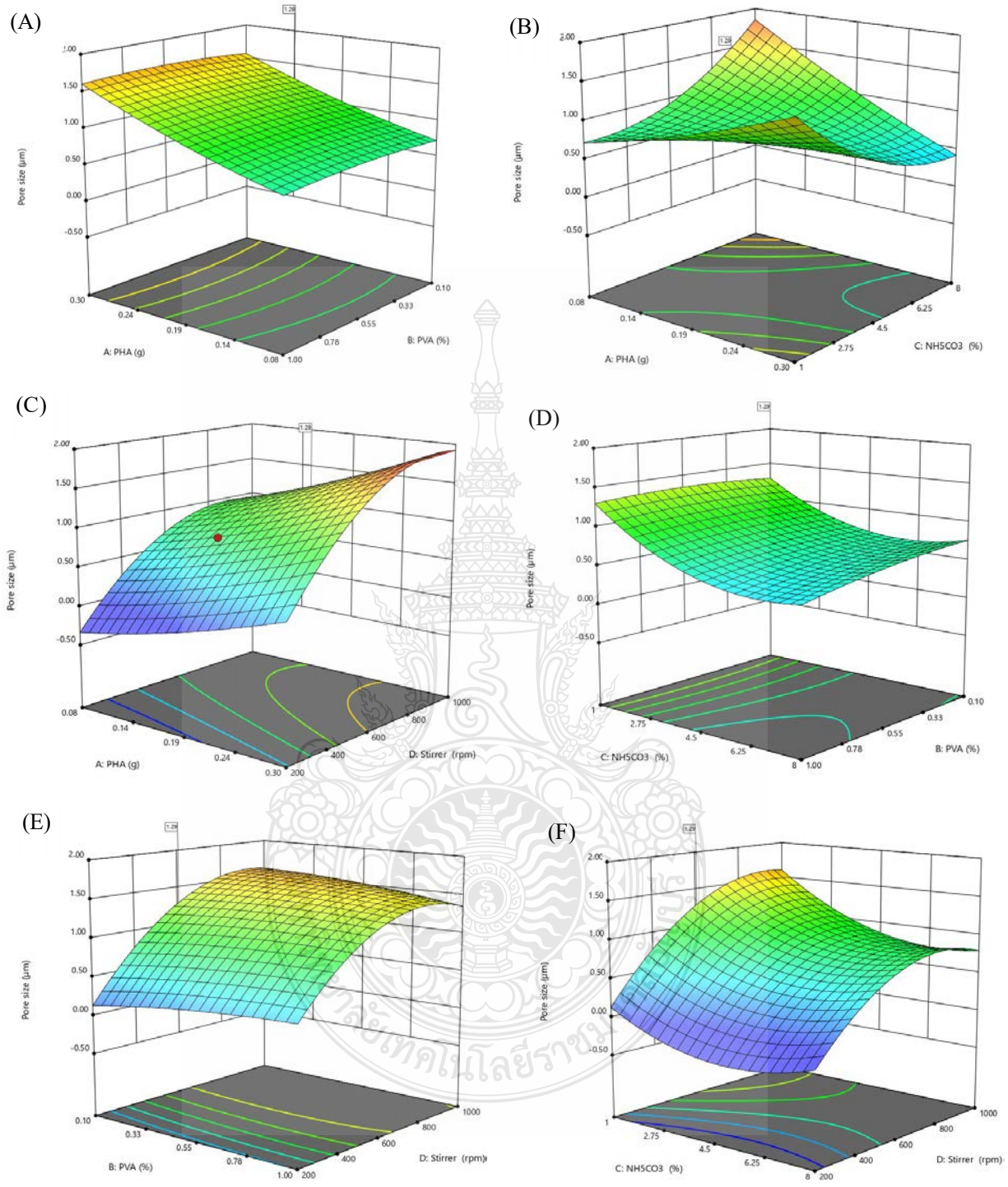

Figure 4.10 3D surface and 2D contour graph of pore size (A), PHA and PVA; (B), PHA and NH_5CO_3; (C), PHA and stirrer; (D), NH_5CO_3 and PVA; (E), PVA and stirrer; and (F), NH_5CO_3 and stirrer

The model construction was arranged in a series by using all coefficients with symbols of all variables in terms of linear, squares, and interactions. The mathematical equation of the full quadratic model is shown in Eqs. (9).

$$\text{Diameter} = -83.92798 - 185.29787A + 75.74132B - 5.28380C + 0.411223D - 332.13020AB - 25.17485AC - 0.340731AD - 0.771294BC - 0.034375BD - 0.008603CD + 2564.06043A^2 - 17.3358B^2 + 1.13295C^2 - 0.000198D^2 \quad (9)$$

Table 4.7 ANOVA results of BBD for Diameter of MC-PHAs

Source	Sum of Squares	df	Mean Square	*F*-value	*p*-value
Model	23596.52	14	1685.47	5.33	0.0017
A-PHA	59.83	1	59.83	0.1893	0.6701
B-PVA	407.48	1	407.48	1.29	0.2753
C-NH_5CO_3	115.66	1	115.66	0.3659	0.5549
D-Stirrer	7815.45	1	7815.45	24.73	0.0002
AB	576.49	1	576.49	1.82	0.1983
AC	201.42	1	201.42	0.6373	0.4380
AD	495.24	1	495.24	1.57	0.2312
BC	6.03	1	6.03	0.0191	0.8921
BD	160.80	1	160.80	0.5087	0.4874
CD	612.57	1	612.57	1.94	0.1856
A^2	1746.56	1	1746.56	5.53	0.0339
B^2	77.45	1	77.45	0.2450	0.6283
C^2	1185.81	1	1185.81	3.75	0.0732
D^2	5540.75	1	5540.75	17.53	0.0009
Residual	4424.97	14	316.07		
Lack of Fit	4424.97	10	442.50		
Pure Error	0.0000	4	0.0000		
Cor Total	28021.49	28			
	$R^2 = 0.8421$				

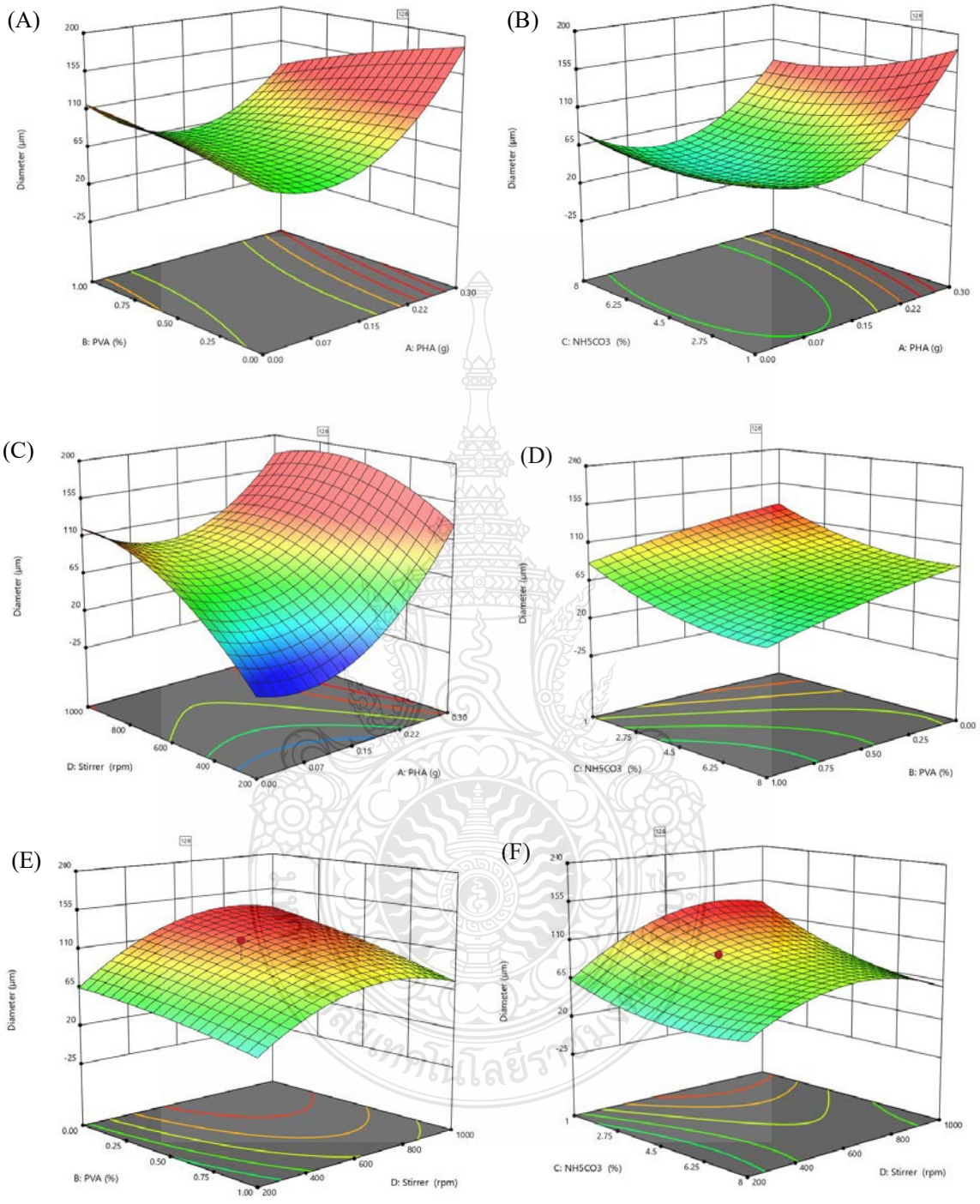

Figure 4.11 3D surface and 2D contour graph of diameter (A), PVA and PHA; (B), NH_5CO_3 and PHA; (C), stirrer and PHA; (D), NH_5CO_3 and PVA; (E), PVA and stirrer; and (F), NH_5CO_3 and stirrer

The Eqs. (8) were employed to create the three-dimensional (3D) response surface graph and the related two-dimensional (2D) contour to determine the optimum combination of the assessed variables (Figure 4.10 A to F). The interaction between PHA + PVA, PHA + NH_5CO_3, and NH_5CO_3 + PVA in this range shows that they slightly affected (Figure 4.10 A, B and D). While the interaction between PHA + stirrer, PVA + stirrer, and NH_5CO_3 + stirrer in this range shows that of microcarrier have pore size widened when speed up stirrer from 200 to 1000 rpm (Figure 4.10 C, E, and F).

The Eqs. (9) were employed to create the three-dimensional (3D) response surface graph and the related two-dimensional (2D) contour to determine the optimum combination of the assessed variables (Figure 4.11 (A) to (F)). The interaction between NH_5CO_3 + PVA in this range shows that they slightly affected (Figure 4.11 D). While the interaction between PVA + PHA, NH_5CO_3 + PHA, and stirrer + PHA in this range shows that of microcarrier have diameter widened when the amount of PHA increases from 0.08 to 0.24 g (Figure 4.11 (A) to (C)). The interaction PVA + stirrer, and NH5CO3 + stirrer in this range shows that of microcarrier have diameter widened when the stirrer is 500 rpm (Figure 4.11 E and F).

However, to optimize the production of microcarriers from PHA, it is essential to consider the four studied variables and other control factors concurrently.

Table 4.8 MC-PHAs under Scanning Transmission Microscope (SEM)

Run	dry weight (g)		
1	0.0323	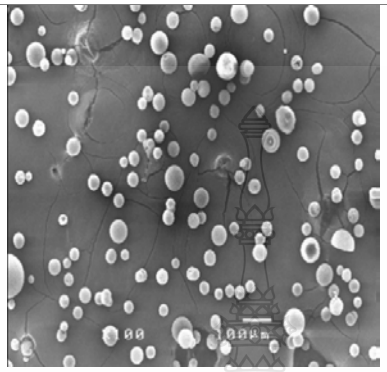	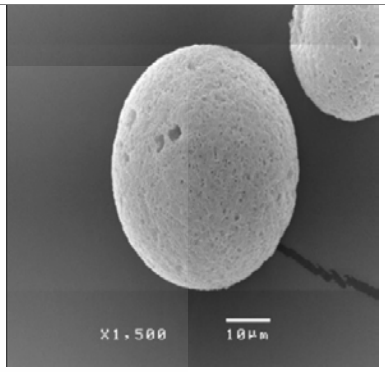
2	0.1634	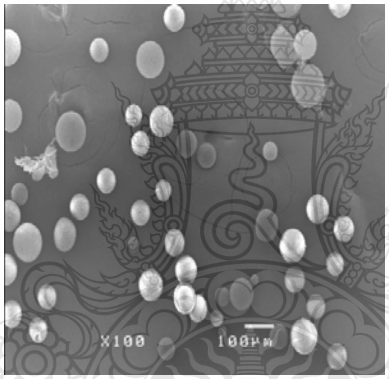	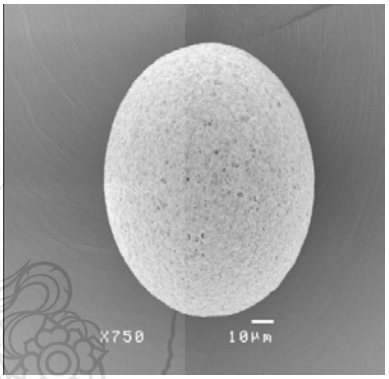
3	0.0307	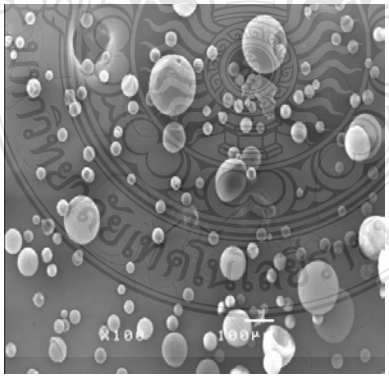	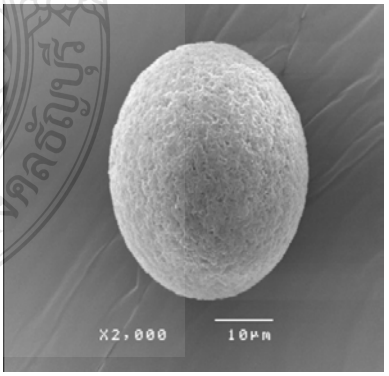

Table 4.8 MC-PHAs under Scanning Transmission Microscope (SEM) (Continued)

Run	dry weight (g)	
4	0.0856	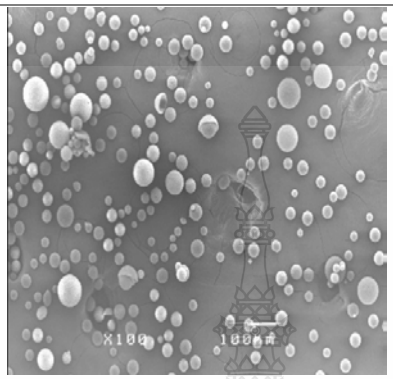 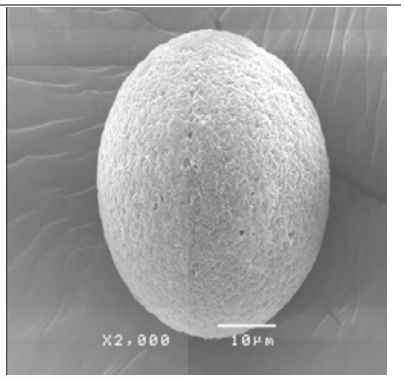
5	0.0914	
6	0.0989	

Table 4.8 MC-PHAs under Scanning Transmission Microscope (SEM) (Continued)

Run	dry weight (g)		
7	0.0628	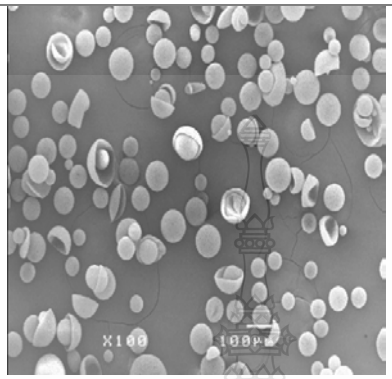	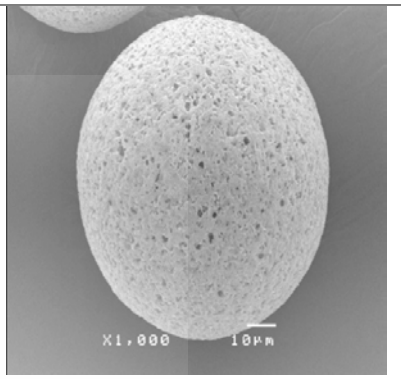
8	0.0199	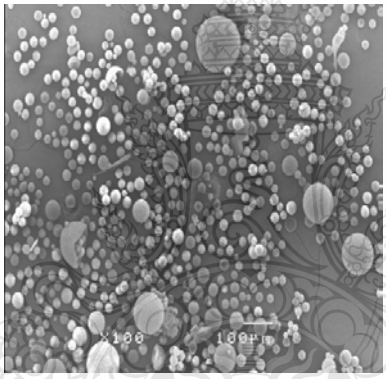	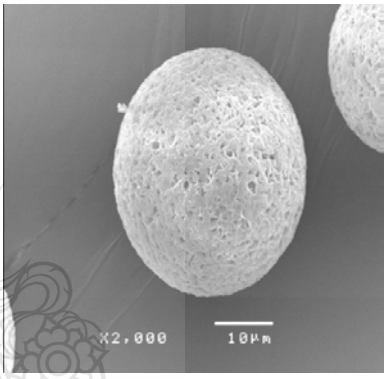
9	0.0500		

Table 4.8 MC-PHAs under Scanning Transmission Microscope (SEM) (Continued)

Run	dry weight (g)		
10	0.1464		
11	0.0079	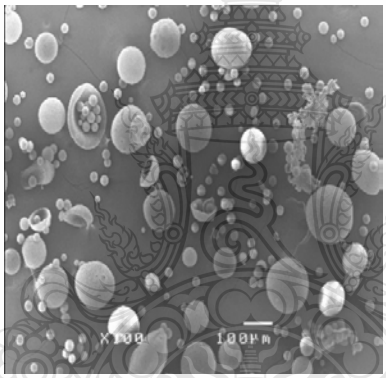	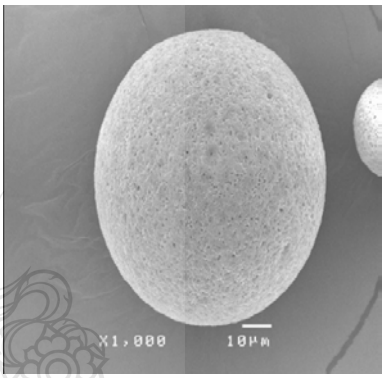
12	0.0925	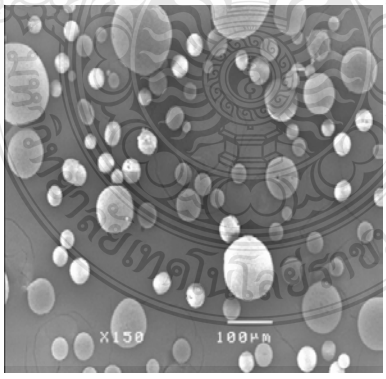	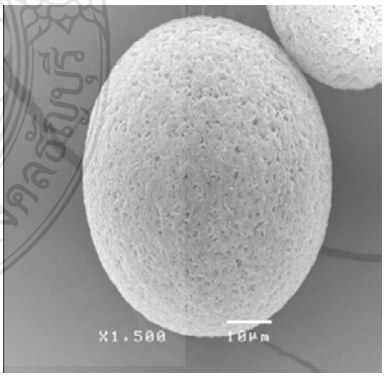

Table 4.*8* MC-PHAs under Scanning Transmission Microscope (SEM) (Continued)

Run	dry weight (g)		
13	0.1007	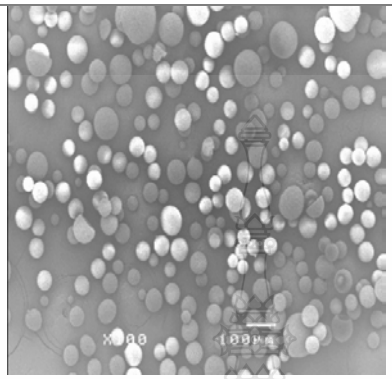	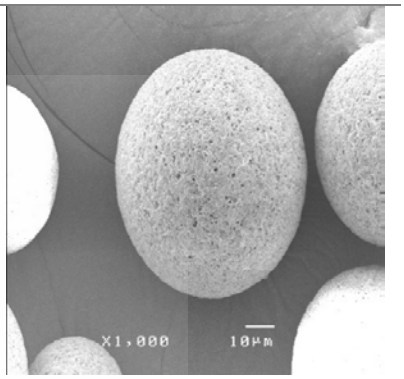
14	0.0533	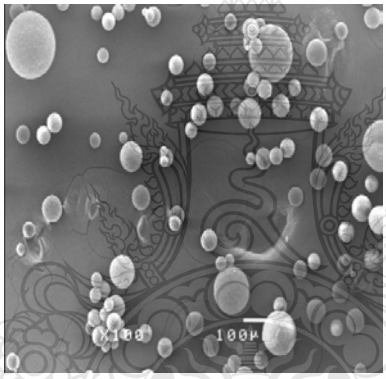	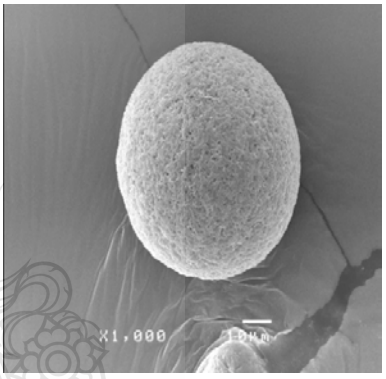
15	0.0754	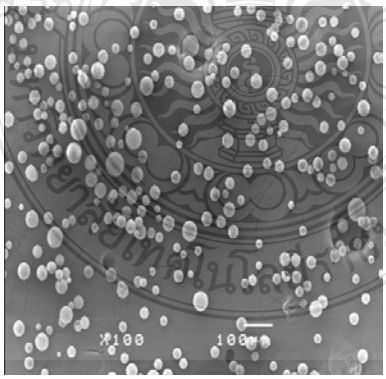	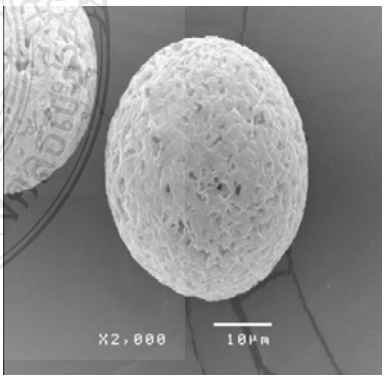

Table 4.*8* MC-PHAs under Scanning Transmission Microscope (SEM) (Continued)

Run	dry weight (g)		
16	0.0948	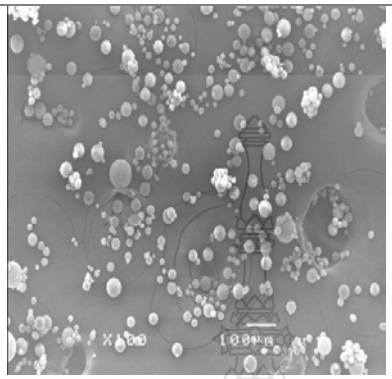	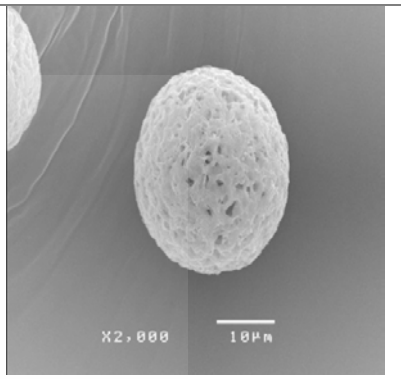
17	0.0210	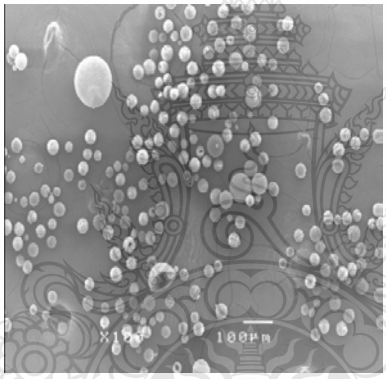	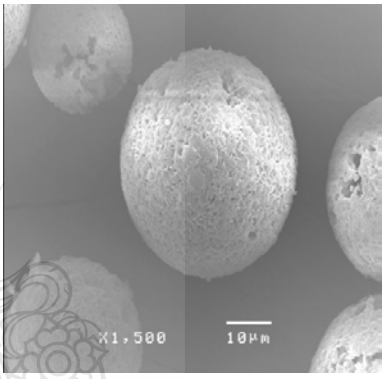
18	0.1640	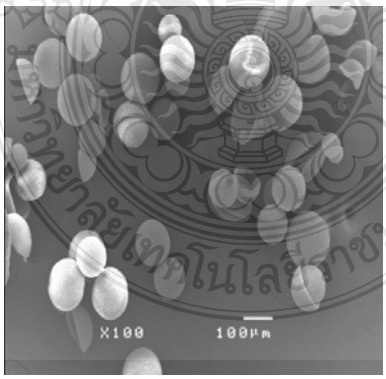	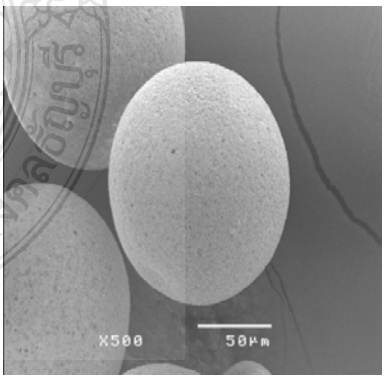

Table 4.*8* MC-PHAs under Scanning Transmission Microscope (SEM) (Continued)

Run	dry weight (g)		
19	0.0166	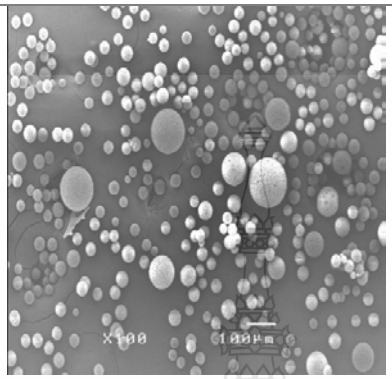	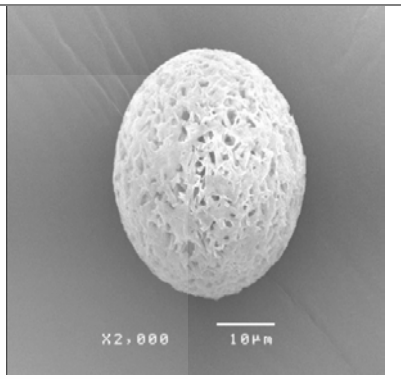
20	0.1546	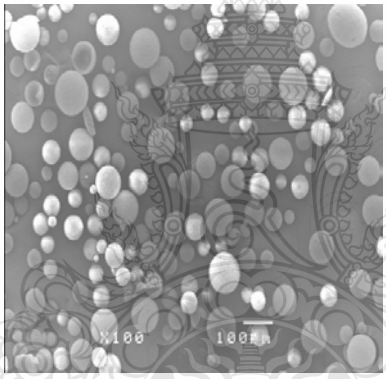	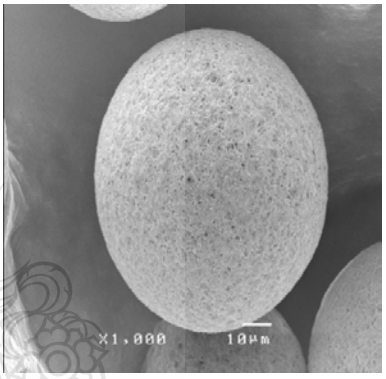
21	0.0645		

Table 4.8 MC-PHAs under Scanning Transmission Microscope (SEM) (Continued)

Run	dry weight (g)		
22	0.1021		
23	0.0677	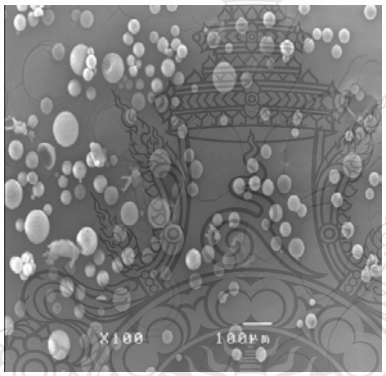	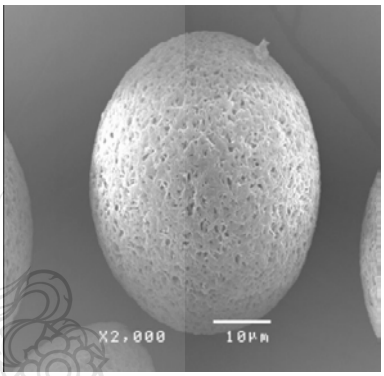
24	0.0638	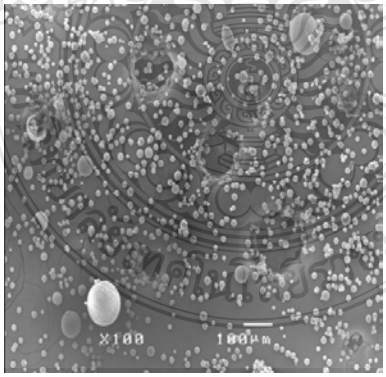	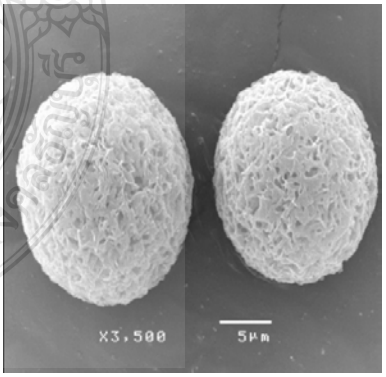

Table 4.8 MC-PHAs under Scanning Transmission Microscope (SEM) (Continued)

Run	dry weight (g)		
25	0.0674	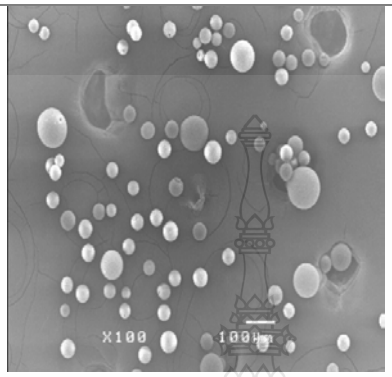	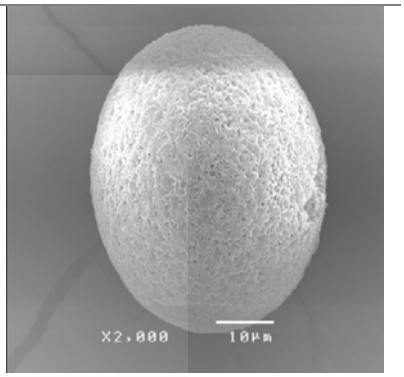
26	0.0674	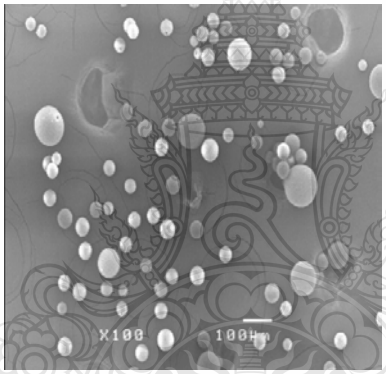	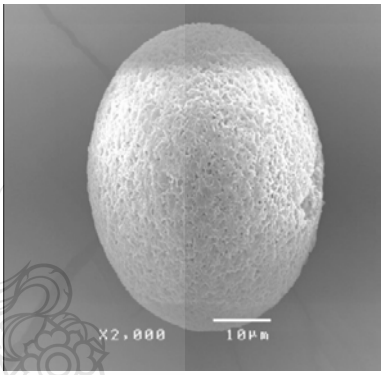
27	0.0674	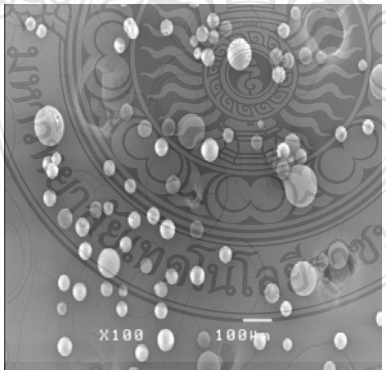	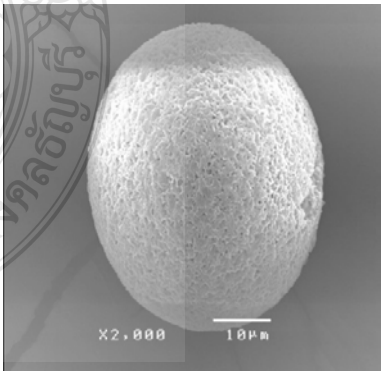

Table 4.8 MC-PHAs under Scanning Transmission Microscope (SEM) (Continued)

Run	dry weight (g)		
28	0.0674	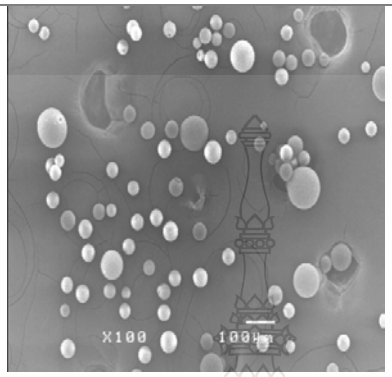	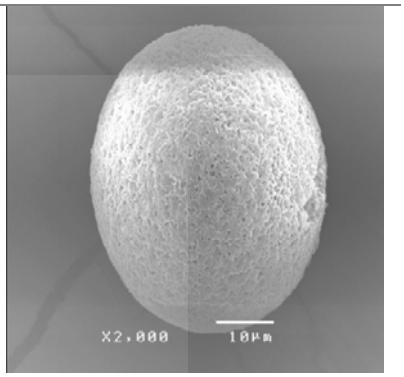
29	0.0674	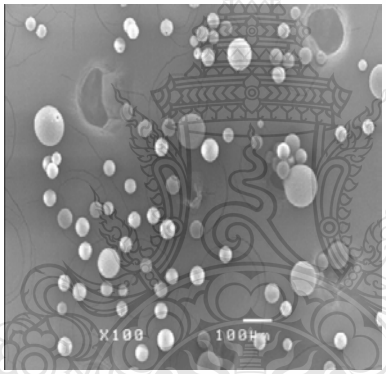	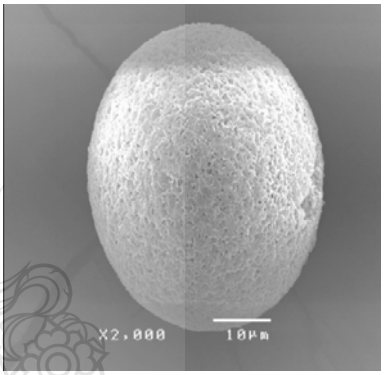

Remark: Experiments 25-29 are the same example.

Table 4.9 Pore size and diameter of microcarriers

Run	Pore size (μm)		Average pore size (μm)	Highest Frequency (μm)	Diameter (μm)
	Minimum size	Maximum size			
1	0.309	0.938	0.583±0.162	0. 566± 0.027	42.863±0.310
2	0.222	1.020	0.479±0.177	0. 427± 0.032	97.152±0.684
3	0.416	0.996	0.656±0.140	0. 633± 0.029	34.234±0.029
4	0.312	1.062	0.599±0.179	0. 478± 0.035	40.428±0.405
5	-	-	-	-	-
6	-	-	-	-	-
7	0.709	2.119	1.412±0.360	1.405 ± 0.048	86.562±0.326
8	0.545	1.409	0.969±0.223	0.972 ± 0.045	32.831±0.093
9	-	-	-	-	-
10	-	-	-	-	-
11	0.437	1.378	0.717±0.172	0. 687± 0.001	80.787±0.978
12	0.495	1.359	0.838±0.245	0. 667± 0.018	56.392±0.458
13	0.303	1.374	0.851±0.274	0. 863± 0.049	65.691±0.543
14	0.413	1.363	0.747±0.230	0.699 ± 0.062	64.367±0.724
15	0.832	2.010	1.259±0.315	1. 148± 0.048	35.323±0.157
16	0.467	1.648	0.881±0.280	0.792 ± 0.038	27.557±0.526
17	0.434	1.251	0.654±0.172	1. 197± 0.060	39.540±0.529
18	0.371	2.132	0.970±0.363	0.891 ± 0.039	125.864±0.512
19	1.061	2.894	1.970±0.458	1.943 ± 0.094	33.264±0.367
20	0.346	1.185	0.707±0.228	0. 745± 0.033	80.755±0.542
21	-	-	-	-	-
22	-	-	-	-	-
23	0.345	2.228	0.920±0.506	0. 731± 0.057	40.014±0.163
24	0.222	1.020	0.479±0.177	0. 427± 0.032	17.172±0.267
25	0.347	1.040	0.665±0.182	0.615 ± 0.026	41.393±0.542

Remark: Experiments 25-29 are the same example. (-) is unable to form.

The forming of PHA polymers into microcarriers using the emulsion technique. The experiment was designed using Box-Behnken (BBD), with a total of 29 experiments. It was found that the microcarriers obtained are easy to form, precipitate quickly when in saturated conditions and can be autoclaved. The morphology of microcarriers was examined under a SEM as shown in Table 4.7. The microcarriers obtained in each experiment are of different sizes. MC-PHAs have diameters in the range of 17-125 μm and pore sizes in the range of 0.479 – 1.970 μm, as shown in Table 4.8. In each experiment the sizes of MC-PHAs are very different and the sizes are not uniform. However, in run 18, the size of MC-PHAs was large and the size was most consistent, it was found that the average diameter was 125.864 μm and the average pore size was 0.970 μm, the formed MC-PHAs had the highest weight of MC-PHAs, which was 0.1640 g (from the PHA precursor content of 0.24 g, accounting for 68.34%. of initial weight). Chung *et al*. (2008) studied biodegradable microcarriers fabricated using gas foaming in double emulsion $W_1/O/W_2$ using PLGA. It was found that the carrier had an average size of approximately 175 μm [94]. Run 24 had the smallest size of MC-PHAs which has an average diameter of 17.172 μm and average pore size of 0.479 μm. As for runs 5, 6, 9, 10, 21, and 22, MC-PHAs had the appearance of a film due to low spinning speed. When spinning for the full time, there was still chloroform remaining and after drying, it formed a film.

This is compared to the size of the commercial microcarrier brand Cytodex1 (Sigma-Aldrich), which has a diameter of 60-87 μm and an average of 190 μm when swelled in liquid solution. The size of the microcarriers that can be formed in the laboratory from PHA is no different from that of the commercial microcarriers. Therefore, the microcarrier suitable for further study is the microcarrier from run 18 because the microcarrier has the most uniform size, is large, and has the highest diameter.

PHAs and ammonium bicarbonate (NH_5CO_3) affects the size of the microcarriers, if the amount of PHA increases, the size of the microcarriers increases. In the research of [83] when increasing the concentration of poly(lactic-co-glycolic acid) PLGA from 1.6 % to 6.3 % (w/v). The microspheres had an increase in particle size from 175.3 μm to 362.4 μm and a decrease in pore size from 29.4 μm to 7.9 μm. PLGA microspheres are prepared by adding increasing amounts of ammonium bicarbonate to the W_1 aqueous phase of the

primary emulsion solution. Ammonium bicarbonate at 0%, 1%, 5%, and 10% (w/v) had average diameters of 343, 403, 439, and 535 μm, respectively. It was shown that the porous PLGA microspheres were larger, caused by increasing the amount of ammonium bicarbonate. This is apparently because of internal gas bubbles that enlarge the size of the gas-developed primary droplets. and creates additional gas bubbles in the solidified polymer phase [142]. Different concentrations of poly (vinyl alcohol) (PVA) allow microcarriers with different pore sizes. Gas bubbles are created and develop through the surface during the evaporation of the aqueous solvent [96]. Therefore, the stirring rate affects the forming of the microcarrier.

Porous structures play an important role in cell culture. This is because it not only promotes cell adhesion and distribution but also promotes the exchange of nutrients and metabolic waste [143]. The pore size should be within an appropriate range, to achieve high performance of cell culture with microcarriers or porous scaffolds [143, 144, 145]. If the pore size is too small, cell migrate is limited, resulting in the formation of a cell capsule nearby the microcarrier [97]. Conversely, if the pore size is too large, there is a decrease in surface area limiting cell adhesion [144]. The optimal pore size can vary for different cell [145, 146]. However, pores should also be connected to each other to allow enough many directions cell–cell interactions within the microcarriers [97].

4.8 Cell adhesion and growth of L292 and Vero cell in dynamic condition on MC-PHAs and Cytodex1

4.8.1 Vero cell growth on Cytodex1

Dynamic cell culture was studied using a microcarrier at 1 g/L, concentration cells were $1x10^6$, incubated at 3°C and 5% CO_2 at 30 rpm stirring rate, samples at 24, 48, 72, 96, 120, and 144 h were stained with crystal violet. Vero cells were able to adhere to the Cytodex1 microcarrier. This can be seen from the dark purple spots of Crystal Violet staining the nuclei of Vero cells (Figure 4.12).

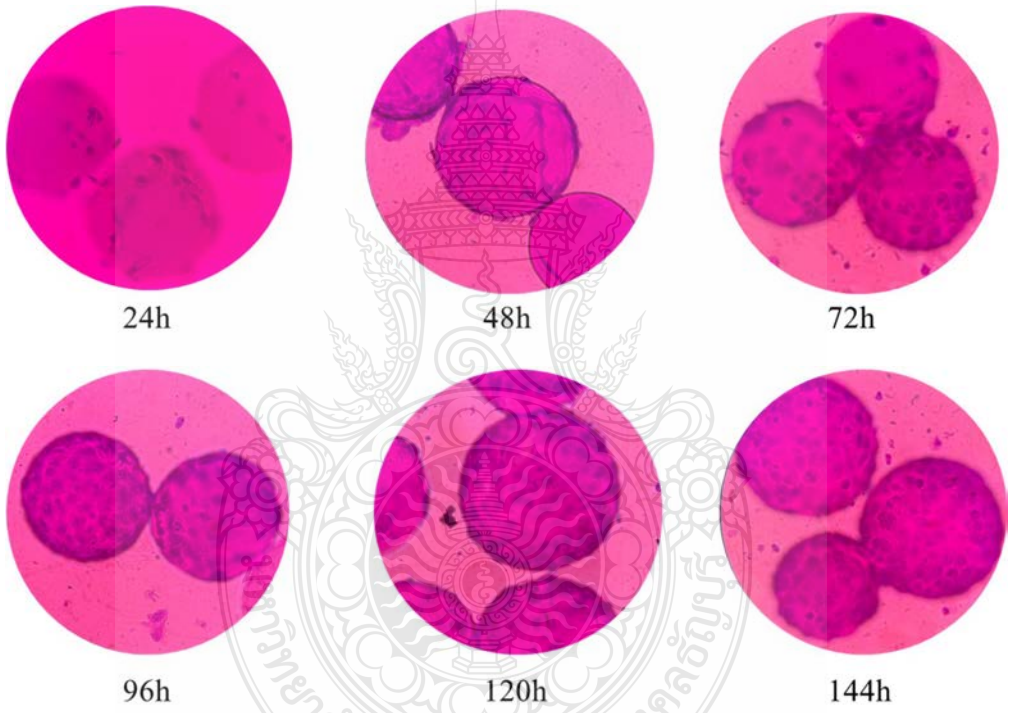

Figure 4.12 Vero cell on Cytodex1 at different cultivation times

4.8.2 Vero cell growth on MC-PHAs

In the study of cell dynamic culture using a microcarrier at 1 g/L, concentration cells were $1x10^6$, incubated at 3°C and 5% CO_2 at 30 rpm stirring rate and samples taken at 24, 48, 72, 96, 120, and 144 h and stained with crystal violet, Vero cells can adhere to the MC-PHAs microcarrier but less than the Cytodex1 microcarrier. This can be seen from the dark purple spots of crystal violet staining the nuclei of Vero cells (Figure 4.13).

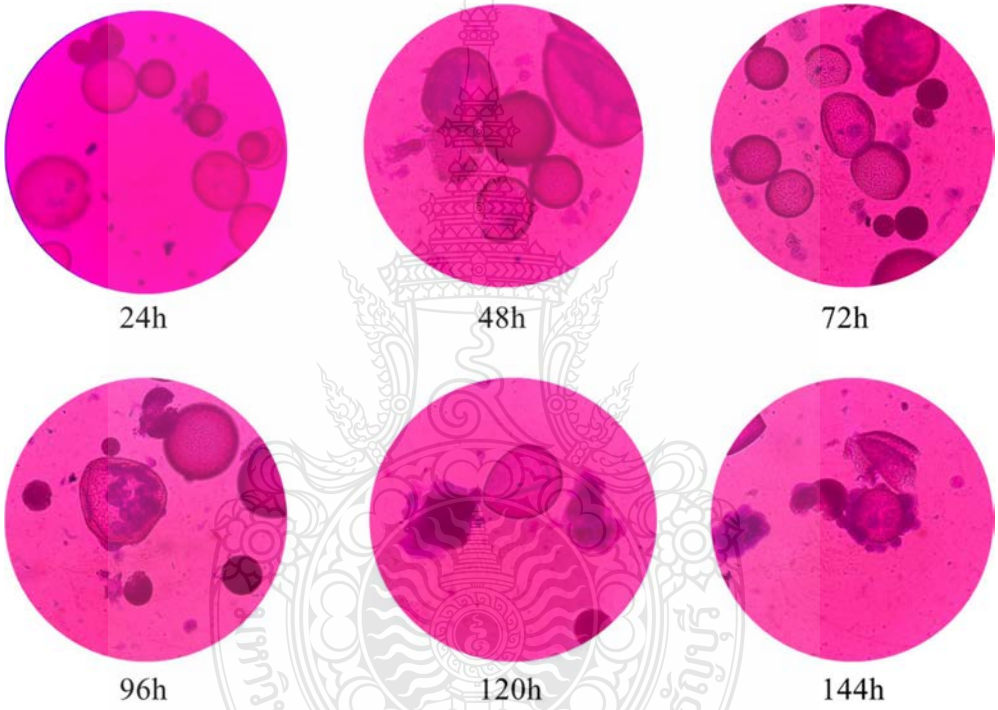

Figure 4.13 Vero cell on MC-PHAs at different cultivation times

4.8.4 L929 cell growth on Cytodex1

Dynamic cell culture was studied using a microcarrier at 1 g/L, concentration cells were $1x10^6$, incubated at 3°C and 5% CO_2 at 30 rpm stirring rate and samples taken at 24, 48, 72, 96, 120, and 144 h were stained with Crystal Violet. L929 cells were able to adhere to the Cytodex1 microcarrier. This can be seen from the dark purple spots of Crystal Violet staining the nuclei of L929 cells (Figure 4.14).

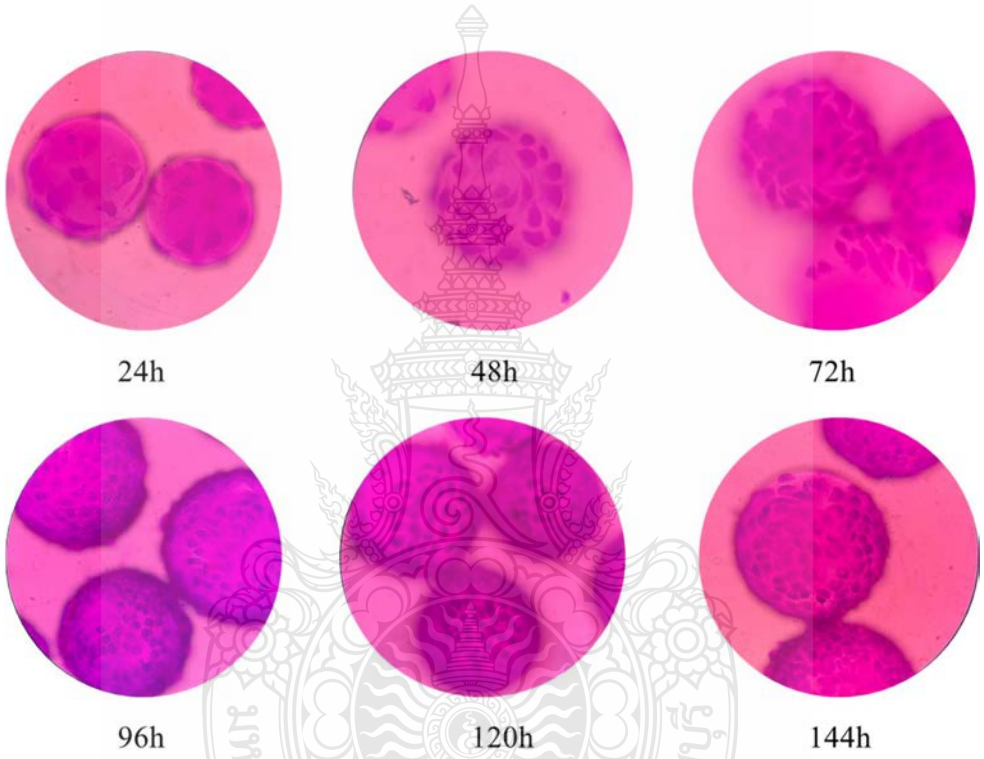

Figure 4.14 L929 cell on Cytodex1 at different cultivation times

4.8.4 L929 cell growth on MC-PHAs

In the study of cell dynamic culture using a microcarrier at 1 g/L, concentration cells were $1x10^6$, incubated at 3°C and 5% CO_2 at 30 rpm stirring rate and samples taken at 24, 48, 72, 96, 120, and 144 h and stained with crystal violet, L929 cells can adhere to the MC-PHAs microcarrier but less than the Cytodex1 microcarrier. This can be seen from the dark purple spots of crystal violet staining the nuclei of L929 cells (Figure 4.15). The figure shows that L929 cells were able to adhere to MC-PHAs more than Vero cells.

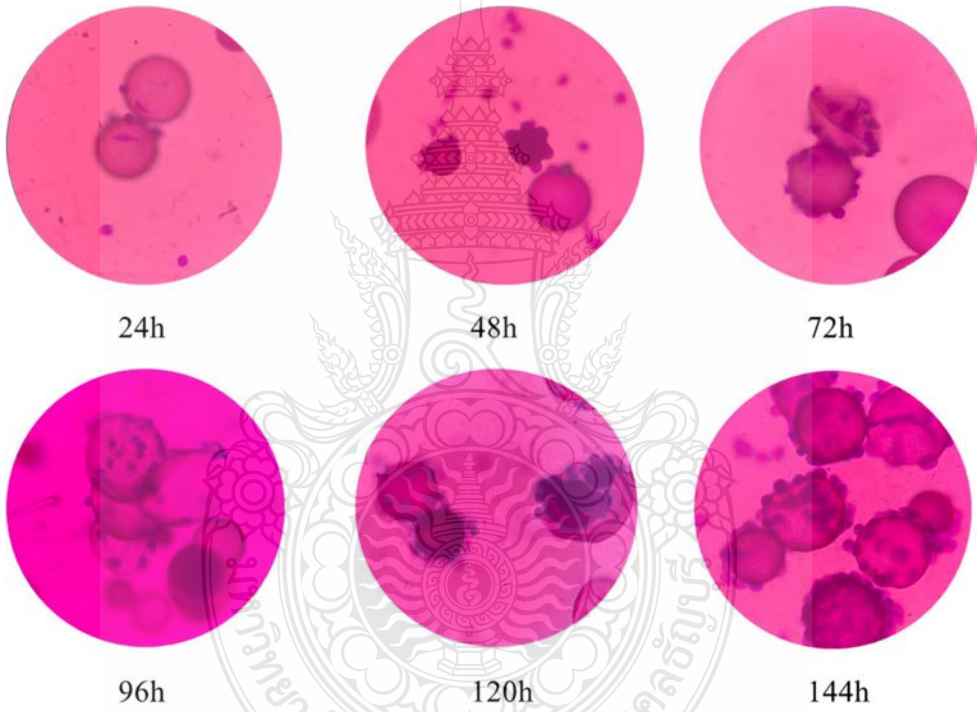

Figure 4.15 L929 cell on MC-PHAs at different cultivation times

4.9 Cytotoxicity of MC-PHAs by MTT assay

Microcarriers should have non-cytotoxic properties, therefore, to ensure that this type of microcarrier is suitable for culture with cells, it is necessary to test it before using it in practice. When comparing the toxicity of the microcarriers Cytodex1 and MC-PHAs to Vero and L929 cells using the MTT assay, it was found that when Vero and L929 cells were grown together with the microcarriers Cytodex1 and MC-PHAs in comparison with a control unit without a microcarrier. Cells that can adhere to the microcarrier can grow and as the number of cells increases, the measured MTT value will be high. Because living cells have activities dehydrogenase of mitochondria reacts with MTT, turning it from light yellow to blue crystals of insoluble formazan. Therefore, the blue intensity of formazan is directly proportional to the number of surviving cells. On the other hand, If the microcarrier is toxic to cells causes cell death the microcarriers have characteristics that are inappropriate for cell adhesion and growth. The number of cells decreases or increases at low doses. As a result, the intensity of the formazan blue color is also low. Cytotoxicity assay of MC-PHAs found that the percent viability of Vero and L929 cells were 92.40 % and 100.00 %, respectively. This study shows that PHA can be fabricated and is not toxic to animal cells (Table 4.9). The standard ISO 10993-5:2009(E) reports that if viability is reduced to < 70 % of the blank, it has a cytotoxic potential.

Table 4.10 Viability of animal cells on MC-PHAs

Condition	% Viability*	
	Vero cell	L929
Cytodex1	100.00±0.000	100.00±0.000
MC-PHAs	92.40±0.032	100.00±0.000

* Viability = 100 - %cytotoxicity

The in vitro cytotoxicity of the chitosan microspheres (CSM), and the viability of L-02 cells incubated with CSM extract displayed no significant change at all the concentrations tested, with cell viability over 100% in all cases [97].

4.10 Biocompatibility of MC-PHAs with Vero and L929 cells by DAPI staining

Microcarrier compatibility studies with Vero and L929 cells, by staining with DAPI, a fluorescence dye that stains cell nuclei. This allows a clear image of the cells on the microcarrier to be seen under the fluorescent camera. The Cytodex1 microcarrier showed higher nuclear fluorescence than the MC-PHAs (Table 4.10).

Table 4.11 Microcarriers stained with DAPI at 96 h.

Condition	Cell	DAPI
Cytodex 1 L929 cell dynamic	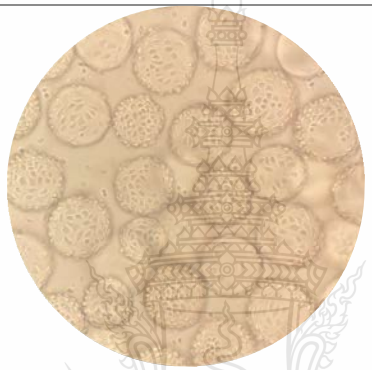	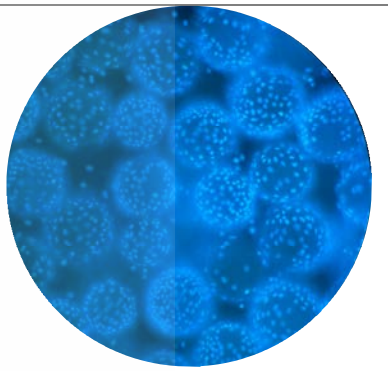
MC-PHAs L929 cell dynamic		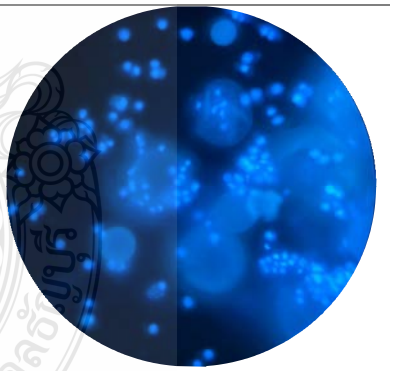
Cytodex 1 Vero cell dynamic	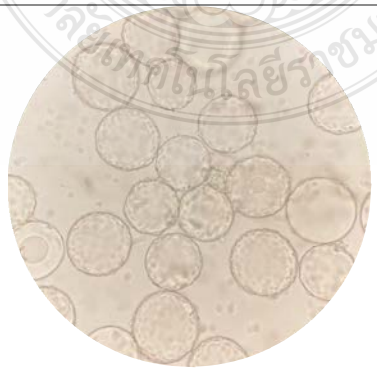	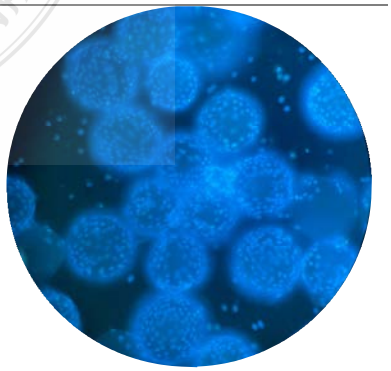

Table 4.11 Microcarriers stained with DAPI at 96 h. (Continued)

Condition	Cell	DAPI
MC-PHAs Vero cell dynamic	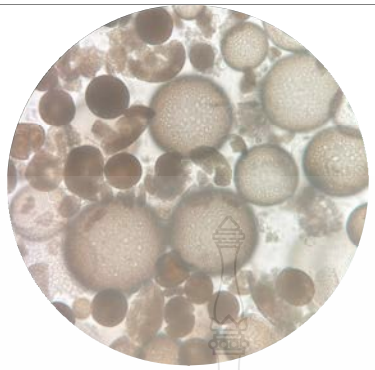	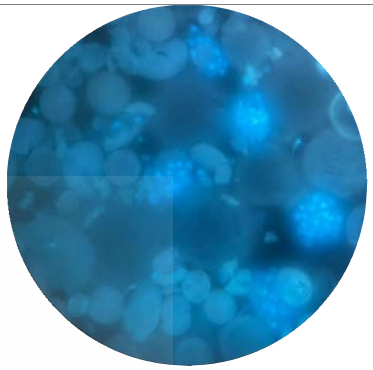

4.11 Cell growth rate and glucose content of cell culture media

4.11.1. Vero cell growth and glucose content of the cell culture medium

The culture of Vero cells adheres to dynamic Cytodex1 and MC-PHAs in Eagle's Minimum Essential Medium (MEM) supplemented with 10% FBS at 0, 24, 48, 72, 96, 120 and 144 h. Using a starter cell concentration of $1x10^6$ cell/mL. It was found that the growth of the cells on MC-PHAs increased cell slowly compared to cell on cytodex1. The amount of glucose in food decreases with cell growth shown in the Figure 4.16.

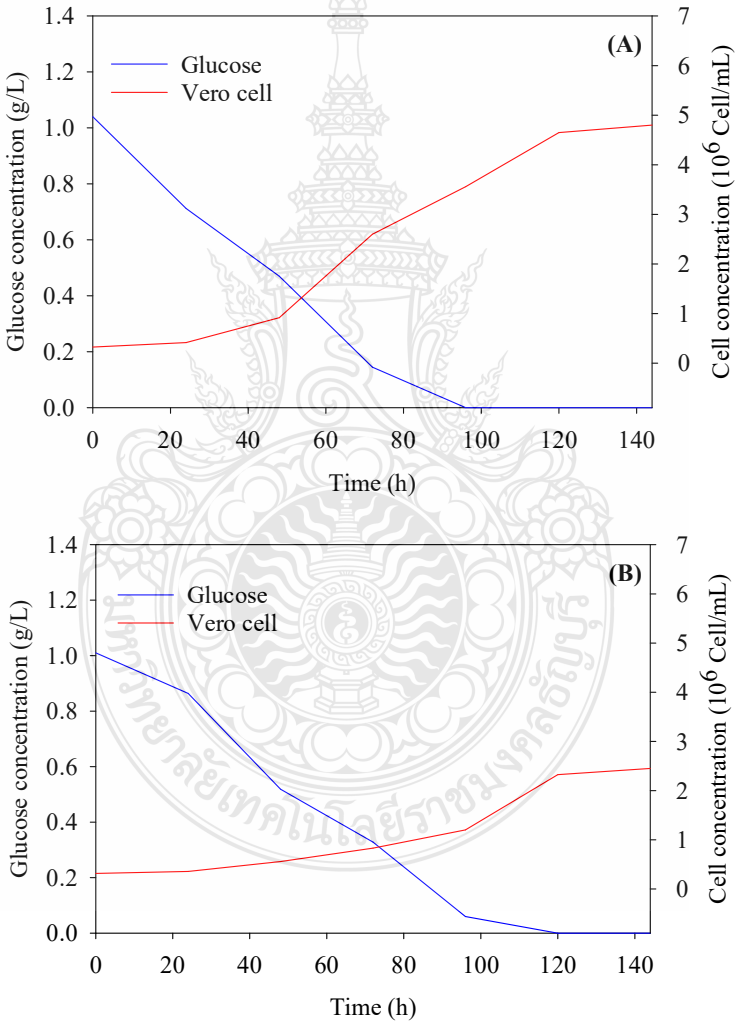

Figure 4.16 Vero cells adhered to microcarriers and the amount of glucose in cell culture at times 0, 24, 48, 72, 96, 120, and 144 h. (A) cytodex1 dynamic and (B) MC-PHAs dynamic

4.11.2. L929 cell growth and glucose content of the cell culture medium

The culture of L929 cells adheres to dynamic Cytodex1 and MC-PHAs in Eagle's Minimum Essential Medium (MEM) supplemented with 10% FBS at 0, 24, 48, 72, 96, 120 and 144 h. Using a starter cell concentration of $1x10^7$ cell/mL. It was found that the growth of the cells on MC-PHAs increased cell slowly compared to cell on cytodex1. The amount of glucose in food decreases with cell growth. Shown in the Figure 4.17.

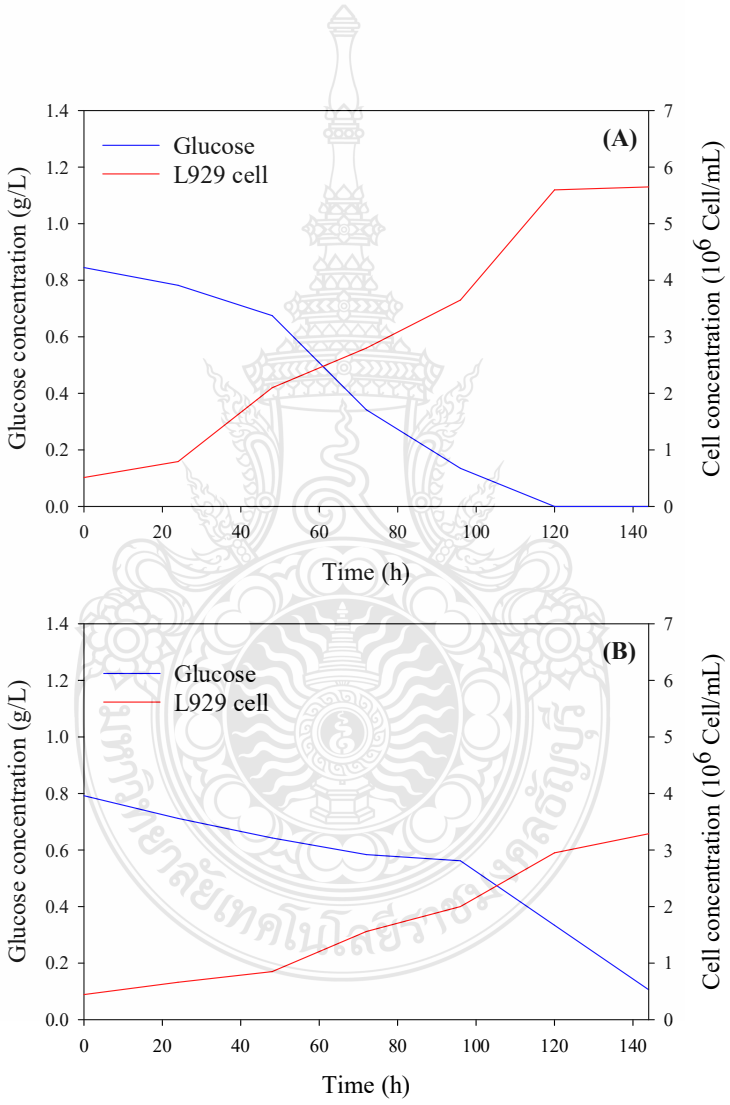

Figure 4.17 L929 cells adhered to microcarriers and the amount of glucose in cell culture at times 0, 24, 48, 72, 96, 120, and 144 h. (A) cytodex1 dynamic and (B) MC-PHAs dynamic

The results of culturing Vero and L929 cells on MC-PHAs showed that the highest cell concentrations were 2.45 x 10^6 and 3.29 x 10^6 cell/mL, respectively, at 144 h. Vero and L929 cells on cytodex1 showed that the highest cell concentrations were 4.80 x 10^6 and 5.65 x 10^6 cell/mL, respectively, at 144 h (Figure 4.16-4.17). From crystal violet staining in Figure 4.12-4.15, cells adhered to MC-PHAs were clearly less adherent than Cytodex1. The properties of MC-PHAs are not as good as Cytodex1 microcarrier. Therefore, MC-PHAs need to be developed for use in animal cell culture in the future.

Collagen conjugated poly(3-hydroxybutyrate) (P3HB) microparticles (Col-P3HB-MPs) had more cells adhered to their surface than the poly(3-hydroxybutyrate) (P3HB) microparticles (P3HB-MP) group did, as demonstrated by staining with the DAPI fluorescent dye. These findings revealed that collagen modification of the P3HB-MP surface was a more significant component promoting cell adhesion than initial electrostatic interactions [147]. The development of anchorage-dependent cells in bioreactor systems is facilitated by microcarriers, which are support matrices. Cells in microcarrier (MC) culture can develop as multilayers within the pores of microporous structures, which are often suspended in culture medium and on the surface of tiny spheres in a monolayer configuration. Many optimization efforts have been made since Van Wezel, 1967 [148] first proposed this intriguing strategy, with the main goal being to enhance the physicochemical characteristics of MC [149], [150]. These investigations have led to different microcarriers with different surfaces, charges, structures, and other properties. This allows the surface properties of the microcarriers to be tailored according to cell type [151]. Cytodex type-1 microcarriers are made of cross-linked dextran matrix these positive charged groups found throughout the entire matrix of the microcarriers are believed to promote attachment and growth of cells especially for anchorage dependent cell lines [148]. In this research, the surface area was improved to increase the charge of the microcarriers, by using gelatin to coat the surface of the MC-PHAs. This allows the cells to adhere to the microcarriers. However, the time required for coating is limited. Therefore, the gelatin has not penetrated well enough into the microcarrier. This causes the cells to still be unable to adhere and spread out well.

CHAPTER 5
CONCLUSIONS

5.1 Conclusion

In this research, we aimed to increase the PHA accumulation in *Novosphingobium* sp. THA_AIK7 by optimizing carbon, nitrogen, and phosphorus sources. The extraction condition by silica gel was investigated to increase the PHA yield. Fabrication process of microcarriers from PHA by emulsion technique and the use of microcarriers in dynamic animal cell culture.

Novosphingobium sp. THA_AIK7 was cultured in mineral salt medium (MSM) with various carbon, nitrogen, and phosphorus sources. Crude glycerol, MSG, and $Na_2HPO_4 \cdot 7H_2O$ were the best sources for growth and PHA production. Experimental and predicted values from the logistic and Gompertz models trended to go in the same direction proving that these models could explain microbial growth and PHA production accurately. The extracted polymer structure was verified as a PHBV copolymer by ^1H NMR spectrometry analysis. The HV monomer contents in the polymers derived from crude glycerol, fructose, and glycerol were 10.85, 10.16, and 6.59 mol%, respectively. Results indicated that *Novosphingobium* sp. THA_AIK7 produced a PHBV copolymer from various carbon sources without precursor addition. The endotoxin-free PHBV polymer produced from *Novosphingobium* sp. THA_AIK7 showed promise for medical applications. The optimum conditions of PHAs extraction using silica gel were 80 mg of the cell, silica gel 30 g, and temperature at 50°C, with the amount of PHA extracted at 41 mg. This extraction method could retrieve PHAs up to 51.25% of cell dry weight, which was higher than the hypochlorite extraction method.

The optimum conditions of the fabrication process of microcarriers from PHA by emulsion technique were PHA 0.24 g, PVA 0.5 %, NH_5CO_3 1 %, and Stirrer speed at 500 rpm. It was found that the average diameter of MC-PHAs was 125.864 µm and the average pore size was 0.970 µm. The diameter of MC-PHAs was not different from that of the commercial microcarriers, Cytodex1. The yield of fabricated MC-PHAs was 0.1640 g from originate PHA 0.24 g, accounting for 68.33%. MC-PHAs were used for Vero and L929 culturing using starter cells at $1x10^6$ cells/mL. It was found that the cells

were able to adhere to MC-PHAs but could not spread and grows the surface of MC-PHAs. Hence, the highest concentrations of Vero and L929 cells reached only $2.45x10^6$ and $3.29x10^6$ cells/mL, respectively, at 144 h. Glucose concentration in the medium decreased with cell growth. Cytotoxicity assay of PHA microcarriers found that the percent viability of Vero and L929 cells were 92% and 100%, respectively.

In summary, *Novosphingobium* sp. THA_AIK7 produced a PHBV copolymer from crude glycerol without precursor addition. Silica gel extraction method could retrieve PHAs up to 51.25% of cell dry weight. PHA can be fabricated into microcarriers and is not toxic to animal cells. However, the properties of MC-PHAs would be improved to enhance cell adhesion and proliferation in the next step.

5.2 Suggestion

Suggestion for future work since PHAs do not have a charge, the charge should be added to MC-PHAs so that cells can adhere and grow on MC-PHAs by coating them with charged substances such as gelatin or collagen, and the coating time should be appropriate. Modify the molding method, such as using a tool to control microcarrier pellet drop to get microcarriers of similar size.

List of Bibliography

[1] G.-Q. Chen, Q. Wu, Y. K. Jung, and S. Y. Lee, "PHA/PHB," *Comprehensive Biotechnology*, pp. 217–227, 2011.

[2] L. M, "Produits de deshydration et de polymerisation de L'acide β=oxybutyrique," *Bull. Soc. Chim. Biol.*, vol. 8, pp. 770–782, 1926.

[3] T. Palmeiro-Sánchez, V. O'Flaherty, and P. N. L. Lens, "Polyhydroxyalkanoate bio-production and its rise as biomaterial of the future," *Journal of Biotechnology*, vol. 348, pp. 10–25, Mar. 2022.

[4] K. Gonzalez, R. Navia, S. Liu, and M. Cea, "Biological approaches in polyhydroxyalkanoates recovery," *Current Microbiology*, vol. 78, no. 1, pp. 1–10, Jan. 2021.

[5] J. Teeka, T. Imai, A. Reungsang, X. Cheng, and E. Yuliani, "Characterization of polyhydroxyalkanoates (PHAs) biosynthesis by isolated *Novosphingobium* sp. THA_AIK7 using crude glycerol," *Journal of Industrial Microbiology and Biotechnology*, vol. 39, no. 5, pp. 749–758, May 2012.

[6] K. Hameed, I. Gatea, and A. Hussein, "Biosynthesis and optimization of polyhydroxyalkanoate (PHA) production by *Acinetobacter lwoffii* Isolate," *Journal of the American Society of Nephrology*, vol. 3, no. 1, pp. 90–103, Feb. 2023.

[7] S. Y. Lee, "Bacterial polyhydroxyalkanoates," *Biotechnology and Bioengineering*, vol. 49, no. 1, pp. 1–14, 1996.

[8] J. Teeka, A. areesirisuk, S. Chamdit, T. Hormsombuta, J. Buaparueanga, N. Chaylim, N. Suksalee and N. Srisamran, "Method for extracting polyhydroxyalkanoate bioplastic from bacteria by silica gel," Thai petty patent, no. 14439, 5 October, 2018.

[9] C. F. Bellani, J. Ajeian, L. Duffy, M. Miotto, L. Groenewegen, and C. J. Connon, "Scale-up technologies for the manufacture of adherent cells," *Frontiers in Nutrition*, vol. 7, p. 575146, Nov. 2020.

List of Bibliography (Continued)

[10] B. Li, X. Wang, Y. Wang, W. Gou, and X. Yuan, "Past, present, and future of microcarrier-based tissue engineering," *Journal of Orthopaedic Translation*, vol. 3, no. 2, pp. 51–57, Apr. 2015.

[11] J. M. B. T. Cavalheiro, M. C. M. D. de Almeida, C. Grandfils, and M. M. R. da Fonseca, "Poly(3-hydroxybutyrate) production by *Cupriavidus necator* using waste glycerol," *Process Biochemistry*, vol. 44, no. 5, pp. 509–515, May 2009.

[12] Z. A. Raza, S. Abid, and I. M. Banat, "Polyhydroxyalkanoates: Characteristics, production, recent developments and applications," *International Biodeterioration & Biodegradation*, vol. 126, pp. 45–56, Jan. 2018.

[13] S. Chanprateep, "Current trends in biodegradable polyhydroxyalkanoates," *Journal of Bioscience and Bioengineering*, vol. 110, no. 6, pp. 621–632, Dec. 2010.

[14] G.-Q. Chen, Q. Wu, Y. K. Jung, and S. Y. Lee, "PHA/PHB," *Comprehensive Biotechnology*, pp. 217–227, 2011.

[15] Z. A. Raza, S. Abid, and I. M. Banat, "Polyhydroxyalkanoates: Characteristics, production, recent developments and applications," *International Biodeterioration & Biodegradation*, vol. 126, pp. 45–56, Jan. 2018.

[16] R. A. J. Verlinden, D. J. Hill, M. A. Kenward, C. D. Williams, and I. Radecka, "Bacterial synthesis of biodegradable polyhydroxyalkanoates," *Journal of Applied Microbiology*, vol. 102, no. 6, pp. 1437–1449, Jun. 2007.

[17] S. F. Williams, D. P. Martin, D. M. Horowitz, and O. P. Peoples, "PHA applications: addressing the price performance issue: I. Tissue engineering," *International Journal of Biological Macromolecules*, vol. 25, no. 1, pp. 111–121, Jun. 1999.

[18] S. Obruca, P. Sedlacek, E. Slaninova, I. Fritz, and C. Daffert, "Novel unexpected functions of PHA granules," *Applied Microbiology and Biotechnology*, vol. 104, no. 11, pp. 4795–4810, Jun. 2020.

[19] G. Y. A. Tan, C. L. Chen, L. Li, L. Ge, and L. Wang, "Start a research on biopolymer polyhydroxyalkanoate (PHA): A review," Polymers, vol. 6, no. 3, Art. no. 3, Mar. 2014.

List of Bibliography (Continued)

[20] S. Khanna and A. Srivastava, "Recent advances in microbial polyhydroxyalkanoates," *Process Biochemistry*, vol. 40, pp. 607–619, Feb. 2005.

[21] A. Peregrina, J. Martins-Lourenço, F. Freitas, M. A. M. Reis, and C. M. Arraiano, "Post-transcriptional control in the regulation of polyhydroxyalkanoates synthesis," *Life*, vol. 11, no. 8, p. 853, Aug. 2021.

[22] M. Koller, "Biodegradable and biocompatible polyhydroxy-alkanoates (PHA): auspicious microbial macromolecules for pharmaceutical and therapeutic applications," *Molecules*, vol. 23, no. 2, Art. no. 2, Feb. 2018.

[23] C. Kourmentza, J. Plácido, N. Venetsaneas, A. Burniol-Figols, C. Varrone, H. N. Gavala, and M. A. M. Reis, "Recent advances and challenges towards sustainable polyhydroxyalkanoate (PHA) production," *Bioengineering (Basel)*, vol. 4, no. 2, p. 55, Jun. 2017.

[24] D. Jendrossek and R. Handrick, "Microbial degradation of polyhydroxyalkanoates," *Annual Review of Microbiology*, vol. 56, pp. 403–432, 2002.

[25] L. L. Madison and G. W. Huisman, "Metabolic engineering of poly(3-hydroxyalkanoates): from DNA to plastic," *Microbiology and Molecular Biology Reviews*, vol. 63, no. 1, pp. 21–53, Mar. 1999.

[26] M. Domínguez Díaz and A. Romo-Uribe, "ice | science Viscoelastic behavior of biodegradable polyhydroxyalkanoates Domínguez-Díaz and Romo-Uribe," *Bioinspired, Biomimetic and Nanobiomaterials*, vol. 1, pp. 214–220, Aug. 2012.

[27] S. F. Williams and D. P. Martin, "Applications of polyhydroxyalkanoates (PHA) in medicine and pharmacy," in *Biopolymers Online*, John Wiley & Sons, Ltd, 2005.

[28] Y. K. Leong, P. L. Show, C. W. Ooi, T. C. Ling, and J. C.-W. Lan, "Current trends in polyhydroxyalkanoates (PHAs) biosynthesis: Insights from the recombinant *Escherichia coli*," *Journal of Biotechnology*, vol. 180, pp. 52–65, Jun. 2014.

[29] B. Lukasiewicz, P. Basnett, R. Nigmatullin, R. Matharu, J. C. Knowles, and I. Roy, "Binary polyhydroxyalkanoate systems for soft tissue engineering," *Acta Biomaterialia*, vol. 71, pp. 225–234, Apr. 2018.

List of Bibliography (Continued)

[30] A. T. Rebocho, J. R. Pereira, F. Freitas, L. A. Neves, and V. D. Alves, "Production of medium-chain length polyhydroxyalkanoates by *Pseudomonas citronellolis* grown in apple pulp waste," *Applied Food Biotechnology*, vol. 6, no. 1, Art. no. 1, Jan. 2019.

[31] S. Y. Lee, H. N. Chang, M. Hiroto, H. Nishimura, Y. Kodera, F. Kawai, P. Rusin, H. L. Ehrlich, S. Y. Lee, H. N. Chang, S. A. Markov, M. J. Bazin, D. O. Hall, A. L. Gutman, M. Shapira, Y. Inada, and A. Matsushima, "Production of poly(hydroxyalkanoic acid)," in *Microbial and Eznymatic Bioproducts*, Berlin, Heidelberg: Springer, 1995, pp. 27–58.

[32] Muhammadi, Shabina, M. Afzal, and S. Hameed, "Bacterial polyhydroxyalkanoates-eco-friendly next generation plastic: Production, biocompatibility, biodegradation, physical properties and applications," *Green Chemistry Letters and Reviews*, vol. 8, no. 3–4, pp. 56–77, Oct. 2015.

[33] J. Ihssen, D. Magnani, L. Thöny-Meyer, and Q. Ren, "Use of extracellular medium chain length polyhydroxyalkanoate depolymerase for targeted binding of proteins to artificial poly[(3-hydroxyoctanoate)-co-(3-hydroxyhexanoate)] granules," *Biomacromolecules*, vol. 10, no. 7, pp. 1854–1864, Jul. 2009.

[34] T. Volova, E. Shishatskaya, V. Sevastianov, S. Efremov, and O. Mogilnaya, "Results of biomedical investigations of PHB and PHB/PHV fibers," *Biochemical Engineering Journal*, vol. 16, no. 2, pp. 125–133, Nov. 2003.

[35] E. I. Shishatskaya, I. A. Khlusov, and T. G. Volova, "A hybrid PHB–hydroxyapatite composite for biomedical application: production, in vitro and in vivo investigation," *Journal of Biomaterials Science, Polymer Edition*, vol. 17, no. 5, pp. 481–498, Jan. 2006.

[36] O. Perlova, K. Gerth, S. Kuhlmann, Y. Zhang, and R. Müller, "Novel expression hosts for complex secondary metabolite megasynthetases: Production of myxochromide in the thermopilic isolate *Corallococcus macrosporus* GT-2," *Microbial Cell Factories*, vol. 8, no. 1, p. 1, Jan. 2009.

List of Bibliography (Continued)

[37] D. Grande, J. Ramier, D. L. Versace, E. Renard, and V. Langlois, "Design of functionalized biodegradable PHA-based electrospun scaffolds meant for tissue engineering applications," *New Biotechnology*, vol. 37, pp. 129–137, Jul. 2017.

[38] S. C. Diniz, M. K. Taciro, J. G. Cabrera Gomez, and J. G. da C. Pradella, "High-Cell-Density cultivation of *pseudomonas putida* IPT 046 and medium-chain-length polyhydroxyalkanoate production from sugarcane carbohydrates," *Applied Biochemistry and Biotechnology* vol. 119, no. 1, pp. 51–69, Oct. 2004.

[39] G. J. Kim, I. Y. Lee, S. C. Yoon, Y. C. Shin, and Y. H. Park, "Enhanced yield and a high production of medium-chain-length poly(3-hydroxyalkanoates) in a two-step fed-batch cultivation of *Pseudomonas putida* by combined use of glucose and octanoate," *Enzyme and Microbial Technology*, vol. 20, no. 7, pp. 500–505, May 1997.

[40] S. Y. Lee, H. H. Wong, J. Choi, S. H. Lee, S. C. Lee, and C. S. Han, "Production of medium-chain-length polyhydroxyalkanoates by high-cell-density cultivation of *Pseudomonas putida* under phosphorus limitation," *Biotechnology and Bioengineering*, vol. 68, no. 4, pp. 466–470, 2000.

[41] B. S. Kim, "Production of medium chain length polyhydroxyalkanoates by fed-batch culture of *Pseudomonas oleovorans*," *Biotechnology Letters*, vol. 24, no. 2, pp. 125–130, Jan. 2002.

[42] B. A. Ramsay, I. Saracovan, J. A. Ramsay, and R. H. Marchessault, "Continuous Production of long-side-chain Poly-β-Hydroxyalkanoates by *Pseudomonas oleovorans*," *Applied and Environmental Microbiology*, vol. 57, no. 3, pp. 625–629, Mar. 1991.

[43] S. Panitsara, "ANH X Kerry," *A.N.H. Scientific Marketing Co.,Ltd.*, www.anhsci.com/kerry, Jun. 2020.

[44] P. Dixit, A. Mehta, G. Gahlawat, G. S. Prasad, and A. R. Choudhury, "Understanding the effect of interaction among aeration, agitation and impeller positions on mass transfer during pullulan fermentation by *Aureobasidium pullulans*," *RSC Advances.*, vol. 5, no. 49, pp. 38984–38994, Apr. 2015.

List of Bibliography (Continued)

[45] G. Gahlawat and A. K. Srivastava, "Development of a mathematical model for the growth associated polyhydroxybutyrate fermentation by *Azohydromonas australica* and its use for the design of fed-batch cultivation strategies," *Bioresour Technol*, vol. 137, pp. 98–105, Jun. 2013.

[46] S. Khanna and A. K. Srivastava, "Computer simulated fed-batch cultivation for over production of PHB: A comparison of simultaneous and alternate feeding of carbon and nitrogen," *Biochemical Engineering Journal*, vol. 27, no. 3, pp. 197–203, Jan. 2006.

[47] G. Kaur and I. Roy, "Strategies for large-scale production of polyhydroxyalkanoates," *Chemical and Biochemical Engineering Quarterly*, vol. 29, pp. 157–172, Jul. 2015.

[48] Md. S. I. Mozumder, H. De Wever, E. I. P. Volcke, and L. Garcia-Gonzalez, "A robust fed-batch feeding strategy independent of the carbon source for optimal polyhydroxybutyrate production," *Process Biochemistry*, vol. 49, no. 3, pp. 365–373, Mar. 2014.

[49] F. Cerrone, R. Davis, S. T. Kenny, T. Woods, A. O'Donovan, V. K. Gupta, M. Tuohy, R. P. Babu, P. O'Kiely, and K. O'Connor, "Use of a mannitol rich ensiled grass press juice (EGPJ) as a sole carbon source for polyhydroxyalkanoates (PHAs) production through high cell density cultivation," *Bioresour Technol*, vol. 191, pp. 45–52, Sep. 2015.

[50] M. S. I. Mozumder, H. De Wever, E. Volcke, and L. Garcia-Gonzalez, "A robust fed-batch feeding strategy independent of the carbon source for optimal polyhydroxybutyrate production," *Process Biochemistry*, vol. 49, no. 3, Art. no. 3, 2014.

[51] C. Haas, T. El-Najjar, N. Virgolini, M. Smerilli, and M. Neureiter, "High cell-density production of poly(3-hydroxybutyrate) in a membrane bioreactor," *New Biotechnol*, vol. 37, no. Pt A, pp. 117–122, Jul. 2017.

List of Bibliography (Continued)

[52] I. Zainab-L and K. Sudesh, "High cell density culture of *Cupriavidus necator* H16 and improved biological recovery of polyhydroxyalkanoates using mealworms," *Journal of Biotechnology*, vol. 305, pp. 35–42, Nov. 2019.

[53] A. Salakkam and C. Webb, "Production of poly(3-hydroxybutyrate) from a complete feedstock derived from biodiesel by-products (crude glycerol and rapeseed meal)," *Biochemical Engineering Journal*, vol. 137, pp. 358–364, Sep. 2018.

[54] Y. J. Sohn, H. T. Kim, K. A. Baritugo, H. M. Song, M. H. Ryu, K. H. Kang, S. Y. Jo, H. Kim, Y. J. Kim, J. I. Choi, S. K. Park, J. C. Joo, and S. J. Park, "Biosynthesis of polyhydroxyalkanoates from sucrose by metabolically engineered Escherichia coli strains," International Journal of Biological Macromolecules, vol. 149, pp. 593–599, Apr. 2020.

[55] W. Blunt, C. Dartiailh, R. Sparling, D. J. Gapes, D. B. Levin, and N. Cicek, "Development of high cell density cultivation strategies for improved medium chain length polyhydroxyalkanoate productivity using *Pseudomonas putida* LS46," *Bioengineering*, vol. 6, no. 4, Art. no. 4, Dec. 2019.

[56] S. Kitamura and Y. Doi, "Staining method of poly(3-hydroxyalkanoic acids) producing bacteria by nile blue," *Biotechnol Tech*, vol. 8, no. 5, pp. 345–350, May 1994.

[57] S. S. Sawant, B. K. Salunke, and B. S. Kim, "Degradation of corn stover by fungal cellulase cocktail for production of polyhydroxyalkanoates by moderate halophile *Paracoccus* sp. LL1," *Bioresource Technology*, vol. 194, pp. 247–255, Oct. 2015.

[58] M. Muhammad, H. Aloui, C. Khomlaem, C. T. Hou, and B. S. Kim, "Production of polyhydroxyalkanoates and carotenoids through cultivation of different bacterial strains using brown algae hydrolysate as a carbon source," *Biocatalysis and Agricultural Biotechnology*, vol. 30, p. 101852, Nov. 2020.

[59] A. Moungprayoon, S. Lunprom, A. Reungsang, and A. Salakkam, "High cell density cultivation of *Paracoccus* sp. on sugarcane juice for poly(3hydrox ybutyrate) production," *Front. Bioeng. Biotechnol.*, vol. 10, p. 878688, May, 2022.

List of Bibliography (Continued)

[60] M. H. Madkour, D. Heinrich, M. A. Alghamdi, I. I. Shabbaj, and A. Steinbüchel, "PHA recovery from biomass," *Biomacromolecules*, vol. 14, no. 9, pp. 2963–2972, Sep. 2013.

[61] C. Pérez Rivero, J. López-Gómez, and I. Roy, "A sustainable approach for the downstream processing of bacterial polyhydroxyalkanoates: State-of-the-art and latest developments," *Biochemical Engineering Journal*, vol. 150, p. 107283, Jun. 2019.

[62] S.-J. Hong, H.-S. Yu, and H.-W. Kim, "Tissue engineering polymeric microcarriers with macroporous morphology and bone-bioactive surface," *Macromolecular Bioscience*, vol. 9, no. 7, pp. 639–645, 2009.

[63] J. Weber, L. Romeo, and P. Dolley-Sonneville, "Human mesenchymal stem cell growth on corning® denatured collagen dissolvable microcarriers in a 5L bioreactor," p. 8.

[64] Z. Zhang, T. W. Eyster, and P. X. Ma, "Nanostructured injectable cell microcarriers for tissue regeneration," *Nanomedicine (Lond)*, vol. 11, no. 12, pp. 1611–1628, Jun. 2016.

[65] L. E. Freed, J. C. Marquis, A. Nohria, J. Emmanual, A. G. Mikos, and R. Langer, "Neocartilage formation in vitro and in vivo using cells cultured on synthetic biodegradable polymers," *Journal of Biomedical Materials Research*, vol. 27, no. 1, pp. 11–23, 1993.

[66] X. Zhang, Z. Deng, H. Wang, Z. Yang, and W. Guo, "Expansion and delivery of human fibroblasts on micronized acellular dermal matrix for skin regeneration," *Biomaterials*, vol. 30, no. 14, pp. 2666–2674, May 2009.

[67] Y. Zhou, Z. Deng, H. Wang, Z. Yang, W. Guo, Y. Li, D. Ma, C. Yu, Y. Zhang, and Y. Jin, "Expansion and delivery of adipose-derived mesenchymal stem cells on three microcarriers for soft tissue regeneration," *Tissue Engineering Part A*, vol. 17, no. 23–24, pp. 2981–2997, Dec. 2011.

[68] J. Malda and C. G. Frondoza, "Microcarriers in the engineering of cartilage and bone," *Trends Biotechnol*, vol. 24, no. 7, pp. 299–304, Jul. 2006.

List of Bibliography (Continued)

[69] G. Yourek, S. M. McCormick, J. J. Mao, and G. C. Reilly, "Shear stress induces osteogenic differentiation of human mesenchymal stem cells," *Regenerative Medicine*, vol. 5, no. 5, pp. 713–724, Sep. 2010.

[70] B. Koh, N. Sulaiman, M. B. Fauzi, J. X. Law, M. H. Ng, R. B. H. Idrus, and M. D. Yazid, "Three dimensional microcarrier system in mesenchymal stem cell culture: a systematic review," *Cell Bioscience*, vol. 10, p. 75, Jun. 2020.

[71] Van Wezel and A. L, "Growth of Cell-strains and Primary Cells on Micro-carriers in Homogeneous Culture," *Nature*, vol. 216, no. 5110, Art. no. 5110, Oct. 1967.

[72] P. H. Jakob, J. Kehrer, P. Flood, C. Wiegel, and U. Haselmann, "A 3-D cell culture system to study epithelia functions using microcarriers," *Cytotechnology*, vol. 68, no. 5, pp. 1813–1825, Oct. 2016.

[73] S. Sart, S. N. Agathos, and Y. Li, "Engineering stem cell fate with biochemical and biomechanical properties of microcarriers," *Biotechnology Progress*, vol. 29, no. 6, pp. 1354–1366, Dec. 2013.

[74] B. Li, X. Wang, Y. Wang, W. Gou, and X. Yuan, "Past, present, and future of microcarrier-based tissue engineering," *Journal of Orthopaedic Translation*, vol. 3, no. 2, pp. 51–57, Apr. 2015.

[75] H. Tavassoli, S. N. Alhosseini, A. Tay, P. P. Y. Chan, S. K. Weng Oh, and M. E. Warkiani, "Large-scale production of stem cells utilizing microcarriers: A biomaterials engineering perspective from academic research to commercialized products," *Biomaterials*, vol. 181, pp. 333–346, Oct. 2018.

[76] S. Derakhti, S. H. Safiabadi-Tali, G. Amoabediny, and M. Sheikhpour, "Attachment and detachment strategies in microcarrier-based cell culture technology: A comprehensive review," *Materials Science and Engineering: C*, vol. 103, p. 109782, Oct. 2019.

[77] C.Y. Wu, D. Stoecklein, A. Kommajosula, J. Lin, K. Owsley, D. Di Carlo, and B. Ganapathysubramanian, "Shaped 3D microcarriers for adherent cell culture and analysis," *Microsyst Nanoeng*, vol. 4, no. 1, Art. no. 1, Aug. 2018.

List of Bibliography (Continued)

[78] P. Li, F. Liu, C. Wu, W. Jiang, and G. Zhao, "Feasibility of human hair follicle-derived mesenchymal stem cells/CultiSpher®-G constructs in regenerative medicine," *Cell Tissue Research,* vol. 362, no. 1, pp. 69–86, Oct. 2015.

[79] T. Hoffman, A. Khademhosseini, and R. Langer, "Chasing the paradigm: Clinical translation of 25 years of tissue engineering," *Tissue Engineering Part A*, vol. 25, Feb. 2019.

[80] L. Nguyen, S. Bang, and I. Noh, "Tissue regeneration of human mesenchymal stem cells on porous gelatin micro-carriers by long-term dynamic in vitro culture," *Tissue Engineering and Regenerative Medicine*, vol. 16, no. 1, pp. 19–28, Feb. 2019.

[81] F. Yang, X. Niu, X. Gu, C. Xu, W. Wang, and Y. Fan, "Biodegradable magnesium-incorporated poly(l-lactic acid) microspheres for manipulation of drug release and alleviation of inflammatory response," *ACS applied materials and interfaces*, vol. 11, no. 26, pp. 23546–23557, Jul. 2019.

[82] D. F. Williams, "On the mechanisms of biocompatibility," *Biomaterials*, vol. 29, no. 20, pp. 2941–2953, Jul. 2008.

[83] Z. Zhou, W. Wu, J. Fang, and J. Yin, "Polymer-based porous microcarriers as cell delivery systems for applications in bone and cartilage tissue engineering," *International Materials Reviews*, vol. 66, no. 2, pp. 77–113, Feb. 2021.

[84] J. Lee, Y. J. Oh, S. K. Lee, and K. Y. Lee, "Facile control of porous structures of polymer microspheres using an osmotic agent for pulmonary delivery," *Journal of Controlled Release*, vol. 146, no. 1, pp. 61–67, Aug. 2010.

[85] S.-W. Choi, Y.-C. Yeh, Y. Zhang, H.-W. Sung, and Y. Xia, "Uniform beads with controllable pore sizes for biomedical applications," *Small*, vol. 6, no. 14, pp. 1492–1498, Jul. 2010.

[86] C. -C. Huang, H. J. Wei, Y. C. Yeh, J. J. Wang, and W. W. Lin, "Injectable PLGA porous beads cellularized by hAFSCs for cellular cardiomyoplasty," *Biomaterials*, vol. 33, no. 16, pp. 4069–4077, Jun. 2012.

List of Bibliography (Continued)

[87] W. L. Randle, J. M. Cha, Y. S. Hwang, K. L. A. Chan, S. G. Kazarian, J. M. Polak, and A. Mantalaris, "Integrated 3-dimensional expansion and osteogenic differentiation of murine embryonic stem cells," *Tissue Engineering*, vol. 13, no. 12, pp. 2957–2970, Dec. 2007.

[88] C. C. Ribeiro, C. C. Barrias, and M. A. Barbosa, "Preparation and characterisation of calcium-phosphate porous microspheres with a uniform size for biomedical applications," *Journal of Materials Science: Materials in Medicine*, vol. 17, no. 5, pp. 455–463, May 2006.

[89] H. Cai, S. Sharma, W. Liu, W. Mu, W. Liu, X. Zhang, and Y. Deng, "Aerogel microspheres from natural cellulose nanofibrils and their application as cell culture scaffold," *Biomacromolecules*, vol. 15, Jun. 2014.

[90] S. Podaralla, R. Sistla, T. Saini, and PrakashV. D. Diwan, "Influence of microencapsulation method and peptide loading on formulation of poly(lactide-co-glycolide) insulin nanoparticles," *Die Pharmazie*, vol. 61, pp. 613–7, Aug. 2006.

[91] ATCC "Vero CCL-81," https://www.atcc.org/products/ccl-81, Mar. 2022.

[92] ATCC "NCTC clone 929 [L cell, L-929, derivative of Strain L] - CCL-1 | ATCC," https://www.atcc.org/products/ccl-1, Dec. 2023.

[93] J. Teeka, D. Kaewpa, A. Thepkila, A. Adam, P. Kodcharin, and T. Imai, "Influence of carbon and nitrogen sources on the performance of Polyhydoxyalkanoates (PHA) production using *Novosphingobium* sp. THA_AIK7 in batch operation," p. 10, 2016.

[94] H. J. Chung, I. K. Kim, T. G. Kim, and T. G. Park, "Highly open porous biodegradable microcarriers: *In Vitro* cultivation of chondrocytes for injectable delivery," *Tissue Engineering Part A*, vol. 14, no. 5, pp. 607–615, May 2008.

[95] D.-X. Wei, J.-W. Dao, H.-W. Liu, and G.-Q. Chen, "Suspended polyhydroxyalkanoate microspheres as 3D carriers for mammalian cell growth," *Artificial Cells, Nanomedicine, and Biotechnology*, vol. 46, no. sup2, pp. 473–483, Nov. 2018.

List of Bibliography (Continued)

[96] T. K. Kim, J. J. Yoon, D. S. Lee, and T. G. Park, "Gas foamed open porous biodegradable polymeric microspheres," *Biomaterials*, vol. 27, no. 2, pp. 152–159, Jan. 2006.

[97] L. Huang, L. Xiao, A. Jung Poudel, J. Li, and P. Zhou, "Porous chitosan microspheres as microcarriers for 3D cell culture," *Carbohydr Polymer*, vol. 202, pp. 611–620, Dec. 2018.

[98] B. A. Ramsay, K. Lomaliza, C. Chavarie, B. Dubé, P. Bataille, and J. A. Ramsay, "Production of poly-(beta-hydroxybutyric-co-beta-hydroxyvaleric) acids.," *Applied and Environmental Microbiology*, vol. 56, no. 7, pp. 2093–2098, Jul. 1990.

[99] M.-H. Liu, Y.-J. Chen, and C.-Y. Lee, "Characterization of medium-chain-length polyhydroxyalkanoate biosynthesis by *Pseudomonas mosselii* TO7 using crude glycerol," *Bioscience, Biotechnology, and Biochemistry*, vol. 82, no. 3, pp. 532–539, Mar. 2018.

[100] K. Zajšek and A. Goršek, "Modelling of batch kefir fermentation kinetics for ethanol production by mixed natural microflora," *Food and Bioproducts Processing*, vol. 88, no. 1, pp. 55–60, Mar. 2010.

[101] J. M. Dodić, D. G. Vučurović, S. N. Dodić, J. A. Grahovac, S. D. Popov, and N. M. Nedeljković, "Kinetic modelling of batch ethanol production from sugar beet raw juice," *Applied Energy*, vol. 99, pp. 192–197, Nov. 2012.

[102] W. J. Hillegas, J. varani, and D. L. Helmreich, "Collagen coated polystyrene microcarrier beads," United States Patent, Fab. 1991.

[103] C. Y. M. Hsu, T. Walsh, B. S. Borys, M. S. Kallos, and D. E. Rancourt, "An integrated approach toward the biomanufacturing of engineered cell therapy products in a stirred-suspension bioreactor," *Molecular Therapy - Methods & Clinical Development*, vol. 9, pp. 376–389, Jun. 2018.

[104] J. Teeka, D. Kaewpa, A. Thepkila, A. Adam, P. Kodcharin, and T. Imai, "Influence of carbon and nitrogen sources on the performance of Polyhydoxyalkanoates (PHA) production using *Novosphingobium* sp. THA_AIK7 in batch operation," p. 10, 2016.

List of Bibliography (Continued)

[105] S. Bloembergen, D. A. Holden, G. K. Hamer, T. L. Bluhm, and R. H. Marchessault, "Studies of composition and crystallinity of bacterial poly(β-hydroxybutyrate-co-β-hydroxyvalerate)," *Macromolecules*, vol. 19, no. 11, pp. 2865–2871, Nov. 1986.

[106] P. Bondioli and L. Della Bella, "An alternative spectrophotometric method for the determination of free glycerol in biodiesel," *European Journal of Lipid Science and Technology*, vol. 107, no. 3, pp. 153–157, 2005.

[107] K. Van Beylen, I. Papantoniou, and J.-M. Aerts, "Microcarrier screening and evaluation for dynamic expansion of human periosteum-derived progenitor cells in a xenogeneic free medium," *Front Bioeng Biotechnol*, vol. 9, p. 624890, 2021.

[108] J. Teeka, T. Imai, X. Cheng, A. Reungsang, T. Higuchi, K. Yamamoto, and M. Sekine, "Screening of PHA-producing bacteria using biodiesel-derived waste glycerol as a sole carbon source," *Journal of Water and Environment Technology*, vol. 8, no. 4, pp. 373–381, 2010.

[109] R. D. Ashby, D. K. Y. Solaiman, and T. A. Foglia, "Bacterial poly(hydroxyalkanoate) polymer production from the biodiesel co-product stream," *Journal of Polymers and the Environment*, vol. 12, no. 3, pp. 105–112, Jul. 2004.

[110] N. Poomipuk, A. Reungsang, and P. Plangklang, "Poly-β-hydroxyalkanoates production from cassava starch hydrolysate by *Cupriavidus* sp. KKU38," *International Journal of Biological Macromolecules*, vol. 65, pp. 51–64, Apr. 2014.

[111] R. Shenbagarathai, "Effect of nitrogen and calcium sources on growth and production of PHA of *Pseudomonas* sp. LDC-5 and its mutant," *Current Research Journal of Biological Sciences*, vol. 2, Jan. 2010.

[112] M. K. Gouda, A. E. Swellam, and S. H. Omar, "Production of PHB by a B*acillus megaterium* strain using sugarcane molasses and corn steep liquor as sole carbon and nitrogen sources," *Microbiological Research*, vol. 156, no. 3, pp. 201–207, 2001.

List of Bibliography (Continued)

[113] M. Beaulieu, Y. Beaulieu, J. Melinard, S. Pandian, and J. Goulet, "Influence of ammonium salts and cane molasses on growth of *Alcaligenes eutrophus* and production of polyhydroxybutyrate," *Applied and Environmental Microbiology*, vol. 61, no. 1, pp. 165–169, Jan. 1995.

[114] J. Quillaguamán, T. Doan-Van, H. Guzmán, D. Guzmán, J. Martín, A. Everest, and R. Hatti-Kaul., "Poly(3-hydroxybutyrate) production by *Halomonas boliviensis* in fed-batch culture," *Applied Microbiology and Biotechnology*, vol. 78, no. 2, pp. 227–232, Feb. 2008.

[115] G. García, J. E. Sosa-Hernández, L. I. Rodas-Zuluaga, C. Castillo-Zacarías, H. Iqbal, and R. Parra-Saldívar, "Accumulation of PHA in the microalgae *Scenedesmus* sp. under nutrient-deficient conditions," *Polymers*, vol. 13, no. 1, Art. no. 1, Jan. 2021.

[116] D. Bustamante, S. Segarra, M. Tortajada, D. Ramón, and C. Del-Cerro, "In silico prospection of microorganisms to produce polyhydroxyalkanoate from whey: Caulobacter segnis DSM 29236 as a suitable industrial strain," *Microbial Biotechnology* vol. 12, no. 3, pp. 487–501, May 2019.

[117] M. Gao, Y. Li, X. Ma, D. Li, and J. Li, "Biotransformation of palm oil wastewater to scl- and mcl-polyhydroxyalkanoates by mixed microbial consortia using different nitrogen and phosphorus sources," *Biomass Conversion and Biorefinery*, Oct. 2021.

[118] M. S. Divyashree, N. K. Rastogi, and T. R. Shamala, "A simple kinetic model for growth and biosynthesis of polyhydroxyalkanoate in Bacillus flexus," *New Biotechnology*, vol. 26, no. 1, pp. 92–98, Oct. 2009.

[119] X. He, H. Lu, W. Hu, T. Deng, and X. Gong, "*Novosphingobium percolationis* sp. nov. and *Novosphingobium huizhouense* sp. nov., isolated from landfill leachate of a domestic waste treatment plant," *International Journal of Systematic and Evolutionary Microbiology*, vol. 72, no. 5, p. 005394, 2022.

List of Bibliography (Continued)

[120] M. Koller and S. Obruča, "Biotechnological production of polyhydroxyalkanoates from glycerol: A review," *Biocatalysis and Agricultural Biotechnology*, vol. 42, p. 102333, Jul. 2022.

[121] Dr. P. Rathore, "Screening of PHA producing bacteria from diverse sources," *International Journal of Biosciences, ISSN: 2220- 6655(Print) 2222- 5234(online)*, vol. Vol.1, pp. 27–32, Jan. 2011.

[122] B. Yadav, A. Talan, R. D. Tyagi, and P. Drogui, "Concomitant production of value-added products with polyhydroxyalkanoate (PHA) synthesis: A review," *Bioresource Technology*, vol. 337, p. 125419, Oct. 2021.

[123] M. Kumar, A. Singhal, P. K. Verma, and I. S. Thakur, "Production and characterization of polyhydroxyalkanoate from lignin derivatives by *Pandoraea* sp. ISTKB," *ACS Omega*, vol. 2, no. 12, pp. 9156–9163, Dec. 2017.

[124] T. Sriyapai, T. Chuarung, K. Kimbara, S. Samosorn, and P. Sriyapai, "Production and optimization of polyhydroxyalkanoates (PHAs) from *Paraburkholderia* sp. PFN 29 under submerged fermentation," *Electronic Journal of Biotechnology*, vol. 56, pp. 1–11, Mar. 2022.

[125] N.-S. Lau, K.-K. Sam, and A. A.-A. Amirul, "Genome features of moderately halophilic polyhydroxyalkanoate-producing *Yangia* sp. CCB-MM3," *Stand Genomic Sci*, vol. 12, p. 12, Jan. 2017.

[126] J. Tao, C. Song, M. Cao, D. Hu, L. Liu, N. Liu, and S. Wang, "Thermal properties and degradability of poly(propylene carbonate)/poly(β-hydroxybutyrate-co-β-hydroxyvalerate) (PPC/PHBV) blends," *Polymer Degradation and Stability*, vol. 94, no. 4, pp. 575–583, Apr. 2009.

[127] R. D. Ashby, D. K. Y. Solaiman, and G. D. Strahan, "Efficient utilization of crude glycerol as fermentation substrate in the synthesis of poly(3-hydroxybutyrate) biopolymers," *Journal of the American Oil Chemists' Society*, vol. 88, no. 7, pp. 949–959, 2011.

List of Bibliography (Continued)

[128] J. Teeka, T. Imai, A. Reungsang, X. Cheng, and E. Yuliani, "Characterization of polyhydroxyalkanoates (PHAs) biosynthesis by isolated *Novosphingobium* sp. THA_AIK7 using crude glycerol," *Journal of Industrial Microbiology and Biotechnology*, vol. 39, no. 5, pp. 749–758, May 2012.

[129] C. Zhu, C. T. Nomura, J. A. Perrotta, A. J. Stipanovic, and J. P. Nakas, "Production and characterization of poly-3-hydroxybutyrate from biodiesel-glycerol by *Burkholderia cepacia* ATCC 17759," *Biotechnology Progress*, vol. 26, no. 2, pp. 424–430, 2010.

[130] G. Adamus, W. Sikorska, H. Janeczek, M. Kwiecień, M. Sobota, and M. Kowalczuk, "Novel block copolymers of atactic PHB with natural PHA for cardiovascular engineering: Synthesis and characterization," *European Polymer Journal*, vol. 48, no. 3, pp. 621–631, Mar. 2012.

[131] M. Patel, D. J. Gapes, R. H. Newman, and P. H. Dare, "Physico-chemical properties of polyhydroxyalkanoate produced by mixed-culture nitrogen-fixing bacteria," *Applied Microbiology and Biotechnology*, vol. 82, no. 3, pp. 545–555, Mar. 2009.

[132] C. Hermann-Krauss, M. Koller, A. Muhr, H. Fasl, F. Stelzer, and G. Braunegg, "Archaeal production of polyhydroxyalkanoate (PHA) co- and terpolyesters from biodiesel industry-derived by-products," *Archaea*, vol. 2013, p. e129268, Dec. 2013.

[133] I. Poblete-Castro, D. Binger, R. Oehlert, and M. Rohde, "Comparison of mcl-Poly(3-hydroxyalkanoates) synthesis by different *Pseudomonas putida* strains from crude glycerol: citrate accumulates at high titer under PHA-producing conditions," *BMC Biotechnology*, vol. 14, no. 1, p. 962, Dec. 2014.

[134] S. O. Kulkarni, P. P. Kanekar, S. S. Nilegaonkar, S. S. Sarnaik, and J. P. Jog, "Production and characterization of a biodegradable poly (hydroxybutyrate-co-hydroxyvalerate) (PHB-co-PHV) copolymer by moderately haloalkalitolerant *Halomonas campisalis* MCM B-1027 isolated from Lonar Lake, India," *Bioresour Technol*, vol. 101, no. 24, pp. 9765–9771, Dec. 2010.

List of Bibliography (Continued)

[135] G. Singh, S. K. Lakhi, I. Y. Kim, S. Kim, P. Srivastava, R. Naidu, and A. Vinu "Highly efficient method for the synthesis of activated mesoporous biocarbons with extremely high surface area for high-pressure CO_2 adsorption," *ACS applied materials & interfaces*, vol. 9, no. 35, pp. 29782–29793, Sep. 2017.

[136] S.-A. Yang, S. Choi, S. M. Jeon, and J. Yu, "Silica nanoparticle stability in biological media revisited," *Scientific Reports*, vol. 8, no. 1, p. 185, Jan. 2018.

[137] B. H. Kenzaoui, M. Ceridono, P. Colpo, A. Valsesia, and P. Urbán, "Dispersion behaviour of silica nanoparticles in biological media and its influence on cellular uptake," *Plos One*, vol. 10, no. 10, 2015.

[138] J. C. Park and H. Song, "Metal@Silica yolk-shell nanostructures as versatile bifunctional nanocatalysts," *Nano Research*, vol. 4, no. 1, pp. 33–49, Jan. 2011.

[139] T. P. L. Ferraz, M. C. Fiúza, M. L. A. Dos Santos, L. Pontes De Carvalho, and N. M. Soares, "Comparison of six methods for the extraction of lipids from serum in terms of effectiveness and protein preservation," *Journal of Biochemical and Biophysical Methods*, vol. 58, no. 3, pp. 187–193, Mar. 2004.

[140] S. H. Neoh, C. Gordon, A. Potter, and H. Zola, "The purification of mouse monoclonal antibodies from ascitic fluid," *Journal of Immunological Methods*, vol. 91, no. 2, pp. 231–235, Jul. 1986.

[141] A. R. Castro, W. E. Morrill, and V. Pope, "Lipid removal from human serum samples," *Clinical and Diagnostic Laboratory Immunology*, vol. 7, no. 2, pp. 197–199, Mar. 2000.

[142] Y. S. Nam, J. J. Yoon, and T. G. Park, "A novel fabrication method of macroporous biodegradable polymer scaffolds using gas foaming salt as a porogen additive," *Journal of Biomedical Materials Research*, vol. 53, no. 1, pp. 1–7, 2000.

[143] S.-W. Choi, J. Xie, and Y. Xia, "Chitosan-based inverse opals: Three-dimensional scaffolds with uniform pore structures for cell culture," *Advanced Materials*, vol. 21, no. 29, pp. 2997–3001, 2009.

List of Bibliography (Continued)

[144] C. M. Murphy, M. G. Haugh, and F. J. O'Brien, "The effect of mean pore size on cell attachment, proliferation and migration in collagen–glycosaminoglycan scaffolds for bone tissue engineering," *Biomaterials*, vol. 31, no. 3, pp. 461–466, Jan. 2010.

[145] F. J. O'Brien, B. A. Harley, I. V. Yannas, and L. J. Gibson, "The effect of pore size on cell adhesion in collagen-GAG scaffolds," *Biomaterials*, vol. 26, no. 4, pp. 433–441, Feb. 2005.

[146] I. V. Yannas, E. Lee, D. P. Orgill, E. M. Skrabut, and G. F. Murphy, "Synthesis and characterization of a model extracellular matrix that induces partial regeneration of adult mammalian skin.," *Proceedings of the National Academy of Sciences*, vol. 86, no. 3, pp. 933–937, Feb. 1989.

[147] A. V. Murueva, A. M. Shershneva, I. V. Nemtsev, E. I. Shishatskaya, and T. G. Volova, "Collagen conjugation to carboxyl-modified poly(3-hydroxybutyrate) microparticles: preparation, characterization and evaluation in vitro," *Journal of Polymer Research*, vol. 29, no. 8, p. 324, Jul. 2022.

[148] Van Wezel and A. L, "Growth of cell-strains and primary cells on micro-carriers in homogeneous Culture," *Nature*, vol. 216, no. 5110, Art. no. 5110, Oct. 1967.

[149] X.-Y. Chen, J.-Y. Chen, X.-M. Tong, J.-G. Mei, Y.-F. Chen, and X.-Z. Mou, "Recent advances in the use of microcarriers for cell cultures and their ex vivo and in vivo applications," *Biotechnology Letters*, vol. 42, no. 1, pp. 1–10, Jan. 2020.

[150] M. H. Amer, M. Alvarez-Paino, J. McLaren, F. Pappalardo, and S. Trujillo, J. Q. Wong, S. Shrestha, S. Abdelrazig, L. A. Stevens, J. B. Lee, D. H. Kim, C. González-García, D. Needham, M. Salmerón-Sánchez, K. M. Shakesheff, M. R. Alexander, C. Alexander, and F. R. Rose, "Designing topographically textured microparticles for induction and modulation of osteogenesis in mesenchymal stem cell engineering," *Biomaterials*, vol. 266, p. 120450, Jan. 2021.

List of Bibliography (Continued)

[151] A. A. Sherstneva, T. S. Demina, A. P. F. Monteiro, T. A. Akopova, C. Grandfils, and A. B. Ilangala, "Biodegradable Microparticles for Regenerative Medicine: A State of the Art and Trends to Clinical Application," *Polymers*, vol. 14, no. 7, Art. no. 7, Jan. 2022.

APPENDIX

APPENDIX A
Cell culture medium

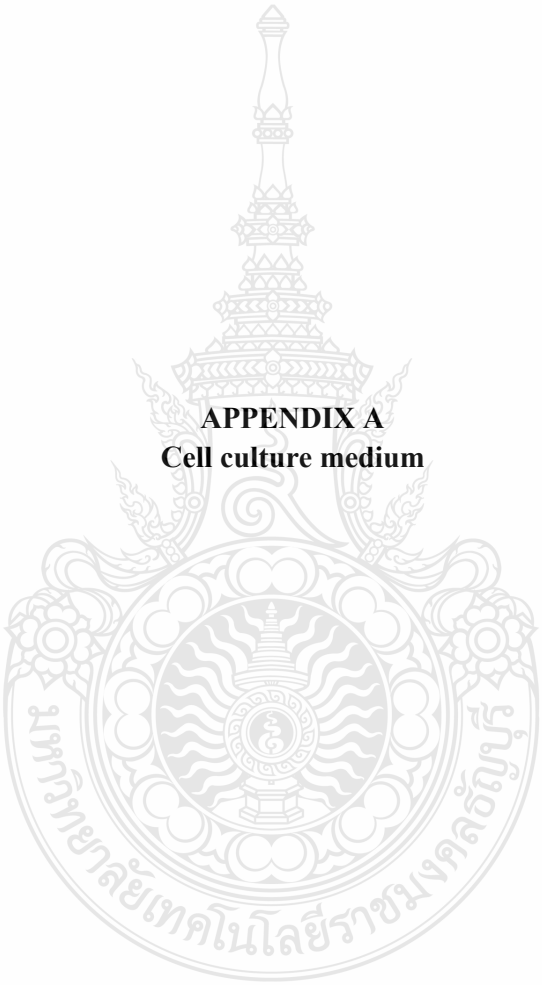

Eagle's Minimum Essential Medium (EMEM) 1000 mL

Medium MEM	9.4	g
Sodium pyruvate	0.11	g
Sodium bicarbonate	2.2	g
Glutamine (GlutaMAX™-I 100x)	20	mL
Non-essential amino acids (100x)	10	mL
Fetal bovine serum	100	mL

APPENDIX B
Phosphate Buffer Saline

Phosphate Buffer Saline (pH 7.4) 1000 mL

NaCl	8	g
KCl	0.2	g
Na_2HPO_4	1.44	g
KH_2PO_4	0.24	g

APPENDIX C
Standard Curve

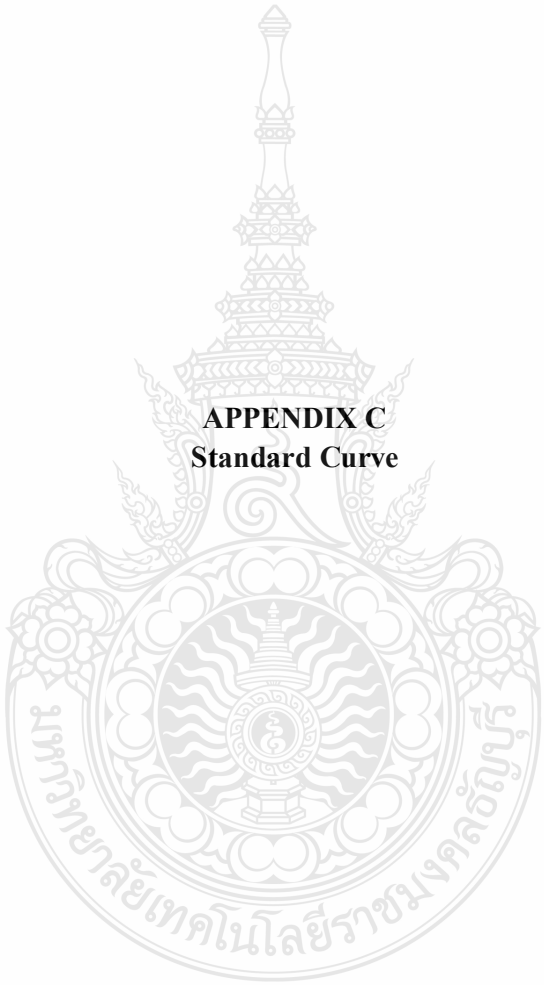

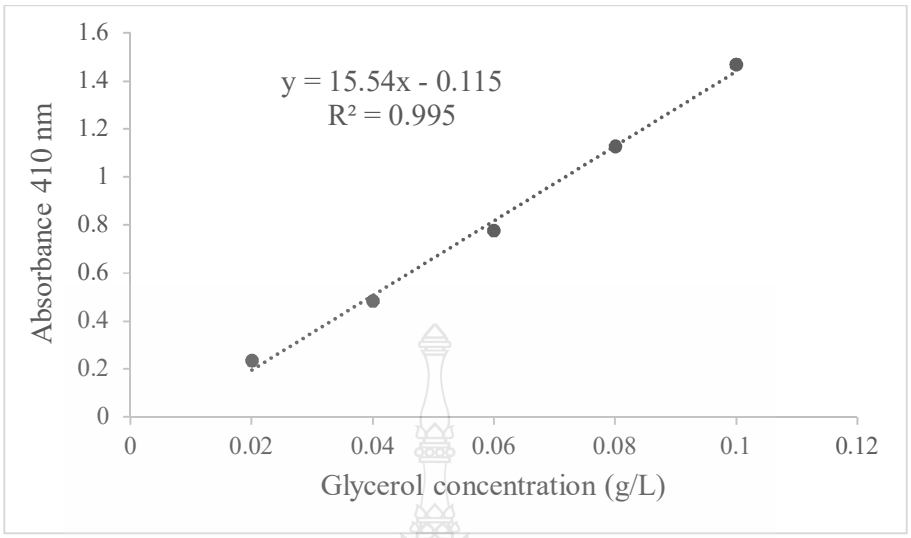

Figure C1 Standard curve of glycerol

APPENDIX D
PHA extracted

Table D1 PHA of extraction process using silica gel

Run	PHA
1	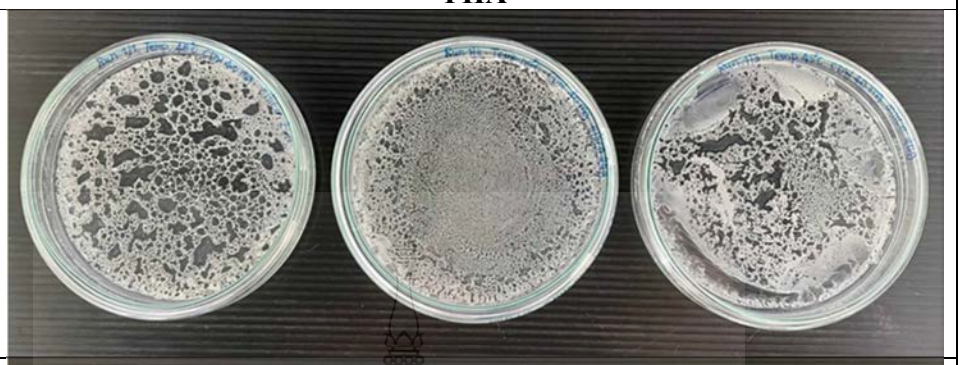
2	
3	
4	

Table D1 PHA of extraction process using silica gel (Continued)

Run	PHA
5	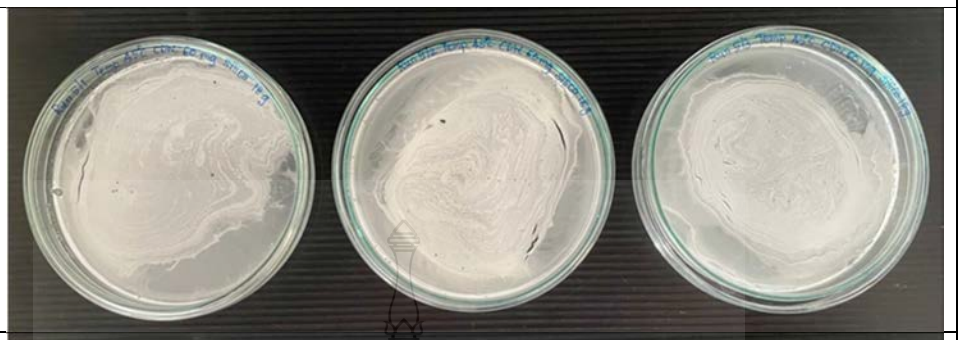
6	
7	
8	

Table D1 PHA of extraction process using silica gel (Continued)

Run	PHA
9	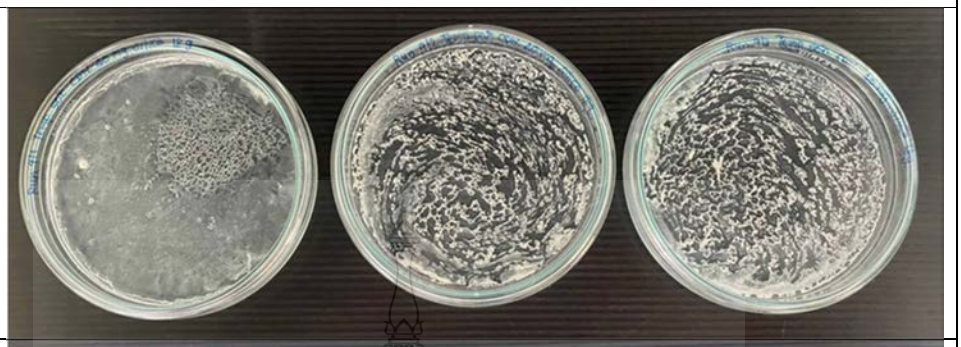
10	
11	
12	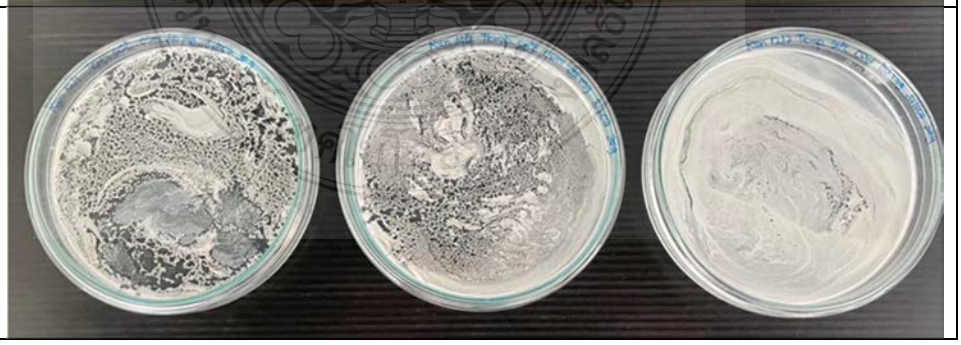

Table D1 PHA of extraction process using silica gel (Continued)

Run	PHA
13	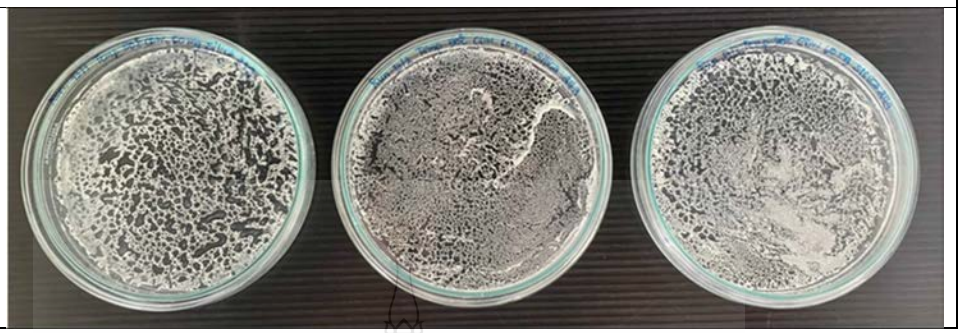

Note Experiments 13-17 are the same example.

Biography

Name - Surname	Miss Sasina Promdee
Date of Birth	February 28, 1997
Address	61/5, M. 8, Wiengsa, Wiengsa, Suratthani, 84190
Education	Mater of Science (Applied Biology Program) (2020-2023)
Telephone Number	090-4891759
Email address	sasina_p@mail.rmutt.ac.th